(2)

POR-2051(EX)
(WT-2051)(EX)
EXTRACTED VERSION

OPERATION DOMINIC, FISH BOWL SERIES

Project Officer's Report—Project 9.1b

Ionospheric Wind and Diffusion Measurements

K. S. W. Champion, Project Officer
Air Force Cambridge Research Laboratories
Bedford, MA

E. R. Manring
Geophysics Corporation of America
Bedford, MA

5 April 1965

NOTICE:

This is an extract of POR-2051 (WT-2051), Operation DOMINIC, Fish Bowl Series, Project 9.1b.

Approved for public release;
distribution is unlimited.

Extracted version prepared for
Director
DEFENSE NUCLEAR AGENCY
Washington, DC 20305-1000

1 September 1985

UNCLASSIFIED
SECURITY CLASSIFICATION OF THIS PAGE

AD-A995431

REPORT DOCUMENTATION PAGE

1a. REPORT SECURITY CLASSIFICATION UNCLASSIFIED	1b. RESTRICTIVE MARKINGS
2a. SECURITY CLASSIFICATION AUTHORITY	3. DISTRIBUTION / AVAILABILITY OF REPORT Approved for public release; distribution is unlimited.
2b. DECLASSIFICATION / DOWNGRADING SCHEDULE	
4. PERFORMING ORGANIZATION REPORT NUMBER(S)	5. MONITORING ORGANIZATION REPORT NUMBER(S) POR-2051 (EX) (WT-2051) (EX)
6a. NAME OF PERFORMING ORGANIZATION 1-AF Cambridge Research Labs 2-Geophysics Corp of America 6b. OFFICE SYMBOL (If applicable)	7a. NAME OF MONITORING ORGANIZATION Defense Atomic Support Agency
6c. ADDRESS (City, State, and ZIP Code) 1-Bedford, MA 2-Bedford, MA	7b. ADDRESS (City, State, and ZIP Code) Washington, DC
8a. NAME OF FUNDING / SPONSORING ORGANIZATION 8b. OFFICE SYMBOL (If applicable)	9. PROCUREMENT INSTRUMENT IDENTIFICATION NUMBER
8c. ADDRESS (City, State, and ZIP Code)	10. SOURCE OF FUNDING NUMBERS PROGRAM ELEMENT NO. / PROJECT NO. / TASK NO. / WORK UNIT ACCESSION NO.

11. TITLE (Include Security Classification) OPERATION DOMINIC, FISH BOWL SERIES; PROJECT OFFICER'S REPORT, PROJECT 9.1b - Ionospheric Wind and Diffusion Measurements, Extracted Version

12. PERSONAL AUTHOR(S)
K. S. W. Champion and E. R. Manring

13a. TYPE OF REPORT	13b. TIME COVERED FROM ____ TO ____	14. DATE OF REPORT (Year, Month, Day)	15. PAGE COUNT
		650405	168

16. SUPPLEMENTARY NOTATION This report has had sensitive military information removed in order to provide an unclassified version for unlimited distribution. The work was performed by the Defense Nuclear Agency in support of the DoD Nuclear Test Personnel Review Program.

17. COSATI CODES		
FIELD	GROUP	SUB-GROUP
18	3	
4	1	

18. SUBJECT TERMS (Continue on reverse if necessary and identify by block number)
Dominic, Fish Bowl, Ionospheric Measurements, Wind, Star Fish Prime, Blue Gill Prime, Blue Gill Triple Prime, King Fish, Tight Rope

19. ABSTRACT (Continue on reverse if necessary and identify by block number)

The aim of this project was to measure high-altitude wind velocities and diffusion coefficients in the altitude region between 60 and 150 km. The method involved the ejection of a sodium vapor trail from a Cajun rocket at dusk or dawn twilight. The sodium was sunlit, and as a result of emission of resonance radiation, was visible against a darkened background for about 20 minutes. The trail was photographed simultaneously from four different sites, allowing for subsequent triangulation to determine the altitude of various parts of the cloud.

A major application of these wind and diffusion data, taken at dusk and dawn following the high-altitude nuclear tests, was to aid in determining the disposition of the nuclear debris.

20. DISTRIBUTION / AVAILABILITY OF ABSTRACT	21. ABSTRACT SECURITY CLASSIFICATION
☒ UNCLASSIFIED/UNLIMITED ☐ SAME AS RPT. ☐ DTIC USERS	UNCLASSIFIED

22a. NAME OF RESPONSIBLE INDIVIDUAL	22b TELEPHONE (Include Area Code)	22c. OFFICE SYMBOL
MARK D. FLOHR	202-325-7559	DNA/ISCM

DD FORM 1473, 84 MAR — 83 APR edition may be used until exhausted. All other editions are obsolete.

SECURITY CLASSIFICATION OF THIS PAGE
UNCLASSIFIED

FOREWORD

Classified material has been removed in order to make the information available on an unclassified, open publication basis, to any interested parties. The effort to declassify this report has been accomplished specifically to support the Department of Defense Nuclear Test Personnel Review (NTPR) Program. The objective is to facilitate studies of the low levels of radiation received by some individuals during the atmospheric nuclear test program by making as much information as possible available to all interested parties.

The material which has been deleted is either currently classified as Restricted Data or Formerly Restricted Data under the provisions of the Atomic Energy Act of 1954 (as amended), or is National Security Information, or has been determined to be critical military information which could reveal system or equipment vulnerabilities and is, therefore, not appropriate for open publication.

The Defense Nuclear Agency (DNA) believes that though all classified material has been deleted, the report accurately portrays the contents of the original. DNA also believes that the deleted material is of little or no significance to studies into the amounts, or types, of radiation received by any individuals during the atmospheric nuclear test program.

OPERATION DOMINIC

FISH BOWL SERIES

PROJECT OFFICERS REPORT – PROJECT 9.1b

IONOSPHERIC WIND AND DIFFUSION MEASUREMENTS

Dr. K.S.W Champion, Project Officer

Air Force Cambridge Research Laboratories
L.G. Hanscom Field
Bedford, Massachusetts

Dr. E.R. Manring

Geophysics Corporation of America
Bedford, Massachusetts

ABSTRACT

The main objective was to measure wind velocities and diffusion coefficients in the altitude region between 60 and 150 km, before and after high-altitude nuclear detonations. A second objective was to determine whether the detonations had any effect on atmospheric circulations at high altitude that would persist for hours.

The method involved the ejection of a sodium vapor trail from a Cajun rocket at dusk or dawn twilight. The sodium was sunlit and, as a result of emission of resonance radiation, was visible for about 20 minutes. The trail was photographed simultaneously by cameras located on Johnston Island and Ships S-1, S-2, and S-4.

The winds were measured in the normal atmosphere on 8 July 1962 before Star Fish Prime, on 25 July before Blue Gill Prime, and on 3 November before Tight Rope. Data was obtained after Star Fish Prime, Blue Gill Triple Prime and at three different times following King Fish. A major change in the wind pattern in the altitude region 80 to 130 km, was produced by Star Fish Prime. Above 100 km the wind was to the south, evidently affected by the motion of field-aligned ionized material. No significant change was caused by Blue Gill Triple Prime in the same altitude region. However, some unusual wind directions were observed following King Fish. In addition to identifying perturbations in the upper atmosphere, the measurements provide data which can be applied to studies of debris motion following the high-altitude detonations.

CONTENTS

FIGURES

CHAPTER 1

INTRODUCTION

1.1 OBJECTIVES

The aim of this project was to measure high-altitude wind velocities and diffusion coefficients in the altitude region between 60 and 150 km. The method involved the ejection of a sodium vapor trail from a Cajun rocket at dusk or dawn twilight. The sodium was sunlit and, as a result of emission of resonance radiation, was visible against a darkened background for about 20 minutes. The trail was photographed simultaneously from four different sites, allowing for subsequent triangulation to determine the altitude of various parts of the cloud.

A major application of these wind and diffusion data, taken at dusk preceding and dawn following the high-altitude nuclear tests, was to aid in determining the disposition of the nuclear debris. The long-time distribution of this material resulting from high-altitude nuclear detonations can be analyzed more completely with measured wind and diffusion data available. Since the atmospheric physical properties are somewhat variable (for example, the altitudes at which

wind shears occur vary by at least 10 km), climatological data based on previous measurements is not adequate for accurate determination of debris motion.

A second objective of the measurements was to determine whether the nuclear detonation had any effect on atmospheric circulations at high altitudes that would persist for hours. These would manifest themselves as unusual wind speed or direction versus altitude profiles or in changes in the altitudes or extent of turbulence.

1.2 BACKGROUND

Direct wind observations in the upper atmosphere over Johnston Island have been made by Smith (Reference 1), who used the rocket-chaff technique in a series of 20 soundings during July and August 1958. Average zonal and meridional components for these soundings are shown in Figure 1.1. Up to the highest point of 275 kilofeet (84 km) the circulation is easterly. Maximum zonal speeds are between 60 and 80 knots (30 to 40 m sec^{-1}) in the layer near 240 kilofeet (73 km). These speeds are based on over 20 observations. Sharp wind shears are observed near 230 and 250 kilofeet. In the altitude region between 140 (43 km) and 180 kilofeet (55 km), only four measurements were made, and so the data may not be representative.

In general, the meridional component is much smaller than the zonal component at all altitudes. The data of Smith is of considerable interest but is severely limited in altitude range.

Both Murgatroyd (Reference 2) and Batten (Reference 3) have constructed plots of zonal wind components as a function of latitude. Neither of these plots appears to be in severe disagreement with observations. Champion and Zimmerman (Reference 4) have plotted wind data obtained at Eglin, Florida, during 1959 and 1960. The data obtained during July and August 1960 is contained in Figure 1.2. Note that the wind is easterly below the shear at 80 km and that it is westerly above that altitude. A second sharp shear near 110 km is followed by easterly winds, up to at least 160 km and possibly to the highest altitude at which hydrodynamic winds exist. The latitude of Eglin is 30.0° N and of Johnston Island is 16.5° N. This would cause each of the wind shears to be about 5 km lower at Johnston than at Eglin during July and August.

Major changes take place in the mean circulation pattern between summer and winter. During winter, the highest shear drops in altitude by about 20 km. The winds above this shear are still easterlies and below it westerlies. However, the

lower shear (~ 80 km in the summer) virtually disappears, and at most latitudes the winds are westerlies, of varying intensity, to ground level. At latitudes between 15° and 20° and altitudes between 15 and 25 km, there is a residual pocket of easterly wind. Spring and fall are the transitional seasons with average zonal winds at a minimum.

It should be emphasized that our knowledge of global circulation patterns above 50 km and at almost all altitudes in the equatorial zone is relatively scanty at present and that the present models require additional data which will probably result in some revisions.

Manring et al (References 5, 6, 7) have employed the sodium trail technique for the determination of horizontal wind profiles and the calculation of diffusion as a function of altitude. Typical results of these experiments are seen in Figures 1.3 and 1.4 where the wind velocity and direction, respectively, are plotted as a function of altitude for three different experiments. Of specific interest is the extremely high shear region between 100 and 110 km. Although the magnitude and specific heights vary to some degree, this interval is almost always turbulent and is a region of high shear.

Detailed studies of Project Firefly by Champion and Zimmerman (References 4, 8, 9, 10, 11) have shown that

turbulence, either isotropic or shear in origin, exists in most or all of the altitude interval between approximately 50 and 120 km. Isotropic turbulence commonly exists where the vertical temperature gradient is negative or nonexistent, conditions known to be present through most of this altitude region. Shear turbulence, of course, occurs in regions of strong wind shears. In addition to the wind shear observed by Manring between 100 and 110 km, the lower wind shear, near 80 km, was also observed.

Zimmerman and Champion (References 12 and 13) have calculated theoretical values of molecular and turbulent diffusion in the upper atmosphere and compared them with experimental values obtained from Project Firefly. Additionally, Manring and Knaflich (Reference 14) have calculated diffusion coefficients from the basic photographic data obtained during sodium trail experiments.

1.3 THEORY

The upper atmospheric winds and diffusion were measured during the Fish Bowl Series by methods developed by Manring et al (References 5 and 7) over the past several years. During the period when the trail was visible, its shape underwent continuous changes due to the wind velocity at various altitudes. If the trail expansion was radial in

a coordinate system moving with the wind, the magnitude and direction of motion of the trail center was a direct measure of the prevailing winds in that region. The positions of the trail at various altitudes and times were obtained from analysis of photographs taken simultaneously at several separate stations. Vertical velocities were either small or they were variable in time as well as in position, for example, due to turbulence. They were assumed to be negligible in the preliminary data analysis outlined below.

Plots were prepared which depict, at a single time, the filament center in x, y coordinates on a tangent plane to the earth at the launch site, Johnston Island. The coordinate system was oriented with the x axis north and y axis west. These plots were called ground projections. Along the curve representing the trail center in the ground projection, the height or z coordinate was located. The change in x, y coordinates for a particular value of z, as determined from two ground projections (at times t_1 and t_2), represented a horizontal displacement D(z) given by

$$D(z) = \left[(x_1 - x_2)^2 + (y_1 - y_2)^2 \right]^{1/2} \qquad (1.1)$$

The magnitude of the velocity at the altitude z was then given by

$$V(z) = \frac{D(z)}{t_2 - t_1} \tag{1.2}$$

whereas the direction was obtained from

$$\tan \theta(z) = - \frac{y_2 - y_1}{x_2 - x_1} \tag{1.3}$$

on a navigator's scale which is zero at north and increases in angle toward the east. Data thus obtained was plotted and resembled Figures 1.3 and 1.4. This then represents the method from which velocity information was obtained from the basic photographs.

The following analysis describes the theory by which diffusion data was obtained. If vapor is ejected at a point in the atmosphere, the resulting cloud will grow radially. The initial expansion is not diffusion controlled if the initial temperature or pressure is higher than that of the ambient existing at the release point. In order for equilibrium to be established and the subsequent expansion controlled by diffusion, several conditions must be met:

1. An initial expansion will occur at about the velocity of sound at the temperature of the expanding gas if the initial pressure is above ambient pressure. A dimension, typical of the equilibrium size, is taken as the diameter of a sphere

which would contain the released material when the number density within the sphere is equal to that of the ambient.

2. If the released material is at a higher temperature than the ambient, a minimum volume such that the enclosed energy density is equal to the ambient energy density is a better criterion for the equilibrium size.

3. Sufficient collisions must occur between the atoms released and the ambient molecules before an equilibrium, diffusion-type expansion can be considered. At very high altitudes and for small amounts of contaminant, this last criterion is the most appropriate.

These conditions are summarized by the following expressions for N atoms released at temperature T_R, ambient number density ρ_a, temperature T_a and mean-free-path L.

$$\frac{N}{\frac{4\pi}{3} r_e^3} < \rho_a \tag{1.4}$$

$$\frac{N}{\frac{4\pi}{3} r_e^3} T_R < \rho_a T_a \tag{1.5}$$

$$r_e > K L \tag{1.6}$$

where r_e is a minimum equilibrium radius and K is a factor equal to perhaps 5.

After the initial expansion has occurred and the released gas is in equilibrium with the ambient, further expansion occurs by diffusion processes. If there is no turbulence (References 11, 15) or if the scale of turbulence is large compared to the cloud dimensions, the standard equation

$$D\nabla^2\rho = \frac{\partial\rho}{\partial t} \tag{1.7}$$

holds where D is the coefficient for molecular diffusion, t the time, and ρ the density of contaminant atoms as a function of position and time. For spherical symmetry a solution of this equation is

$$\rho(r, t) = \frac{N}{(4\pi\ Dt)^{3/2}}\ \exp\left(-\frac{r^2}{4Dt}\right) \text{atoms/unit volume} \tag{1.8}$$

where N is the total number of atoms released and r is the radius from the cloud center. This equation results if the atoms are all at the center at zero time t_o, and negligible initial or forced expansion occurs.

If the initial expansion is forced or if the release does not occur at a point, other boundary conditions must be imposed. However, it is found that all such solutions quickly approach Equation 1.8, if an appropriate value is used for t_o. For the release pressures and temperatures in the experiments

to be described, Equation 1.8 is applicable over most of the period of observation for non-turbulent regions. For these experiments, τ_o coincides with the release time, to within experimental error, for heights below 140 km, and negligible error is involved in considering it coincident to the maximum heights reported.

The photographic image density of the cloud is a function of its surface brightness. Releases were timed to occur during twilight when the cloud is illuminated by solar radiation, but the sky background is low. From known absorption cross sections for the contaminant atoms released and from the solar spectrum, the scattering efficiency of an atom bathed in sunlight can be determined. For those parts of the cloud which are optically thin, the apparent surface brightness is proportional to the number of atoms in a column of unit area along the direction in which it is viewed. That is, the surface brightness is given by

$$B = \frac{q}{4\pi} \int_0^\infty \rho(r, t)\, ds \text{ photons/cm}^2 \cdot \text{sec} \cdot \text{steradian} \qquad (1.9)$$

where q is the number of photons scattered per atom per second uniformly into 4π steradians, $\rho(r, t)$ the density of scattering atoms, and ds is a differential of path length along the line of sight. The quantity $\int_0^\infty \rho(r, t)\, ds$ is defined as τ_1.

For a spherical cloud with a Gaussian distribution of contaminant as defined in Equation 1.8, the quantity η, after integrating along a line of sight, is given by

$$\eta = \frac{N}{\sqrt{4\pi\ Dt}} \exp -\left(\frac{a^2}{4Dt}\right) \qquad (1.10)$$

where a is the perpendicular distance from the cloud center to the line of sight in question.

If the contaminant is released continuously from a moving rocket, the resulting cloud has a cylindrical cross section. The diffusion equation and subsequent integration along a line of sight yields

$$\eta = \frac{M}{\sqrt{4\pi\ Dt}} \exp -\left(\frac{a^2}{4Dt}\right) \qquad (1.11)$$

for cylindrical case. Parameters have the same meaning as before except the M is the number of atoms released per unit length along the rocket trajectory. In all cases considered, the line of sight could be regarded as perpendicular to the axis of the cylinder, as only those portions of the cloud were chosen for analysis which satisfied this condition. Otherwise η as given in Equation 1.11 would not be unique.

After the rapid initial expansion of the sodium to pressure equilibrium, the trail expands according to the relation (Reference 13, Equation 12)

$$r_o^2 = 4Dt\left[1 + \ln\left(\frac{r_{o\ max}^2}{2r_e^2}\right) - \ln\left(\frac{2Dt}{r_e^2}\right)\right] \qquad (1.12)$$

for molecular diffusion, where r_o is the observed radius of the trail, which is defined as that radius at which the cloud contains the minimum number of particles per column of unit area which can be detected against its ambient background.

r_e is the radius when pressure equilbrium is reached. When turbulence is present expansion is more rapid and different expressions are used for r_o (Reference 13, Equations 10 and 11).

If r_o^2 is plotted as a function of t a straight line is obtained at times when the last term of Equation 1.12 is small. However, at later times the plot of r_o^2 deviates from a straight line, and a maximum ($r_{o\ max}^2$) is reached. The diffusion coefficient D can be calculated from Equation 1.12 when $r_{o\ max}$ and r_e are known and r_o has been determined as a function of time. An alternative method, which is probably more satisfactory to use with densitometry, is based on the following considerations. As defined, η is proportional to the surface brightness. Hence a line of constant η will be along isophotes on the cloud photograph. From Equation 1.11 at a given time t

$$\ln \eta_1/\eta_2 = \frac{r_2^2 - r_1^2}{4Dt} \quad . \qquad (1.13)$$

where r_1 and r_2 are the radial distances from the isophotes in question to the axis of the cloud. Since the values of η enter as a ratio, absolute units are not required. The ratio can be measured with a densitometer; then, knowing the values r_1 and r_2 measured from the plates, and the time after release at which the photograph was taken, D can be computed.

In the cases where the quantity η is of the order of, or larger than, the reciprocal of the atomic scattering cross section σ, the surface brightness is no longer proportional to η. For such regions of the cloud, the surface brightness is proportional to the solar flux times the absorption line widths. For regions in which η represents several optical thickness (one optical thickness = $1/\sigma$), the brightness becomes essentially independent of η.

Since the clouds of released material are usually optically dense near their centers, valid measurements of η can be made only in the region of the cloud edges. In practice a densitometer is utilized to determine photographic density of the image along a cut through the cloud center. If the

film characteristics are known, it is then possible to determine η at the cloud edges for all $\eta < 1/\sigma$. Since the background light level is constantly changing throughout the twilight period, conventional film calibration is very difficult. A method exists, however, by which the photographic density of the optically dense cloud center and the photographic density outside the cloud can be employed to calibrate each negative. Briefly, the difference between these two densities represents a constant and known increment of surface brightness. Between these two limits of density, for such increments of light level, it is known photographic theory that the density varies as log of the light intensity within the increment.

The trail material employed in the measurements was sodium, although lithium and potassium have also been employed. These materials scatter sunlight radiation incident upon the trail by a resonance process. The resulting scattered light is nearly monochromatic and is characteristic of the scattering atom (neutral sodium in this case). To maximize photographic contrast, the vapor was released from the carrier rocket during twilight periods at times when the trail was sunlit, but the background was a minimum. The number of photons n emitted per solar illuminated atom by resonance radiation is given by

$$n = \frac{g_1}{\tau g_2} \; P \exp(-E/kT) \qquad (1.14)$$

Where: τ = radiative lifetime

g_1, g_2 = Statistical weights of upper and lower states

E = energy of incident photon

k = Boltzmann constant

T = temperature of the sun

P = dilution factor (= 5.4×10^{-6})

Thus, if the sun's temperature is assumed to be 6000^{o}K and a Fraunhofer intensity of about 5×10^{-2} is used (Reference 16), then the sodium resonance line from solar rays would give $n = 0.85$ sec^{-1} (Reference 17).

A typical sodium payload is of the order of 2 kg which is equivalent to 5×10^{25} atoms. Typical trail dimensions are 50-km length and 1-km diameter (4×10^{16}cm^3). It thus follows that an average trail density is 1.2×10^9 atoms cm^{-3}. For such densities practically all photons will undergo at least one resonance transition within a path length of about three meters (Reference 18). The trail has maximum brightness when viewed from the same direction as the incident solar photons and minimum brightness from the opposite direction. The maximum from any direction can be no more than one-half of the total emission or about 5×10^{11} photons/cm^2 sec (Reference 17). Photometric measurements have shown that the intensity of the emission decreased slowly as attenuation of

the incident solar energy by the earth's atmosphere increased. The intensity fell suddenly to about the night-time value as the earth's shadow reached the region.

To further increase contrast for optimum photographic registration of the characteristics of the emitted trail, filters and film types were used to augment as far as possible the ratio of light scattered by the cloud to background light. Interference filters could not be used effectively owing to the wide angles over which the cloud extended.

Film development techniques were also carefully scrutinized to provide maximum contrast for future data reduction. The film of all four sites was processed at essentially the same time and under the same conditions to assure minimum deviations. Film calibration and processing for subsequent densitometry was also considered. The changing background intensity during twilight was taken into account; lens apertures and exposure times were adjusted accordingly.

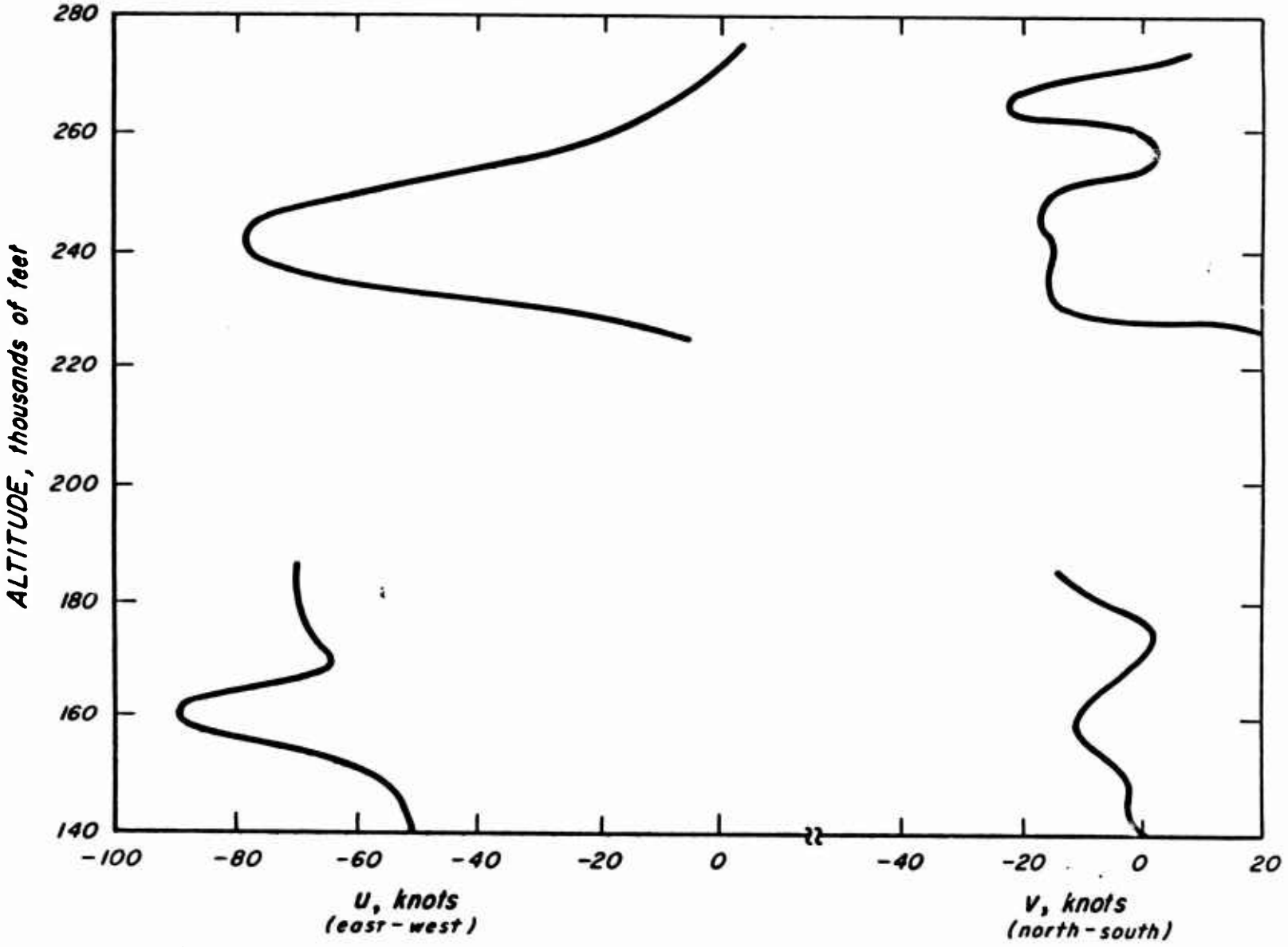

Figure 1.1 Vertical variations of u and v components of winds over Johnston Island during summer.

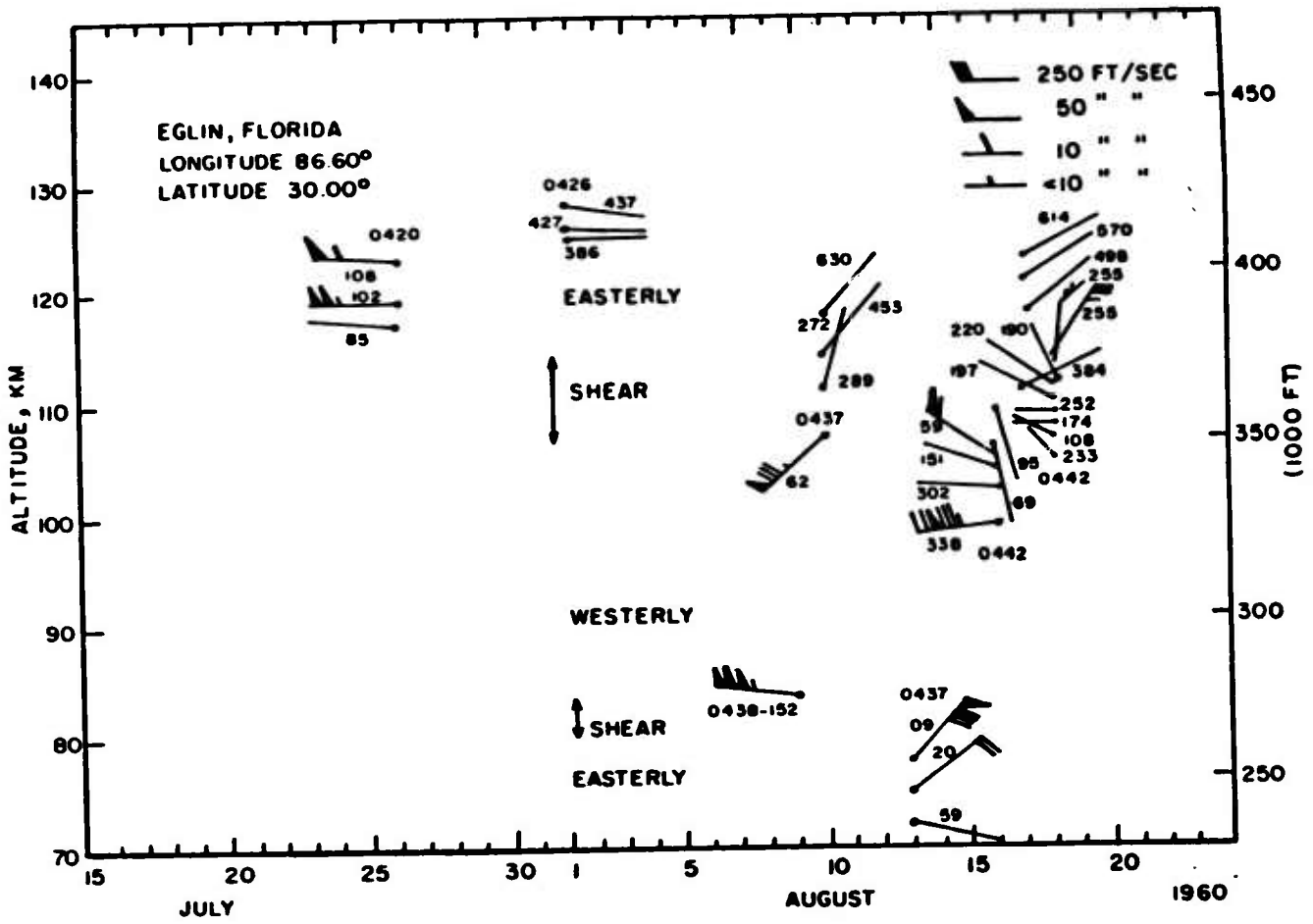

Figure 1.2 Upper atmosphere winds measured by chemical releases, Eglin, Florida, July and August 1960.

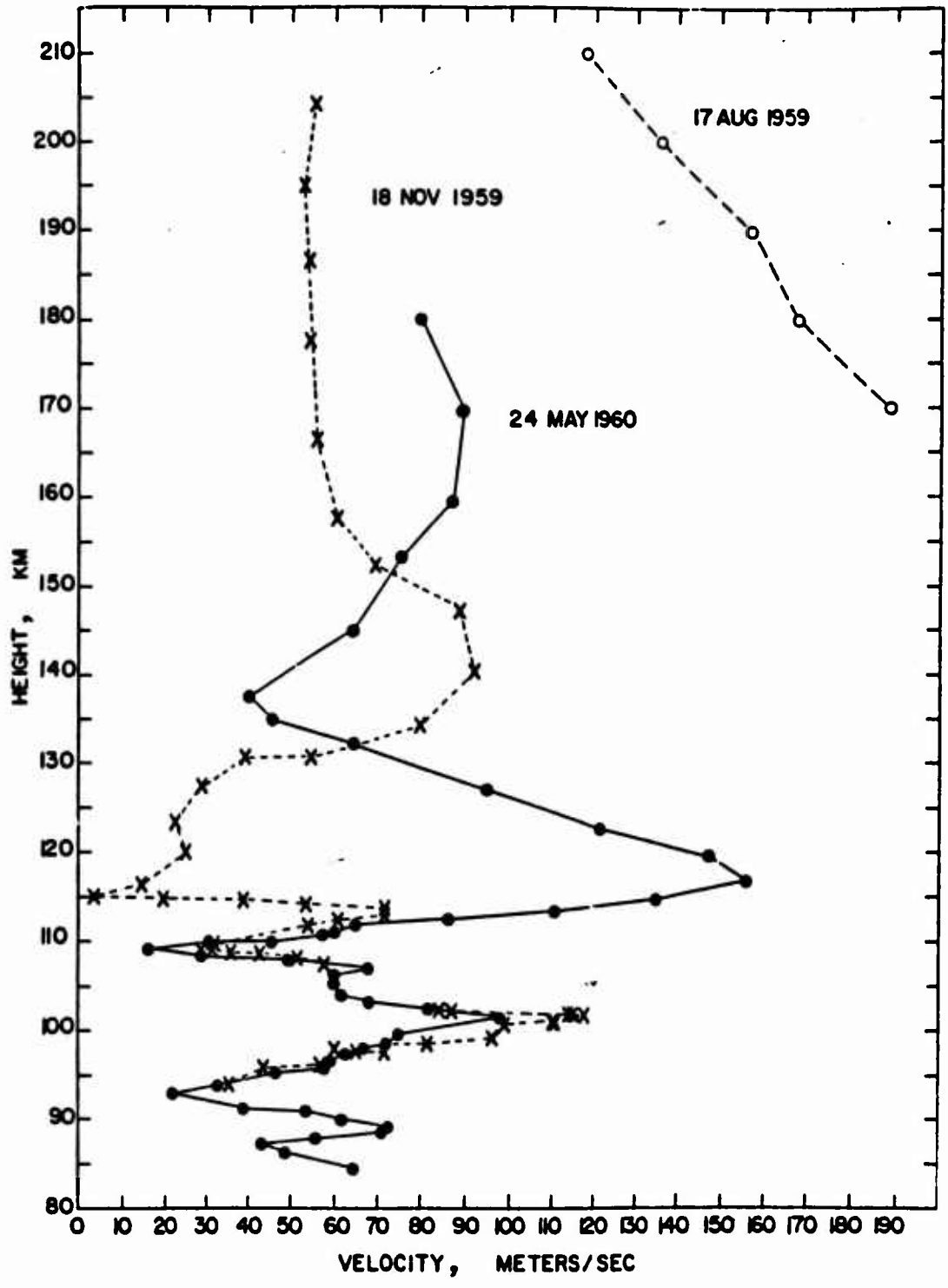

Figure 1.3 Observed wind vector magnitude as a function of height.

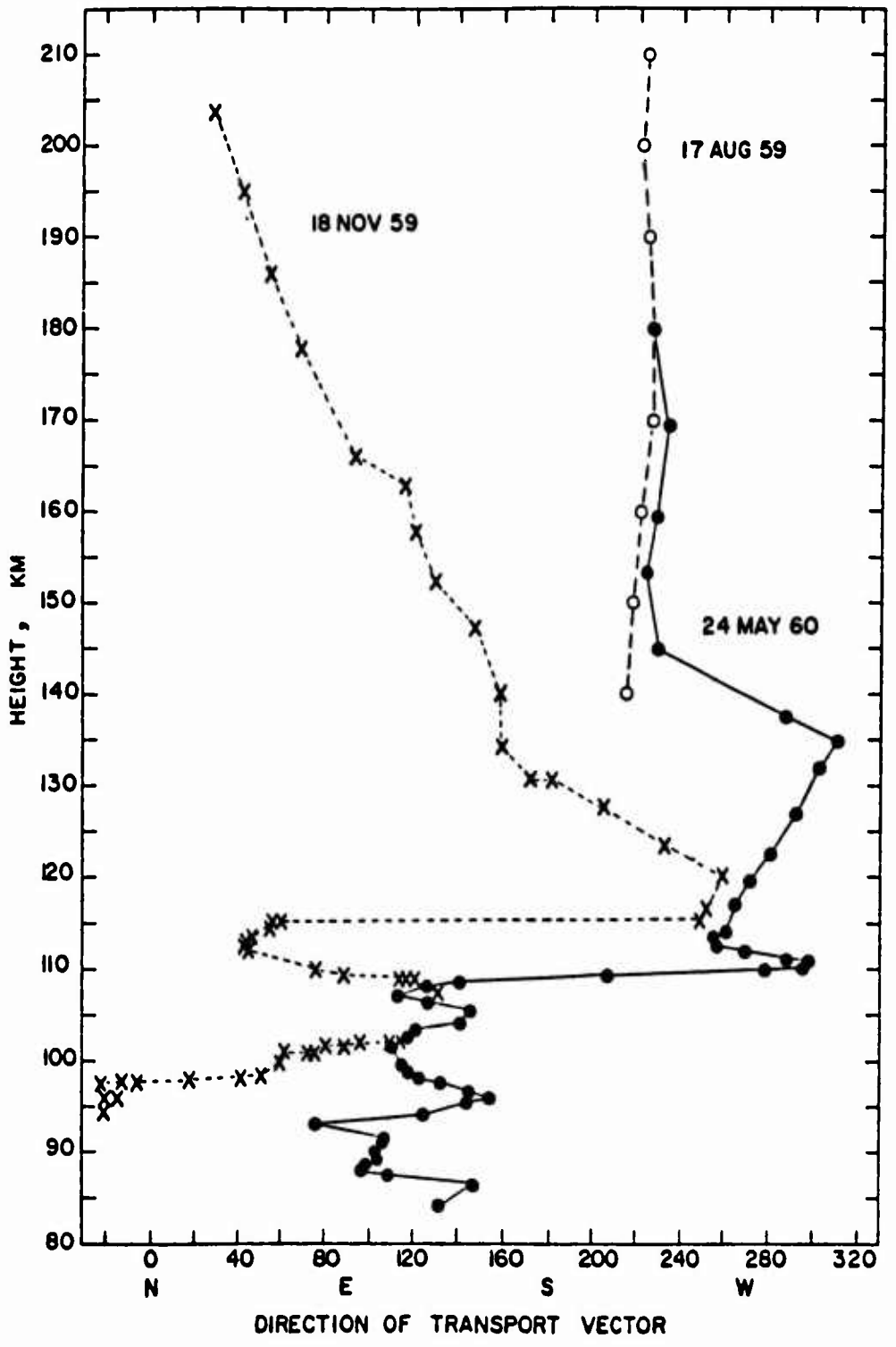

Figure 1.4 Observed wind vector direction as a function of height.

CHAPTER 2

PROCEDURE

2.1 SHOT PARTICIPATION

Sodium trails were produced during twilights either preceding or following each of the events listed in Table 2.1. A total of eight successful trails were produced. These occurred during the evening twilight before and the morning twilight following Star Fish Prime, the evening before Blue Gill Prime, the morning following Blue Gill Triple Prime, the morning 4-1/2 hours after King Fish, the morning 28-1/2 hours after King Fish, the evening 41 hours after King Fish, and the evening before Tight Rope. In order that the sodium trail may be photographed, it must be sunlit and the sky background low. Thus, the sodium trail rockets must be fired within a 10-minute window during each twilight, and cloud cover is a major problem. Since the aim of the project was to measure winds and other atmospheric properties immediately before and after nuclear detonations, the sodium rocket firings were cancelled only if cloud coverage approached 100% throughout the window.

As a result of this procedure, clouds are conspicuous on many photographs. However, the desired data was obtained from all sodium trails.

The camera operation and cloud cover relative to the sodium experiments are summarized in Table 2.2. The percentage cloud cover over Johnston Island and the Ships S-1, S-2, and S-4 is given in each case as is the number of cameras that were available at each site. Despite a generally high percentage of cloud cover, most sites obtained some data.

The sodium trail Nike-Cajun rockets were launched from Pad 21 (see Figure 2.1) at an effective elevation of 85° and azimuth of 155° T. Since only one launcher was available for Project 9.1b, it was necessary to reload for the dawn twilight shot. In the figure the payload is covered by plastic with aluminum sheet inside to protect it from water and heat from sunlight, respectively. Banks of three K-24 cameras were located on Johnston Island, Ships S-1, S-2, and S-4. The Star Fish ship locations were approximately: S-1, 575 km magnetic south of Johnston; S-2, 240 km magnetic north; and S-4, 280 km west. The distances of the ships (particularly S-1) from Johnston were considerably greater than desired by this project and resulted in degradation of data. The roll of the ships resulted in blurring of the photographs. This problem could be minimized by appropriate orientation of the ships. This was requested but not, in general, done.

Using the line-of-sight equation,

$$R = (h^2 + 2ch)^{1/2} \qquad (2.1)$$

With the radius of the earth $\alpha \approx 6 \times 10^3$ km, the trail should be within line of sight from S-1 above about 40 km. However, in practice it is not as simple as this and due to refraction, strong scattering of light near the horizon, and frequent clouds, the minimum effective height is usually considerably greater than this altitude.

During Blue Gill Prime, Ships S-1, S-2, and S-4 were all within 70 km of Johnston, and this distance was satisfactory. However, the revised bearings from the island resulted in the three ships being relatively close together, and this was not satisfactory for two reasons. One was that the locations were poor for triangulation purposes, and the other was that, being so close together, if clouds obscured the view of one ship, they were almost certain to obscure the view from all three ships.

Table 2.3 contains the minimum-maximum elevation angles (for trail altitudes of 60 and 150 km, respectively) from each of the photographic sites computed from the law of cosines:

$$\theta = \sin^{-1}\left(\frac{h^2 + 2\alpha h - R^2}{2\alpha R}\right) \qquad (2.2)$$

or more simply by

$$\theta = \tan^{-1}\frac{h}{R^1} \qquad (2.3)$$

where R = slant range, and R^1 = ground range in the convenient flat earth approximation in Equation 2.3. The values in the table are typical, but not exact, since it was not worthwhile to recalculate the table every time the ship locations were changed. The quite low elevation angles subtended by the cameras on the ships for Star Fish is apparent.

2.2 INSTRUMENTATION

2.2.1 Rocket and Payload. The sodium was carried in the payload section of a Nike-Cajun rocket. The total payload, attached to the front of the Cajun rocket, consisted of three parts. The first was cylindrical and contained the chemicals; the second was also cylindrical and contained the batteries, electrical and other control equipment. The third was the conical nose cone, which subtended a total angle of 20° at its tip. The chemical makeup of the payload was sodium and thermite in proper ratio as described in detail in Reference 19. The control instrumentation included two parallel timing circuits, batteries, and igniters for firing the chemical canister. Each firing circuit was complete, and the duplication was to ensure that, in the event of malfunction of one circuit, firing would still be accomplished. In the circuit shown in

Figure 2.2 a mechanical timer, set at approximately 40 seconds, was initiated by an acceleration switch which was activated at launch. In Figure 2.3 an electronic timer was initiated by a lanyard switch which was released at rocket takeoff. The electronic timer was also set at 40 seconds. By means of an umbilical cable, which was manually pulled away before launch, the payload was monitored at the blockhouse during its final preparation. The safety circuit provided for opening the circuit between the batteries and igniters in the event the payload malfunctioned.

Figure 2.4 shows the typical trajectory of a Nike-Cajun rocket with a 70-pound payload at 80-and 85-degree launch angles. Trail generation starts at 40 to 50 seconds after launch, continues through apogee, and during a relatively short part of the downward section of the flight. Thus, trail generation takes place for about 160 seconds. Although all rockets were fired with nominal effective elevations of 85 degrees, fluctuations in low-altitude winds, for which exact compensation was not always possible, resulted in actual effective elevation of 85±2 degrees.

2.2.2 Rocket Performance. With regard to rocket performance, the following comments cover Project 9.1b through the whole of Fish Bowl. For cases where both Nike and Cajun ignited:

1. All flights were successful for which the Nike was spun at 2 rps (ARC SVG* or Aerolab fins) and the Cajun was spun at 8 rps at Cajun burnout (ARC SVG wedged Capache fins —7 flights) or 10 rps (White Sands fins with bevels and spoilers——1 flight).

2. Unsuccessful flights occurred when the Nike was spun at 2 rps (ARC SVG fin) and zero spin was put on the Cajun (ARC SVG fins, no wedges——1 flight) or the Nike was spun at 8 rps (Aerolab fins) and about 3 rps was put on the Cajun (Aerolab fins with experimental wedges——1 flight).

For more detailed information on rocket performance, Tables 2.4-2.10 should be consulted. These contain the radar trajectory data for each of the successful flights, except that of 26 October 1962, for which no trajectory data exist.

2.2.3 Photographic Equipment. All the cameras specified in Table 2.2 were of the K-24 type. The K-24 is a military aerial reconnaissance camera employing a fixed-

*Atlantic Research Corporation, Space Vehicles Group

focus, 7-inch, f/2.5 Aero Ektar lens, and a removable magazine. Other lenses are also available including the 20-inch, f/5.6 Aero Ektar. The K-24 accepts 5-1/2-inch film in either 26- or 56-foot lengths and has a 5-in^2 format. The shutter is a curtain type, and a night curtain was installed so that it could be operated on a time setting. The cameras were fitted within a combination adjustable mount and carrying box. Azimuth angles were set in by compass, and zenith angles by protractor level, or by use of the calibrated scale on each mount. The units could be operated electrically using an automatic timing unit. In the case of malfunction of the electrical equipment, the units could be hand operated. A bank of three cameras was located at each of the four principal photographic sites. Having three cameras at each site provided a backup in case one, or even two, failed.

In addition to the K-24 cameras at the main site on Johnston Island, there was a polaroid camera. This provided the photographs used for the quick-look data reduction. There were also two stereo sites equipped with press cameras, one at the east and the other at the west end of Johnston Island. Exposures were made at 30-or 60-second intervals at both sites. The stereo photographs could be used

both to help determine the altitude of sections of the trail by triangulation and also to develop three-dimensional images or models of the trails.

Two methods were used to obtain as much contrast as possible between the sodium cloud and the background. The first has already been mentioned; namely, the cloud was released during twilight intervals when the background was as low as possible, subject, of course, to the condition that the cloud be sunlit at all heights of interest for a time interval sufficiently long to make good measurements. Secondly, as has already been touched upon, the background was reduced as much as possible by proper selection of film and filter for the material released in the cloud.

For sodium, the wavelengths of interest are 5,890 Å and 5,896 Å (D lines). Accordingly, panchromatic film of the Tri-X or Royal X variety was employed. It is sensitive to these wavelengths but relatively insensitive to radiation of a longer wavelength. A Wratten 23 A filter was employed on two of the cameras because it transmits 5,890 Å with negligible attenuation but absorbs radiation of shorter wavelengths. The passband of the resulting film and filter combination is some 300 Å wide. One camera was set a stop slower than the other. This procedure gives greater

assurance that the rapidly changing background light levels encountered during twilight and the fluctuations due to varying cloud cover will be adequately accounted for. The third camera was used without a filter to obtain star photographs for determining with greater accuracy the site positions.

The cameras had been serviced, with many parts rebuilt, and they had undergone extensive laboratory and field testing. When checked manually, they operated sluggishly but effectively; when operated automatically, using the control box, the camera motor did not operate positively enough to warrant operation in this manner. Camera operation on Johnston Island was satisfactory, but there were some problems on the ships.

A fiducial lamp assembly was added to the K-24 cameras by simply allowing two small collimated light sources to illuminate etched cross-hairs on the diagonal opposite corners of the format. Methods were devised to operate two of these units manually in a staggered sequence.

Figure 2.5 shows six K-24 cameras mounted in operating positions. The adjustable legs on this unit were removable and fitted inside the box. The cameras were mounted on a platform which became a variable zenith control. When

the cameras were recessed down into the box, the front top section hinged over and was securely clamped, resulting in a portable unit which was handy for shipment and field use.

When two photographic sites are separated by a distance, such that the angle subtended by them at the cloud is a few degrees, the photographs are sufficiently similar to be studied using stereo methods. In this project the trail was photographed with press cameras located at opposite ends of Johnston Island, a separation of about one mile, resulting in a subtended angle of about one degree. One advantage of stereo photographs is that they can be used to produce three-dimensional representations of the trail. Other advantages in this case were that the two close sites had the same cloud conditions (that is, both were clear at the same time); there was no blurring of the photographs due to rolling (as on the ships); and finally, the film was readily available for development and quick-look data reduction.

2.3 DATA REQUIREMENTS

In this section, timing, weather, and communications requirements are enumerated. In the sections that follow, radar data and its interpretation (Section 2.4) and photographic data and its reduction (Sections 2.5 and 2.6) are discussed.

To enable quick-look wind data to be available within one to two hours after firing of the sodium trail rocket, the photographs obtained with the polaroid camera were anayzed in the following way: The position of the camera remained fixed during the photographs, and thus its bearing could be used to mark azimuth directions on the photograph. (Two photographs taken 6 to 8 minutes apart were chosen, and corresponding portions of the trail were identified.) The distance and direction that each identified point moved on the photograph was carefully measured. Then, using the focal length of the camera and the altitude of the identified point, its speed could be calculated. The altitude of the peak of the trail was obtained from quick-look radar data. Radar data could also be used to determine, less accurately, the altitude of other points on the trail. Some help in assignment of altitude could be obtained by using the fact that the upper limit of atmospheric turbulence occurs near 110 km.

Timing, weather, and communications requirements of the project were as follows: For dusk firings a countdown was broadcast over a worldwide countdown net. This was heard at Johnston Island and on the three ships on which cameras were located.

A ten-minute window was allowed for launching. This was essential, as cloud cover was often severe, and it was a question of looking for a gap in the clouds. It was necessary to estimate likely visibility from the ships, since the latest weather reports available were one to two hours old, and weather conditions could change appreciably in that time.

About five minutes before the estimated firing time, an accurate stopwatch was set by WWVH or (less accurately) by the worldwide countdown. The cameras were then set at the appropriate azimuths and elevations, and photographs were taken at twenty-second intervals starting after the trail was visually observed. Thus, photographs were obtained simultaneously from all stations, except when a trail was not visible from any given station.

For the firings at dawn, after the nuclear event, radio silence was broken to provide a countdown on the worldwide net to the ships on one frequency only. The rest of the procedure was the same as for the dusk firings.

2.4 RADAR TRAJECTORY DATA

For accurate determination of the initial location of the sodium trail, radar altitude and azimuth data is extremely valuable. When sodium cloud data from only one site is

available, the radar tracking information must be used to find the heights and horizontal distances to those points in the cloud whose velocities are to be determined, as the usual triangulation method cannot be applied. In Section 2.5 the methods used to apply the radar data to the analysis of the sodium trail films is outlined.

The Range Tracker skin-tracked the Cajun rockets and summarized tracking data on seven of them is included in Tables 2.4-2.10. In the absence of a beacon, radar acquisition was achieved by using an optical viewfinder during the rocket burn phase.

It should be noted that the time given in each table is radar time, which is in general arbitrary and non-zero at launch time. Thus, a zero correction has to be determined for each flight and used to correct each radar time to obtain the flight time. The horizontal range (slant range for 25 July) and azimuth are from the particular radar in use. All data in the tables is from the FPS 16 or the MPS 26. The altitude is measured relative to a plane tangent to the earth at the site of the radar. These values have been corrected for the curvature of the earth to give actual height above the earth before being entered in the tables. Where data is not shown in the tables, there was no radar

track of the rocket. A track at least through the trajectory peak was desired. This was achieved on four rockets (Tables 2.4, 2.6, 2.9, and 2.10) but not on the other three (Tables 2.5, 2.7, and 2.8), although the data obtained on the flight of these three rockets was of considerable value. Edrick, using the Univac in the PMR computer van near the motor pool, reduced the radar data for Rockets 1 and 2. Ysnago reduced the last five trajectories presented in the tables.

Note that the times given in the table captions are local times. In Table 2.8, the radar tracked the Nike-Cajun combination to a radar time of 40 seconds and then tracked the Nike until 75 seconds, at which time it switched back to the Cajun which it tracked from that time onward.

On the rocket flight for which data is given in Table 2.9, for some unknown reason the radar time did not start until the Cajun reached an altitude of approximately 286,900 feet. Thus, data reduction at one-second intervals, starting at the time the rocket was first tracked, ended up with fractional times when it passed radar time zero. The data was recomputed, starting at radar time zero and at even seconds after that time. Thus, two partially overlapping sets of data were provided. These have been combined in Table 2.9.

2.5 REDUCTION OF WIND DATA

2.5.1 Star Fish Prime, Blue Gill Prime. Throughout this report the wind data will be designated by the GMT date of the rocket firing, and morning and evening twilights will be distinguished by use of AM and PM after the GMT date. Rocket launching times and tracking data will be left in Honolulu standard time.

Clouds, stack smoke, ship roll, and equipment difficulties combined to render the ship data useless for triangulation purposes. While there was some good data from both S-2 and S-4, there were too few quality simultaneous photographs to warrant use of triangulation methods (see Table 2.2). The results from the ships were very sparse compared to those obtained on Johnston Island. Thus, only the Johnston Island results could be used in the determination of the upper atmospheric wind vectors for Star Fish Prime and Blue Gill Prime.

Since the regular triangulation method could not be used, the following approximations had to be made:

1. It was necessary to make an educated guess as to the height for the different parts of the cloud. This is possible to do within ±5 km, from previous experience,

2. Since the radar tracking only gave a time-height variation (Tables 2.4 and 2.5) for Star Fish Prime, the range had to be estimated from knowledge of previous Nike-Cajun shots (Figure 2.4) and the azimuth determined from the cloud photographs which also showed the rocket,

3. The plate constants had to be estimated graphically.

The first thing needed was a scale drawing of the launch site (Johnston Island) and the rocket trajectory. The only way to do this with the information available was to assume the photograph to be the same projection from all parts of the plate. This is of course not true, since the projection is correct only at the optical center and is distorted toward the edges. To find the place on the photograph which represents the zenith of Johnston Island, stars were used. Because of the inaccuracy of this method, it was not necessary to obtain a more accurate position of the plate center. A celestial globe of 8-inch radius was set for the correct sidereal time for the plate on which the star field was identified and the latitude of Johnston Island. The 7-inch focal length plates were placed on the globe with the star field fitting as well as possible. The zenith point over Johnston Island was then marked, accounting for

the slight difference in scale, and the north-south line drawn. Now, on a piece of paper, the fiducial marks of the plate, the zenith mark of Johnston Island, and north-south line could be drawn. Then, each plate on which the rocket appeared could be placed under the paper with the fiducial marks coinciding and the very end of the rocket marked. The time and length of exposure was known for each picture. A straight line could now be passed through all the rocket points and extended back to the point representing Johnston Island. The azimuth of the ground range could now be measured. Since only the height vs. time was known, the range was determined by picking a previous rocket flight which was similar in time vs. height and from which the range was known. The distance of Johnston Island to the point under the maximum height of the rocket could now be laid out to scale in kilometers and the intermediate heights marked off.

It was now necessary to know the position of the height throughout the cloud. Normally, this is done with two or more pictures using some triangulation method (Reference 7). However, here an educated guess had to be made, since only one picture was available. Up to July 1962 about seventeen other shots had been reduced using normal triangulation

methods. From the type of configuration the cloud makes it was possible to estimate to within ±5 km where key heights are located within the cloud. These estimates were then marked off on a series of clouds, say every minute for five or six minutes. The outline of the cloud for each minute was drawn on the graphical plot with fiducial marks matching. The expansion of the cloud was easily noted, and knowing the scale, the distance between marked points could be measured and converted into meters/second, since each picture was taken exactly 20 seconds apart. The average of each interval was obtained for better accuracy. The direction of the transport vector could be determined by drawing the best straight line through the above-described points and extending it to meet the rocket trajectory. This should then give a second approximation to the assigned height, since the line should meet the trajectory close to where the ground projection of the rocket was at that height. The north-south line was known, so the azimuth of this line could be measured with a protractor.

2.5.2 Blue Gill Triple Prime, King Fish, Tight Rope. During this series of shots, it was possible to find one set of pictures from a ship which was good enough to use with

Johnston Island in a triangulation method for all except 4 November 1962 (PM) when the amount of sodium emitted from the rocket was much smaller than normal, at the same time the sky was cloudy, and all the ships but S-2 were in the harbor at Johnston Island.

The triangulation method used was as follows: This method involves the solution of the following formulas, in order to obtain an accurate azimuth and zenith angle for the center of each plate.

$$H = \text{sidereal time} - \alpha$$

$$\cos z = \sin \phi \sin \delta + \cos \phi \cos \delta \cos H \qquad (2.4)$$

$$\cos A = \frac{\sin \delta - \sin \phi \cos z}{\cos \phi \sin z} \qquad (2.5)$$

Where H = hour angle

α = right ascension of star

δ = declination of star

A = azimuth of star

z = zenith angle of star

ϕ = latitude of observer

To obtain any angles around the optical center of the plate a protractor was used. To obtain the sides of the triangle from the center of the plate to any two stars near the optical center an inch rule read to the nearest 0.005 inch was used. The measured distance between the plate center and each star is then divided by the focal length of the camera objective. This ratio is the tangent of the angular distance of the star from the plate center.

Two stars were identified in order to form a spherical triangle with the optical center of the plate. Then, a second spherical triangle was formed with the same two stars and the point representing the observer's zenith. Finally, two more triangles were formed using a star, the plate center, and the observer's zenith. Using spherical trigonometry it was now possible to obtain the zenith angle and azimuth of the plate center.

The triangle formed by the two stars and the observer's zenith can obviously be solved uniquely. The second triangle including the same two stars and the plate center can be solved using the plate measurements. The angular distance between the stars thus obtained should, of course, be equal to the unique determination. This will not be so unless the plate center is known to a tenth of an inch.

It is possible to experiment with different focal lengths until a match is made. From these experiments it can be seen that the exact position of the optical center is not as important as the focal length.

In order to solve the above equations the positions of the ships and Johnston Island must be known. The position of Johnston Island used was: Lat = 16^{o} 43.618' N and Long = 11^{h} 18^{m} 04^{s} W. For the ships the original positions given by the ships' navigators were used (see Table 2.11).

It was now possible to calculate the zenith angle and azimuth for each plate center. It was very difficult to find a time when the ships were not rolling during the exposure, but in each case it was possible to pick a plate where stars were identifiable as dots rather than streaks and the cloud was not blurred.

By examination of the appearance of the cloud from Johnston Island and the ship, places which appeared to be in common were picked as a first trial. By using the spherical triangle formed by the plate center, observer's zenith, and unknown point, the azimuth and zenith angle of this point may be calculated.

On graph paper the positions of Johnston Island and the ship were marked. . From the rocket trajectory information from radar[a] (see Tables 2.7-2.10) the rocket trajectory from Johnston Island could be drawn and the ground position versus height plotted to scale. Since the down trail was also clearly visible on the first three observations, the whole trajectory could be included. Knowing the azimuth and zenith angle of the unknown point, the ground position of the cloud could be found graphically where the two azimuth lines cross. Two determinations of the height were then possible by multiplying the ground distance from the ship to the azimuth cross by cot z_{ship} and multiplying the Johnston Island to azimuth cross ground distance by cot z_{JI}. These two heights should be the same if the point chosen is indeed common. If the heights do not agree, two things are possible: (1) The points are not common and (2) the position of the ship is not accurate. Through a method of trial and error, and by using the down as well as up trail it was possible to locate the ships in their actual positions very accurately (see Table 2.11).

[a]Since there was no radar trajectory information for 26 October 1962 (PM), the approximate trajectory method outlined in Section 2.5.1 was used.

Because of the complications already mentioned, the above triangulation method could not be used for 4 November 1962 (PM) and the one-station method used for the July data had to be utilized.

2.6 REDUCTION OF THE DIFFUSION COEFFICIENT DATA

Many of the photographs obtained, although of some value for wind determination, were too obscured by clouds for good densitometry. However, diffusion data has been obtained from the sodium trails at dusk on 25 July (26 July GMT) and dawn on 2 November. The measurements were made by R. Almasian of Air Force Cambridge Research Laboratories (AFCRL), Bedford, Massachusetts, using techniques developed by E. Manring and H. Knaflich (Reference 14). A double beam microdensitometer was used to scan the density across the photographs of the trail. Traces were made in a direction perpendicular both to the axis of the trail and to the line of sight at a number of altitudes. This was repeated with photographs obtained at different times after formation of the trail. Figure 2.6 shows a typical trace of cloud density with respect to r, the radial distance from the cloud axis to various points in the cloud. To obtain the dimensions of the actual cloud from the densitometer trace the following equation was used

$$r = \frac{S\, f_s\, d_c}{f\, f_m} \qquad (2.6)$$

where r is the distance in the cloud, d_c is the distance measured on the chart, S is the slant range, f is the focal length of the camera, f_m is the magnification factor of the densitometer, and f_s is the foreshortening factor.

$$f_s = [1 + (d_p/f)^2]^{-1} \qquad (2.7)$$

where d_p is the distance from the center of the plate to the image of the cloud.

The density was normalized to lie between zero and one and was plotted as a function of distance from the axis of the trail at a series of times after release of the sodium from the rocket. This was replotted in the form of radial distance squared (r^2) as a function of time for different isophotes (usually between 0.2 and 0.8). Figure 3.44 is a typical plot of this kind. Values of r and η so obtained were substituted in Equation 1.13 to obtain the diffusion coefficient.

TABLE 2.1 EVENT DESCRIPTION

Event	Time (Zulu)	Yield	Altitude
	1962	kt	km
Star Fish Prime	090900 Jul	1,400	400
Blue Gill Prime	26 Jul	aborted	---
Check Mate	200830 Oct		
Blue Gill Triple Prime	261000 Oct		
King Fish	011210 Nov		
Tight Rope	040730 Nov		

TABLE 2.2 CAMERA OPERATION AND CLOUD COVER

Date (Zulu)	Twil	Johnston Island	Ship S-1	Ship S-2	Ship S-4
9 July (Star Fish - 2-2/3 hr)	PM	25% cloud cover	Overcast	50% cover	Overcast
9 July (Star Fish + 7 hr)	AM	25% cloud cover	Overcast	Overcast	50% cover
26 July	PM	Scattered to heavy cumulus-- no higher clouds	75% cover	Overcast	Overcast
26 October (Blue Gill + 6-2/3 hr)	AM	25% cloud cover 3 cameras operating	50% cover 2 cameras	75% cover 3 cameras	70% cover 2 cameras
1 November (King Fish + 4-1/2 hr)	AM	25% cover 3 cameras	50% cover 2 cameras	25% cover 2 cameras	50% cover 2 cameras
2 November (King Fish + 28-1/2 hr)	AM	Clear 2 cameras	Clear 2 cameras	50% cover 2 cameras	50% cover 2 cameras
3 November (King Fish + 41 hr)	PM	50% cover 3 cameras	50% cover 2 cameras	70% cover 3 cameras	Local rain
4 November (Tight Rope - 2-1/3 hr)	PM	25% cover 3 cameras	50% cover 2 cameras	50% cover 2 cameras	70% cover 3 cameras

TABLE 2.3 MINIMUM AND MAXIMUM CAMERA ELEVATION ANGLES

	Star Fish		Blue Gill*	
Site	θ min	θ max	θ min	θ max
Johnston Island	50.2°	71.6°	50.2°	71.6°
S-1	6.1	15.0	82.4	86.9
S-2	11.7	27.3	82.4	86.9
S-4	11.9	27.7	71.6	82.4

* Calculated for the planned positions of the ships.

TABLE 2.4 RADAR TRAJECTORY DATA, ROCKET 1, 8 JULY, 2024 HONOLULU STANDARD TIME (9 JULY, 0624Z)[a]

Radar Time[b]	Altitude	Radar Time	Altitude
seconds	feet	seconds	feet
60	155,041	90	265,431
61	159,291	91	268,606
62	163,430	92	271,759
63	167,469	93	274,910
64	171,473	94	277,980
65	175,493	95	281,035
66	179,476	96	284,096
67	183,403	97	287,107
68	187,319	98	290,067
69	191,200	99	292,994
70	195,044	100	295,894
71	198,869	101	298,730
72	202,641	102	301,549
73	206,418	103	304,424
74	210,153	104	307,223
75	213,838	105	309,990
76	217,491	106	312,699
77	221,126	107	315,343
78	224,728	108	317,978
79	228,299	109	320,609
80	231,824	110	323,215
81	235,328	111	325,802
82	238,814	112	328,456
83	242,220	113	330,917
84	245,634	114	333,331
85	249,021	115	335,712
86	252,347	116	338,187
87	255,682	117	340,595
88	258,940	118	342,812
89	262,193	119	345,179

TABLE 2.4 CONTINUED

Radar Time[b]	Altitude	Radar Time	Altitude
seconds	feet	seconds	feet
120	347,394	150	401,393
121	349,710	151	402,983
122	352,031	152	404,476
123	354,084	153	405,827
124	356,287	154	406,853
125	358,460	155	407,756
126	360,650	156	408,791
127	362,686	157	410,231
128	364,645	158	411,544
129	366,672	159	412,563
130	368,643	160	413,389
131	370,568	161	414,296
132	372,451	162	415,396
133	374,427	163	416,457
134	376,278	164	417,571
135	378,055	165	419,003
136	379,895	166	420,053
137	381,807	167	420,162
138	383,501	168	420,630
139	385,127	169	421,584
140	386,621	170	422,354
141	388,201	171	423,042
142	389,935	172	423,752
143	391,625	173	424,414
144	393,117	174	425,029
145	394,638	175	425,690
146	396,063	176	426,412
147	397,252	177	426,924
148	398,402	178	427,073
149	399,823	179	427,292

TABLE 2.4 CONTINUED

Radar Time[b]	Altitude	Radar Time	Altitude
seconds	feet	seconds	feet
180	427,803	195	431,763
181	428,451	196	431,348
182	429,392	197	430,901
183	430,044	198	430,449
184	430,251	199	429,812
185	430,557	200	429,103
186	430,821	201	428,566
187	431,177	202	428,247
188	431,572	203	427,913
189	431,872	204	427,385
190	432,142	205	427,004
191	432,473	206	426,634
192	432,648	207	426,447
193	432,461		
194	432,096		

[a]Complete radar data is filed at Air Force Cambridge Research Laboratories, Bedford, Mass.

[b]Radar time is 16 seconds fast.

TABLE 2.5 RADAR TRAJECTORY DATA, ROCKET 2, 9 JULY, 0609:30 HONOLULU STANDARD TIME (9 JULY 1609:30Z)

Radar Time[a]	Altitude	Radar Time	Altitude
seconds	feet	seconds	feet
60	217,168	90	311,172
61	220,759	91	313,798
62	224,318	92	316,408
63	227,853	93	319,091
64	231,347	94	321,586
65	234,797	95	324,036
66	238,221	96	326,563
67	241,636	97	329,118
68	245,021	98	331,519
69	248,353	99	333,899
70	251,640	100	336,291
71	254,911	101	338,570
72	258,166	102	340,911
73	261,362	103	343,145
74	264,554	104	345,373
75	267,677	105	347,631
76	270,806	106	349,833
77	273,910	107	351,963
78	276,939	108	354,066
79	279,981	109	356,136
80	282,991	110	358,223
81	285,895	111	360,241
82	288,851	112	362,227
83	291,770	113	364,176
84	294,646	114	366,147
85	297,495	115	368,033
86	300,251	116	369,891
87	303,061	117	371,760
88	305,770	118	373,612
89	308,391	119	375,369

TABLE 2.5 CONTINUED

Radar Time[a]	Altitude	Radar Time	Altitude
seconds	feet	seconds	feet
120	377,103	150	415,046
121	378,667	151	415,835
122	380,355	152	416,601
123	382,127	153	417,301
124	383,788	154	417,976
125	385,327	155	418,607
126	386,881	156	419,361
127	388,426	157	419,974
128	390,043	158	420,563
129	391,573	159	421,130
130	392,904	160	421,562
131	394,173	161	421,871
132	395,519	162	422,477
133	396,860	163	423,053
134	398,123	164	423,502
135	399,359	165	424,012
136	400,687	166	424,346
137	401,926	167	424,487
138	403,296	168	424,792
139	404,427	169	425,186
140	405,508	170	425,438
141	406,759	171	425,805
142	407,650	172	426,433
143	408,613	173	427,062
144	409,617	174	427,366
145	410,551	175	427,536
146	411,519	176	427,781
147	412,491	177	428,164
148	413,413	178	428,480
149	414,261	179	428,563

TABLE 2.5 CONTINUED

Radar Time[a]	Altitude	Radar Time	Altitude
seconds	feet	seconds	feet
180	428,750	190	420,424
181	429,214	191	422,941
182	429,359	192	425,535
183	429,359	193	428,051
184	429,359	194	430,449
185	429.359		
186	430,258		
187	422.343		
188	415,511		
189	418.005		

[a]Radar time correct ± 2 seconds.

[b]Probable peak time, radar ceased to track after 182 seconds.

TABLE 2.6 RADAR TRAJECTORY DATA. ROCKET 3, 25 JULY, 2020 HONOLULU STANDARD TIME (26 JULY 0620Z)

Radar Time[a]	Slant Range	Azimuth	Elevation
seconds	feet	degrees	degrees
25	82,461	161.0595	81.5576
26	87,348	160.9194	81.5837
27	92,175	160.8240	81.5992
28	96,957	160.7052	81.6205
29	101,715	160.5765	81.6291
30	106,440	160.4721	81.6390
31	111,111	160.3482	81.6356
32	115,734	160.3207	81.6407
33	120,339	160.2795	81.6407
34	124,911	160.2795	81.6486
35	129,459	160.2270	81.6418
36	133,932	160.1247	81.6284
37	138,402	160.0780	81.6352
38	142,836	159.9949	81.6315
39	147,231	159.9945	81.6133
40	151,590	159.9193	81.5985
41	155,928	159.9139	81.5752
42	160,248	159.8926	81.5700
43	164,508	159.8538	81.5700
44	168,732	159.8551	81.5422
45	172,185	159.8236	81.5422
46	177,123	159.7649	81.5158
47	181,041	159.7525	81.5072
48	185,166	159.7484	81.4855
49	189,258	159.7470	81.4564
50	193,278	159.7497	81.4306
51	197,304	159.8809	81.4018
52	201,312	159.8675	81.4083
53	205,239	159.7903	81.3987
54	209,166	159.7381	81.3983

TABLE 2.6 CONTINUED

Radar Time[a]	Slant Range	Azimuth	Elevation
seconds	feet	degrees	degrees
55	213,057	159.6897	81.3640
56	216,906	159.7655	81.3077
57	220,740	159.8133	81.2995
58	224,538	159.8891	81.2693
59	228,300	159.8373	81.2541
60	232,044	159.7995	81.2311
61	235,746	159.7844	81.1845
62	239,397	159.7539	81.1817
63	243,051	159.7700	81.1628
64	246,654	159.7649	81.1391
65	250,251	159.8019	81.1038
66	253,776	159.8036	81.0959
67	257,301	159.7772	81.0725
68	260,778	159.7628	81.0423
69	264,231	159.7079	80.9517
70	267,678	159.7412	80.9596
71	271,050	159.8823	80.9870
72	274,416	160.0127	80.9129
73	277,743	160.0914	80.8607
74	281,061	160.0227	80.8858
75	284,331	159.8854	80.8480
76	287,535	159.8287	80.8089
77	290,778	159.8085	80.7594
78	293,946	159.8091	80.7786
79	297,087	159.7985	80.7711
80	300,174	159.8112	80.7168
81	303,300	159.9211	80.6822
82	306,324	159.9496	80.6111
83	309,348	159.9506	80.6039
84	312,321	159.9719	80.6087

TABLE 2.6 CONTINUED

Radar Time[a]	Slant Range	Azimuth	Elevation
seconds	feet	degrees	degrees
85	315,324	159.9623	80.5936
86	318,252	159.9465	80.5208
87	321,165	159.9121	80.4511
88	323,961	159.9011	80.4103
89	326,892	159.9794	80.3821
90	329,646	159.9949	80.3831
91	332,463	159.9619	80.3910
92	335,193	160.0206	80.3505
93	337,899	160.1078	80.2963
94	340,578	160.1703	80.2225
95	343,239	160.2108	80.2455
96	345,900	160.1487	80.2135
97	348,474	160.1188	80.1665
98	351,054	160.1765	80.1239
99	353,565	160.2417	80.0711
100	356,046	160.3186	80.0460
101	358,536	160.2445	80.0354
102	360,996	160.1810	79.9955
103	363,411	160.0989	79.9197
104	365,754	160.0793	79.8774
105	368,115	160.2070	79.8335
106	370,455	160.3605	79.7658
107	372,732	160.4299	79.8160
108	374,988	160.5308	79.8060
109	377,217	160.5198	79.7693
110	379,407	160.5390	79.6924
111	381,603	160.5950	79.6464
112	383,724	160.6314	79.5623
113	385,848	160.6990	79.5451
114	387,948	160.7207	79.5032

TABLE 2.6 CONTINUED

Radar Time[a]	Slant Range	Azimuth	Elevation
seconds	feet	degrees	degrees
115	389,946	160.5809	79.4775
116	391,980	160.4512	79.4225
117	393,996	160.2259	79.3868
118	395,937	160.0804	79.3703
119	397,833	160.0701	79.3576
120	399,747	160.0347	79.2855
121	401,610	160.0392	79.2320
122	403,461	160.2119	79.2303
123	405,303	160.5061	79.2093
124	407,022	160.8116	79.1049
125	408,750	160.9346	79.0497
126	410,538	160.9775	78.9402
127	412,206	160.8096	78.8959
128	413,838	160.7066	78.9278
129	415,464	160.6005	78.8794
130	417,066	160.4453	78.7695
131	418,611	160.3320	78.6789
132	420,144	160.2228	78.6607
133	421,686	160.2627	78.6779
134	423,141	160.3945	78.6480
135	424,596	160.6177	78.5556
136	426,030	160.7612	78.4646
137	427,392	160.8463	78.4430
138	428,790	160.9740	78.4070
139	430,095	160.9830	78.4159
140	431,403	161.0434	78.3651
141	432,642	161.0863	78.2854
142	433,884	161.0832	78.1938
143	435.054	160.9469	78.0911
144	436,344	160.8024	77.9933

TABLE 2.6 CONTINUED

Radar Time [a]	Slant Range	Azimuth	Elevation
seconds	feet	degrees	degrees
145	437,370	160.6479	77.9531
146	438,510	160.5284	78.0245
147	439,674	160.4371	77.9878
148	440,631	160.4772	77.9679
149	441,666	160.5202	77.8882
150	442,707	160.5229	77.7976
151	443,613	160.5837	77.6870
152	444,612	160.6554	77.6403
153	445,581	160.8717	77.5868
154	446,322	161.0805	77.5428
155	447,285	161.2923	77.5239
156	448,044	161.4787	77.4532
157	448,917	161.4938	77.3475
158	449,613	161.3658	77.2362
159	450,330	161.2054	77.1525
160	451,038	160.9030	77.1799
161	451,725	160.7220	77.1013
162	452,358	160.6702	77.0567
163	453,012	160.6613	77.0141
164	453,486	160.6805	76.9056
165	454,161	160.7914	76.7662
166	454,668	160.8885	76.6588
167	455,115	161.0104	76,6179
168	455,640	161.2096	76.6828
169	456,081	161.3198	76.6351
170	456,465	161.4516	76.6492
171	456,822	161.4554	76.5513
172	457,239	161.3853	76.4287
173	457,506	161.3620	76.2804
174	457,767	161.2748	76.1349

TABLE 2.6 CONTINUED

Radar Time[a]	Slant Range	Azimuth	Elevation
seconds	feet	degrees	degrees
175	458,061	161.1690	76.0662
176	458,358	161.0932	76.0236
177	458,469	160.9510	76.0109
178	458,727	160.8099	75.9285
179	458,760	160.7213	75.8650
180	458,949	160.6252	75.7606
181	459,057	160.6644	75.6051
182	459,105	160.6884	75.5117
183	459,144	160.9325	75.4510
184	459,165	161.1824	75.4386

[a]Radar time 10 seconds fast.

TABLE 2.7 RADAR TRAJECTORY DATA, ROCKET 5, 1 NOVEMBER, 0638 HONOLULU STANDARD TIME, (1 NOVEMBER, 1638Z)

Radar Time	Altitude	Horizontal Range	Azimuth
seconds	feet	feet	degrees
7	20,289	4,167	170.4247
8	21,170	4,587	167.1724
9	21,995	5,024	165.3308
10	23,021	5,361	165.0510
11	23,962	5,547	165.9539
12	24,829	5,668	167.7351
13	25,663	5,761	169.7607
14	26,383	5,774	171.6665
15	27,113	5,735	173.6179
16	28,506	5,854	175.4128
17	31,661	6,370	177.1105
21	49,771	7,489	159.2262
22	61,722	8,161	158.7146
23	68,764	8,940	158.3167
24	72,853	9,477	157.9473
25	77,860	10,033	157.5580
26	82,651	10,593	157.2661
27	87,396	11,173	157.0083
28	92,098	11,741	156.8799
29	96,757	12,291	156.7034
30	101,372	12,840	156.5294
31	105,944	13,400	156.3553
32	110,475	13,958	156.2262
33	114,972	14,515	156.1534
34	119,432	15,066	155.9904
35	123,859	15,630	155.8637
36	128,247	16,201	155.7971
37	132,602	16,763	155.7387
38	136,927	17,315	155.6536
39	141,217	17,869	155.5162

TABLE 2.7 CONTINUED

Radar Time	Altitude	Horizontal Range	Azimuth
seconds	feet	feet	degrees
40	145,472	18,423	155.4108
41	149,694	18,997	155.3796
42	153,885	19,573	155.4225
43	158,046	20,112	155.2443
44	162,173	20,650	154.9813
45	166,265	21,229	155.0431
46	170,325	21,821	155.1262
47	174,351	22,378	155.1444
48	178,351	22,920	154.9463
49	182,314	23,458	154.7712
50	186,244	24,024	154.7959
51	190,143	24,618	154.7966
52	194,017	25,210	154.7510
53	197,850	25,770	154.8234
54	201,643	26,358	154.8612
55	205,404	26,955	154.9566
56	209,153	27,480	155.0064
57	212,879	27,991	154.7698
58	216,567	28,503	154.5573
59	220,212	29,076	154.4664
60	223,828	29,648	154.6215
61	227,412	30,226	154.7012
62	230,960	30,768	154.5779
63	234,482	31,329	154.4688
64	237,971	31,913	154.4650
65	241,427	32,477	154.4392
66	244,861	33,074	154.5704
67	248,261	33,663	154.6861
68	251,629	34,160	154.7286
69	254,946	34,712	154.6500

TABLE 2.7 CONTINUED

Radar Time	Altitude	Horizontal Range	Azimuth
seconds	feet	feet	degrees
70	258,250	35,245	154.4317
71	261,525	35,772	154.2937
72	264,757	36,343	154.2864
73	267,956	36,952	154.6112
74	271,129	37,468	154.7870
75	274,277	37,993	154.6641
76	277,380	38,548	154.5450
77	280,460	39,193	154.5731
78	283,504	39,780	154.5930
79	286,535	40,292	154.6435
80	289,527	40,808	154.6081
81	292,497	41,325	154.5632
82	295,425	41,856	154.5553
83	298,343	42,332	154.6792
84	301,224	42,757	154.7637
85	304,008	43,546	154.6373
86	306,746	44,413	154.5347
87	309,560	44,827	154.4409
88	312,375	44,863	154.3688
89	315,103	45,232	154.3098
90	317,718	46,156	154.4063
91	370,281	47,313	154.5975
92	322,867	48,070	155.0576
93	325,513	48,194	155.2508
94	328,108	48,361	155.2409
95	330,637	48,846	155.1231
96	331,130	49,441	154.8684
97	335,578	50,060	154.7939
98	337,994	50,715	154.7022
99	340,400	51,236	154.5906

TABLE 2.7 CONTINUED

Radar Time	Altitude	Horizontal Range	Azimuth
seconds	feet	feet	degrees
100	342,739	51,764	154.6459
101	345,092	52,378	154.4708
102	347,389	53,003	154.4887
103	349,616	53,555	154.5388
104	351,862	53,886	154.4742
105	354,083	54,346	154.3695
106	356,212	55,128	154.4554
107	358,307	55,949	154.7283
108	360,437	56,545	154.9958
109	362,518	57,033	155.2203
110	364,635	57,293	155.2944
111	366,686	57,617	155.2635
112	368,669	58,210	155.1705
113	370,603	58,970	154.9305
114	372,539	59,561	154.8897
115	374,465	59,993	154.8145
116	376,364	60,455	154.8691
117	378,197	61,013	154.9576
118	379,988	61,636	155.0078
119	381,771	62,221	155.0380
120	383,530	62,692	155.0833
121	385,287	62,995	155.0521
122	387,042	63,414	154.9995
123	388,729	64,017	154.7994
124	390,344	64,808	154.5542
125	391,862	65,592	154.4718
126	393,373	66,327	154.5158
127	394,879	66,747	154.7438
128	396,421	66,889	155.0648
129	397,917	67,185	155.2989

TABLE 2.7 CONTINUED

Radar Time	Altitude	Horizontal Range	Azimuth
seconds	feet	feet	degrees
130	399,376	67,904	155.6608
131	400,752	68,671	155.9159
132	402,125	69,221	155.8469
133	403,492	69,596	155.5025
134	404,788	70,242	155.1588
135	406,042	71,220	154.8763
136	407,206	72,132	154.4863
137	408,109	72,419	154.3561
138	408,976	72,133	154.3864
139	410,681	72,005	154.4300
140	472,838	71,735	154.6514
141	414,780	70,332	154.8114
142	416,781	68,100	154.9645
143	419,352	66,163	155.1200

TABLE 2.8 RADAR TRAJECTORY DATA, ROCKET 6, 2 NOVEMBER, 0638 HONOLULU STANDARD TIME (2 NOVEMBER 1638Z)

Radar Time	Altitude	Horizontal Range	Azimuth
seconds	feet	feet	degrees
16	23,311	4,190	176.8046
17	24,226	4,065	175.2676
18	25,096	4,027	174.6932
19	25,924	4,119	174.6681
20	26,702	4,209	174.5408
21	27,428	4,257	174.3468
22	28,106	4,298	174.1490
23	28,746	4,347	173.9980
24	29,341	4,398	173.8366
25	29,902	4,448	173.6900
26	30,431	4,498	173.5771
27	30,929	4,550	173.4023
28	31,394	4,600	173.2489
29	31,828	4,648	173.0631
30	32,236	4,700	172.9488
31	32,600	4,751	172.8317
32	32,928	4,801	172.6930
33	33,219	4,852	172.5605
34	33,479	4,905	172.5049
35	33,704	4,960	172.3851
36	33,901	5,014	172.2882
37	34,063	5,067	172.1931
38	34,189	5,118	172.1228
39	34,290	5,167	171.9449
40	34,358	5,219	171.8199
tracking booster 41 - 75 sec.			
76	259,524	29,414	164.8313
77	264,074	29,968	164.2219
78	268,890	30,265	164.1302
79	271,894	30,534	164.5257

TABLE 2.8 CONTINUED

Radar Time	Altitude	Horizontal Range	Azimuth
seconds	feet	feet	degrees
80	274,379	31,098	164.8834
81	277,473	31,731	165.1399
82	280,719	32,190	165.1214
83	283,875	32,722	165.0582
84	287,035	33,010	165.0132
85	290,138	33,225	164.6170
86	293,190	33,814	164.1920
87	296,204	34,503	164.1546
88	299,233	34,891	164.5549
89	302,202	35,280	165.1128
90	305,133	35,828	165.5007
91	308,027	36,314	165.3119
92	310,915	36,696	164.9480
93	313,756	37,149	164.7334
94	316,579	37,670	164.8951
95	319,355	38,193	165.0345
96	322,120	38,637	165.0064
97	324,847	39,041	165.0942
98	327,519	39,713	165.2422
99	330,179	40,197	165.2656
100	332,851	40,114	164.8869
101	335,531	40,070	164.6850
102	338,054	40,999	164.4921
103	340,488	42,227	164.1327
104	342,924	43,266	163.8085
105	345,412	43,642	163.6760
106	347,944	43,401	163.7151
107	350,412	43,476	164.1240
108	352,789	44,186	164.6109
109	355,085	44,938	165.0839

TABLE 2.8 CONTINUED

Radar Time	Altitude	Horizontal Range	Azimuth
seconds	feet	feet	degrees
110	357,423	45,204	165.5797
111	359,730	45,410	166.0113
112	361,978	45,996	166.1496
113	364,158	46,727	166.2516
114	366,357	47,122	166.2100
115	368,563	47,244	166.0099
116	370,695	47,543	165.8327
117	372,829	47,996	165.7260
118	374,934	48,615	165.5708
119	376,944	49,241	165.4019
120	378,956	49,483	165.1320
121	380,974	49,708	164.9799
122	382,885	50,516	164.8604
123	384,691	51,745	164.9051
124	386,539	52,438	165.0856
125	388,438	52,529	165.4156
126	390,327	52,607	166.0037
127	392,112	53,171	166.4071
128	393,852	53,760	166.6698
129	395,563	54,333	166.9152
130	397,217	55,010	166.9516
131	398,873	55,657	166.7425
132	400,587	55,857	166.5180
133	402,255	55,906	166.1022
134	403,847	56,208	165.7857
135	405,290	57,066	165.3033
136	406,707	58,069	164.9926
137	408,270	58,704	164.7262
138	410,100	58,876	164.5202
139	412,246	58,323	164.1491
140	414,764	57,004	163.9283
141	417,526	55,337	163.6056
142	420,452	53,873	163.2506

TABLE 2.9 RADAR TRAJECTORY DATA, ROCKET 7, 2 NOVEMBER, 1907 HONOLULU STANDARD TIME (3 NOVEMBER, 0507Z)

Radar Time	Altitude	Horizontal Range	Azimuth
seconds	feet	feet	degrees
-53.7	76,922	11,343	155.8417
-52.7	81,418	11,989	155.6161
-51.7	86,563	12,685	155.5279
-50.7	91,298	13,351	155.4064
-49.7	95,995	14,007	155.2450
-48.7	100,646	14,671	155.0867
-47.7	105,258	15,334	155.1334
-46.7	109,834	15,989	154.9923
-45.7	114,369	16,644	154.8279
-44.7	118,870	17,297	154.6967
-43.7	123,339	17,956	154.7554
-42.7	127,771	18,609	154.6432
-41.7	132,166	19,270	154.5635
-40.7	136,529	19,924	154.4945
-39.7	140,859	20,583	154.4152
-38.7	145,160	21,227	154.4207
-37.7	149,422	21,887	154.3434
-36.7	153,655	22,552	154.2834
-35.7	157,854	23,204	154.2247
-34.7	162,020	23,853	154.1962
-33.7	166,155	24,529	154.1742
-32.7	170,254	25,215	154.1972
-31.7	174,322	25,865	154.0156
-30.7	178,359	26,521	153.9486
-29.7	182,371	27,144	153.8951
-28.7	186,350	27,793	153.9884
-27.7	190,282	28,474	154.1464
-26.7	194,185	29,154	154.0447
-25.7	198,066	29,792	153.9273
-24.7	201,919	30,426	153.9462

TABLE 2.9 CONTINUED

Radar Time	Altitude	Horizontal Range	Azimuth
seconds	feet	feet	degrees
-23.7	205,734	31,078	154.0001
-22.7	209,524	31,703	154.0602
-21.7	213,270	32,380	154.1350
-20.7	216,985	33,020	154.2906
-19.7	220,677	33,681	154.3204
-18.7	224,330	34,382	154.1302
-17.7	227,949	35,120	153.8357
-16.7	231,536	35,794	153.7340
-15.7	235,096	36,466	153.8233
-14.7	238,635	37,074	154.0125
-13.7	242,146	37,628	154.1062
-12.7	245,616	38,236	154.1405
-11.7	249,031	39,013	154.1179
-10.7	252,404	39,800	153.9761
-9.7	255,792	40,363	153.8346
-8.7	259,161	40,850	153.7258
-7.7	262,485	41,510	153.7224
-6.7	265,747	42,232	153.7107
-5.7	269,016	42,836	153.6324
-4.7	272,203	43,530	153.7248
-3.7	275,379	44,279	153.8824
-2.7	278,527	45,000	154.0798
-1.7	281,681	45,489	154.0973
-0.7	284,783	46,049	154.0619
0.3	287,842	46,734	154.1553
1	289,954	47,275	154.1079
2	292,935	48,064	154.1817
3	295,895	48,825	154.3270
4	298,832	49,525	154.2796
5	301,774	50,023	154.0568

TABLE 2.9 CONTINUED

Radar Time	Altitude	Horizontal Range	Azimuth
seconds	feet	feet	degrees
6	304,673	50,535	153.9280
7	307,524	51,199	153.9033
8	310,322	51,998	153.9390
9	313,094	52,732	154.0873
10	315,869	53,275	154.2247
11	318,615	53,824	154.4128
12	321,309	54,535	154.5433
13	323,944	55,338	154.4052
14	326,579	55,975	154.3273
15	329,195	56,523	154.1762
16	331,759	57,184	153.9867
17	334,291	57,879	153.8405
18	336,806	58,546	153.8109
19	339,269	59,356	153.9057
20	341,696	60,087	154.2181
21	344,140	60,579	154.6026
22	346,552	60,967	154.6864
23	348,942	61,400	154.7705
24	351,286	62,041	154.8825
25	353,539	62,903	154.8660
26	355,760	63,699	154.6555
27	357,991	64,383	154.4842
28	360,220	64,867	154.2902
29	362,436	65,191	154.1244
30	364,630	65,690	154.0262
31	366,709	66,533	153.9115
32	368,709	67,508	154.0702
33	370,698	68,480	154.2768
34	372,726	69,144	154.5151
35	374,803	69,499	154.6373

TABLE 2.9 CONTINUED

Radar Time	Altitude	Horizontal Range	Azimuth
seconds	feet	feet	degrees
36	376,849	69,771	154.6164
37	378,764	70,190	154.6655
38	380,569	70,897	154.5209
39	382,422	71,588	154.3507
40	388,303	72,254	154.3984
41	386,094	72,944	154.2820
42	387,795	73,845	154.2315
43	389,432	74,875	154.2549
44	391,093	75,824	154.2628
45	392,822	76,141	154.3287
46	394,543	76,237	154.3346
47	396,181	76,649	154.4828
48	397,754	77,601	154.5580
49	399,266	78,447	154.6195
50	400,765	79,034	154.7108
51	402,256	79,602	154.7214
52	403,678	80,483	154.7180
53	405,079	81,225	154.7383
54	406,503	81,713	154.8358
55	407,901	82,236	154.8104
56	409,212	83,029	154.7922
57	410,478	83,797	154.7389
58	411,763	84,349	154.7173
59	413,020	84,854	154.6246
60	414,249	85,420	154.4519
61	415,443	85,987	154.3846
62	416,536	86,681	154.3338
63	417,564	87,651	154.3215
64	418,679	88,496	154.3074
65	419,797	89,072	154.2325

TABLE 2.9 CONTINUED

Radar Time	Altitude	Horizontal Range	Azimuth
seconds	feet	feet	degrees
66	420,880	89,307	154.3362
67	421,944	89,512	154.6075
68	422,915	90,093	154.9903
69	423,760	91,147	155.2539
70	424,594	92,133	155.6103
71	425,489	92,901	155.9674
72	426,405	93,696	156.1977
73	427,279	94,830	156.3402
74	428,330	95,928	156.4219

TABLE 2.10 RADAR TRAJECTORY DATA, ROCKET 8, 3 NOVEMBER, 1907 HONOLULU STANDARD TIME, (4 NOVEMBER, 0507Z)

Radar Time	Altitude	Horizontal Range	Azimuth
seconds	feet	feet	degrees
27	57,891	7,124	164.2277
28	64,175	7,968	163.7333
29	68,903	8,619	163.7038
30	73,732	9,123	163.4851
31	78,574	9,644	163.2880
32	83,336	10,164	163.1555
33	88,052	10,693	163.1480
34	92,719	11,219	163.0182
35	97,342	11,747	162.8984
36	101,923	12,278	162.7538
37	106,468	12,802	162.7377
38	110,974	13,335	162.7806
39	115,439	13,865	162.6580
40	119,870	14,395	162.4699
41	124,264	14,923	162.4386
42	128,628	15,459	162.5468
43	132,955	15,995	162.4881
44	137,253	16,526	162.3140
45	141,515	17,049	162.2931
46	145,742	17,593	162.3490
47	149,939	18,128	162.3889
48	154,106	18,650	162.2423
49	158,229	19,175	162.2460
50	162,328	19,717	162.2107
51	166,399	20,250	162.2316
52	170,433	20,779	162.1812
53	174,431	21,309	162.0778
54	178,397	21,853	162.1121
55	182,325	22,403	162.1781
56	186,233	22,926	162.2615

TABLE 2.10 CONTINUED

Radar Time	Altitude	Horizontal Range	Azimuth
seconds	feet	feet	degrees
57	190,115	23,444	162.2663
58	193,947	23,976	162.1630
59	197,748	24,517	162.1647
60	201,527	25,052	162.2677
61	205,278	25,576	162.2014
62	208,988	26,105	162.0644
63	212,665	26,646	162.0521
64	216,309	27,208	162.1444
65	219,926	27,745	162.2533
66	223,520	28,246	162.2474
67	227,083	28,754	162.2433
68	230,606	29,293	162.2138
69	234,089	29,808	162.2591
70	237,544	30,335	162.2069
71	240,974	30,899	162.1657
72	244,380	31,464	162.0929
73	247,743	31,954	162.0946
74	251,077	32,490	162.2443
75	254,371	33,047	162.2900
76	257,633	33,660	162.2587
77	260,863	34,234	162.3593
78	264,076	34,749	162.5743
79	267,259	35,261	162.6416
80	270,403	35,766	162.4489
81	273,532	36,206	162.4342
82	276,633	36,599	162.4476
83	279,684	37,122	162.4651
84	282,677	37,830	162.3188
85	285,652	38,515	162.2045
86	288,606	38,996	162.0943

TABLE 2.10 CONTINUED

Radar Time	Altitude	Horizontal Range	Azimuth
seconds	feet	feet	degrees
87	291,539	39,504	162.2179
88	294,441	40,023	162.2529
89	297,319	40,509	162.3144
90	300,139	41,083	162.3233
91	302,930	41,715	162.4888
92	305,693	42,274	162.6337
93	308,411	42,918	162.7435
94	311,115	43,474	162.8139
95	312,809	43,817	162.8644
96	316,471	44,231	162.8743
97	319,068	44,860	162.4102
98	321,663	45,407	162.6103
99	324,218	45,875	162.4235
100	326,742	46,356	162.4369
101	329,233	46,850	162.3751
102	331,703	47,378	162.3075
103	334,105	48,009	162.3686
104	336,506	48,525	162.4893
105	338,905	48,953	162.6649
106	341,251	49,470	162.7562
107	343,520	49,983	162.7919
108	345,794	50,429	162.8475
109	348,055	50,891	162.9145
110	350,263	51,487	162.8754
111	352,412	52,255	162.8424
112	354,531	52,992	162.7573
113	356,648	53,402	162.7923
114	358,761	53,812	162.9004
115	360,841	54,286	162.9746
116	362,879	54,702	163.0796

TABLE 2.10 CONTINUED

Radar Time	Altitude	Horizontal Range	Azimuth
seconds	feet	feet	degrees
117	364,904	55,220	163.0961
118	366,855	56,194	163.1689
119	368,699	57,014	163.1775
120	370,606	57,366	163.0717
121	372,517	57,521	163.0446
122	374,387	57,744	162.5712
123	376,217	58,109	162.7936
124	378,002	58,746	162.6505
125	379,665	59,652	162.4695
126	381,350	60,325	162.5880
127	383,107	60,576	162.8685
128	384,812	60,769	163.0676
129	386,403	61,445	163.2125
130	387,941	62,344	163.3378
131	389,459	63,056	163.5706
132	390,981	63,388	163.7543
133	392,549	63,554	163.7961
134	394,087	63,835	163.9180
135	395,491	64,410	163.9709
136	396,849	65,289	163.9929
137	398,201	66,272	164.1093
138	399,528	66,886	164.0293
139	400,831	67,125	163.8140
140	402,134	67,408	163.6217
141	403,380	67,986	163.3824
142	404,639	68,376	163.1867
143	405,865	68,802	162.9320
144	406,980	69,653	162.6865
145	408,049	70,578	162.6766
146	409,179	70,889	162.7960

TABLE 2.10 CONTINUED

Radar Time	Altitude	Horizontal Range	Azimuth
seconds	feet	feet	degrees
147	410,267	71,126	162.9626
148	411,294	71,607	163.2472
149	412,279	72,255	163.6176
150	413,254	72,835	163.8892
151	414,169	73,466	164.0495
152	415,038	74,237	164.0499
153	415,922	74,775	163.8967
154	416,801	75,117	163.8102
155	417,580	75,780	163.7244
156	418,408	76,376	163.4381
157	419,239	76,479	163.2602
158	419,988	76,735	163.1291
159	420,706	77,299	163.0597
160	421,423	77,587	163.0704
161	422,072	77,923	163.0824
162	422,616	78,966	163.0910
163	423,065	80,099	163.4168
164	423,567	80,590	163.5847
165	424,178	80,589	163.8198
166	424,749	80,703	163.9754
167	425,198	81,111	164.0560
168	425,552	81,968	164.0591
169	425,825	83,071	164.0087
170	426,108	84,038	163.9232
171	426,481	84,393	163.7587
172	426,887	84,352	163.6763
173	427,230	84,536	163.5963
174	427,496	84,959	163.5630
175	427,701	85,369	163.5847
176	427,804	86,075	163.6276

TABLE 2.10 CONTINUED

Radar Time	Altitude	Horizontal Range	Azimuth
second	feet	feet	degrees
177	427,912	87,055	163.8686
178	428,000	87,857	164.0766
179	427,985	88,419	164.1875
180	428,056	88,761	164.1893
181	428,121	89,150	164.3650
182	428,179	89,263	164.4309
183	428,235	89,310	164.2126
184	428,194	89,834	164.0684
185	427,956	90,926	164.0035
186	427,800	91,547	163.9730
187	427,757	91,649	163.9874
188	427,595	92,066	163.9963
189	427,241	93,126	163.9664
190	426,879	94,095	163.9386
191	426,600	94,461	164.0251
192	426,355	94,665	164.1285
193	426,032	94,996	164.2631
194	425,601	95,725	164.2778
195	425,110	96,611	164.2699
196	424,634	97,397	164.3424
197	424,220	97,728	164.3784
198	423,798	97,992	164.2795
199	423,282	98,338	164.0265
200	422,679	98,755	163.6990
201	422,097	99,209	163.5126
202	421,519	99,648	163.3749
203	420,860	100,191	163.5623
204	420,202	100,676	163.8785
205	419,531	101,080	164.2260
206	418,776	101,491	164.4231

TABLE 2.10 CONTINUED

Radar Time	Altitude	Horizontal Range	Azimuth
second	feet	feet	degrees
207	417,909	102,273	164.5267
208	417,070	103,003	164.5552
209	416,197	103,601	164.4347
210	415,316	104,051	164.3757
211	414,456	104,535	164.2191
212	413,530	105,193	164.1151
213	412,501	106,158	164.0588
215	410,696	107,254	163.8713
218	407,234	108,380	164.1123

TABLE 2.11 POSITIONS OF SHIPS

			Given Position		Actual Position	
Type of Twilight	Date GMT	Ship	Latitude	Longitude	Latitude	Longitude
AM	26 Oct 62	S-2	16° 11.360'	11^{h} 18^{m} 16^{s}	16° 13.295'	11^{h} 18^{m} 39^{s}
AM	1 Nov 62	S-2	16° 52.5'	11^{h} 20^{m} 32^{s}	16° 53.648'	11^{h} 20^{m} 32^{s}
AM	2 Nov 62	S-4	16° 32.775'	11^{h} 17^{m} 20^{s}	16° 36.787'	11^{h} 17^{m} 10^{s}
PM	3 Nov 62	S-1	14° 59'	11^{h} 17^{m} 46^{s}	14° 59'	11^{h} 17^{m} 46^{s}

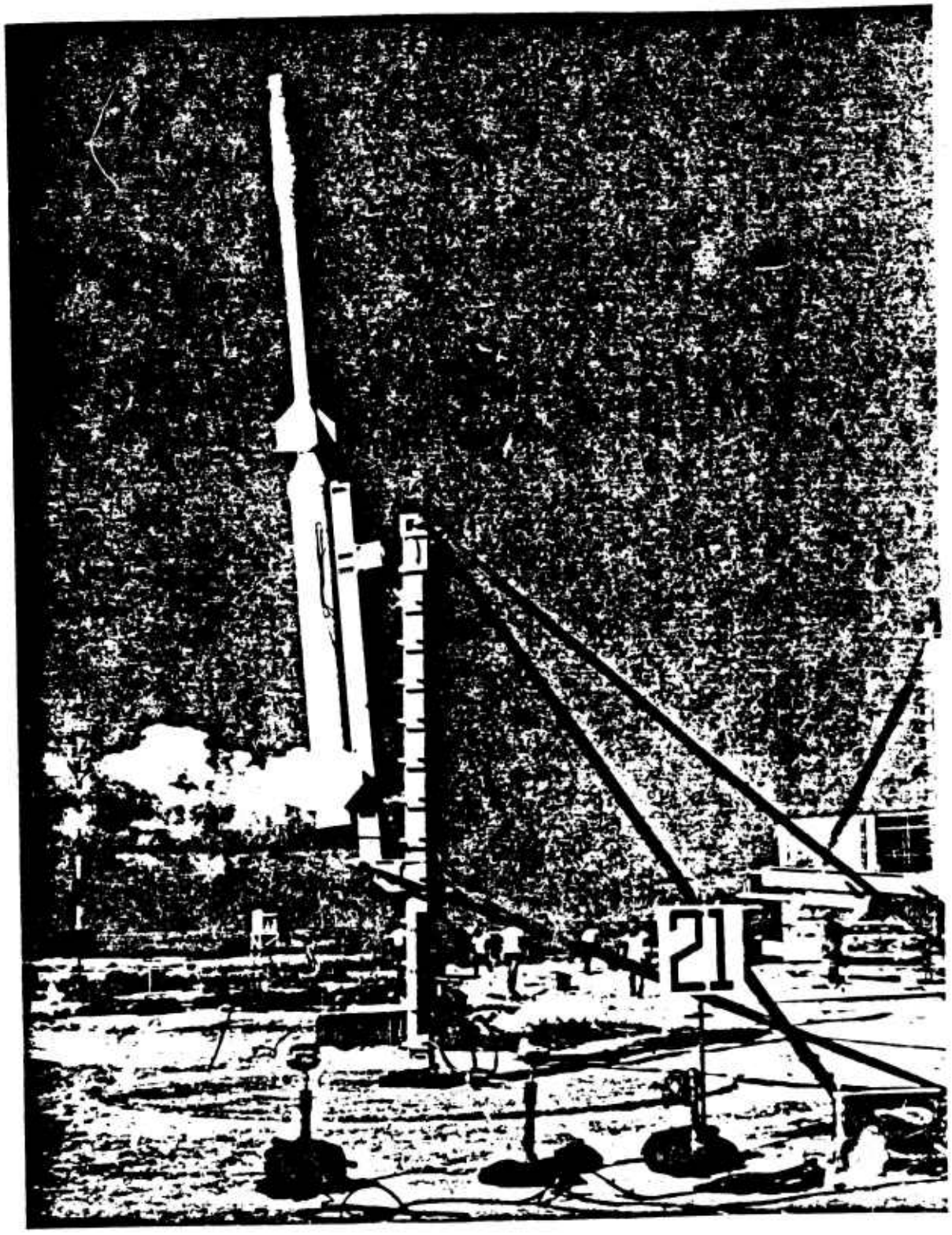

Figure 2.1 Nike-Cajun with sodium payload on launcher. (AFCRL photo)

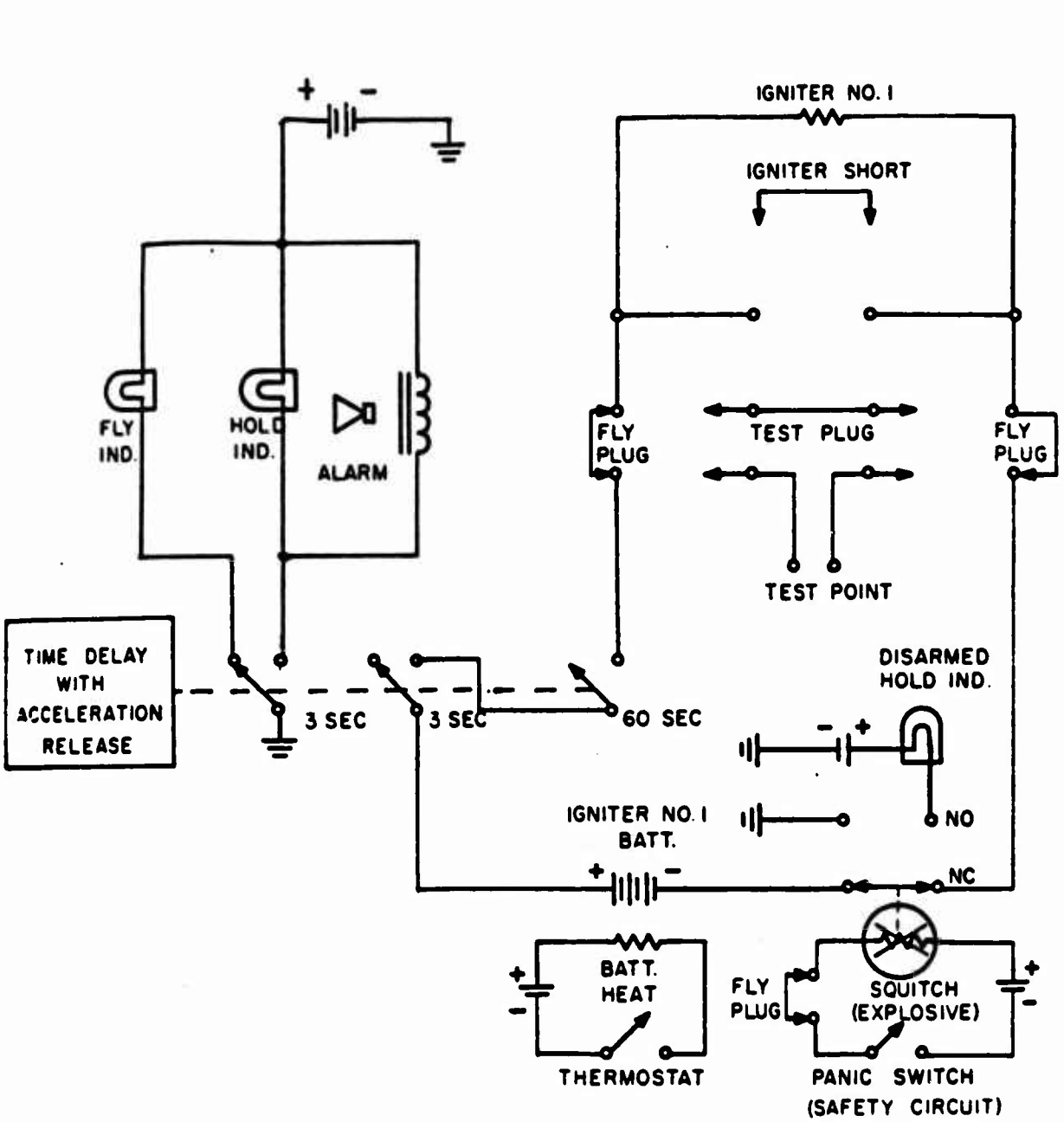

Figure 2.2. Igniter Circuit 1.

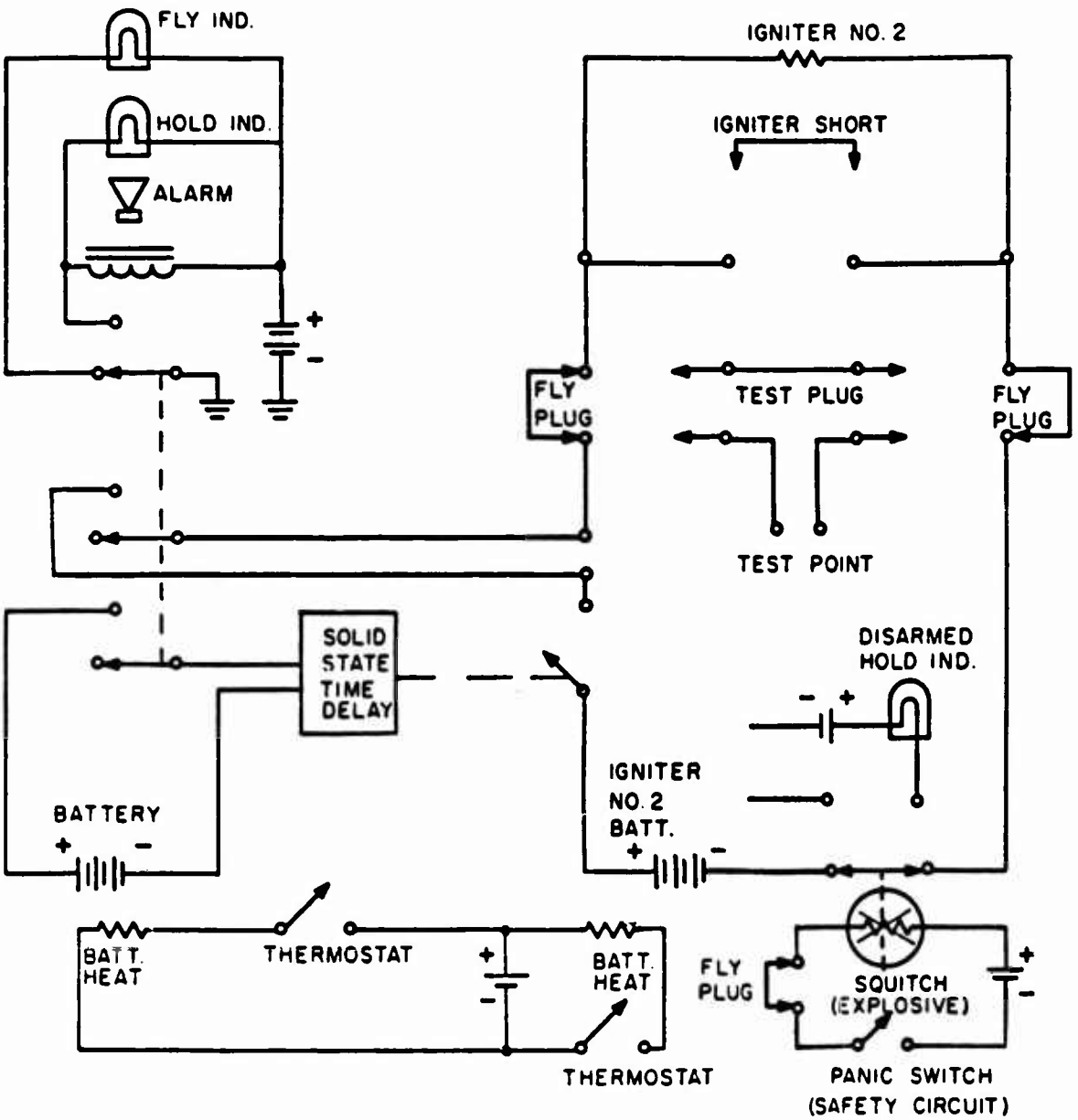

Figure 2.3. Igniter Circuit 2.

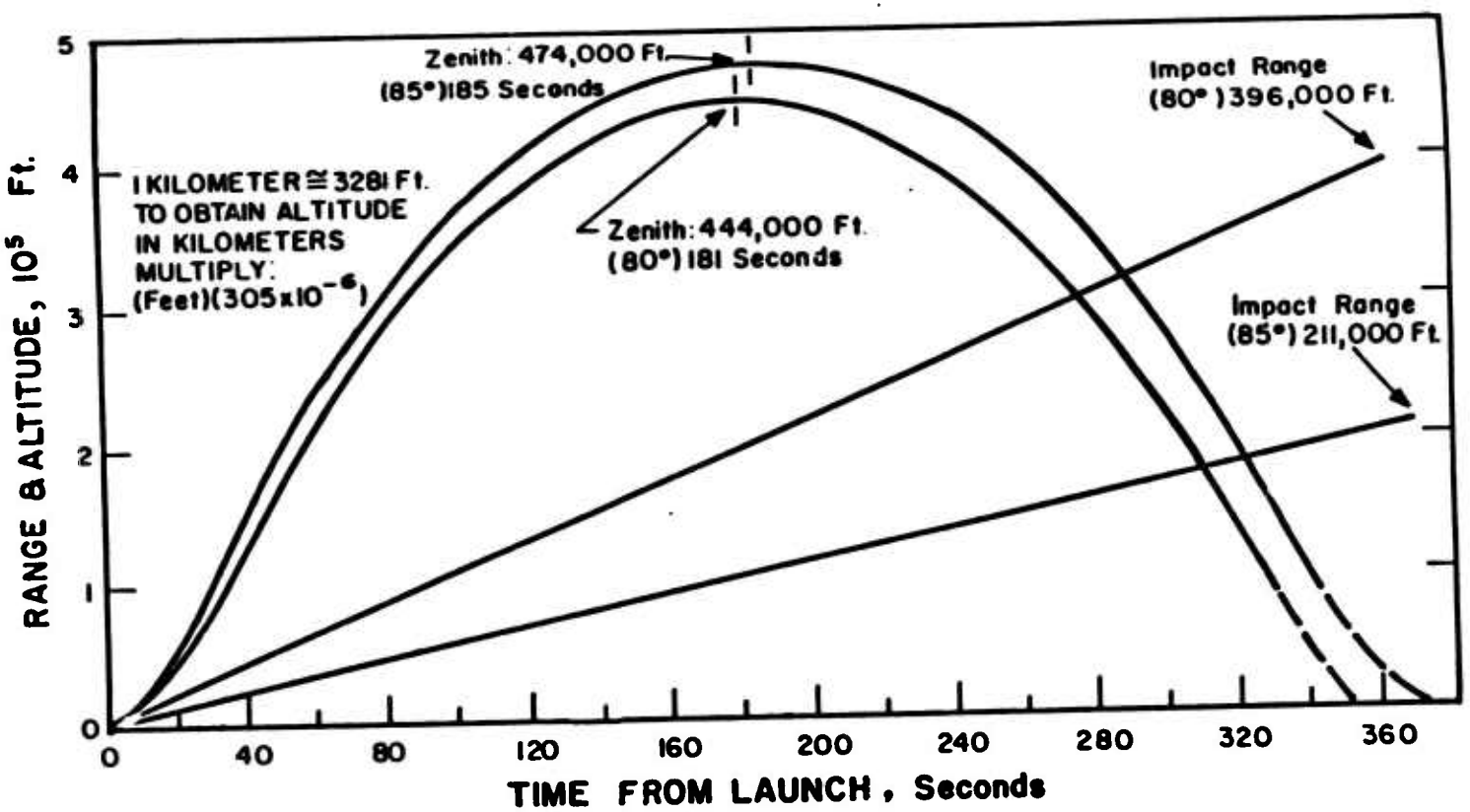

Figure 2.4. Nike-Cajun trajectories for 70-pound payload with 80° and 85° launch angles.

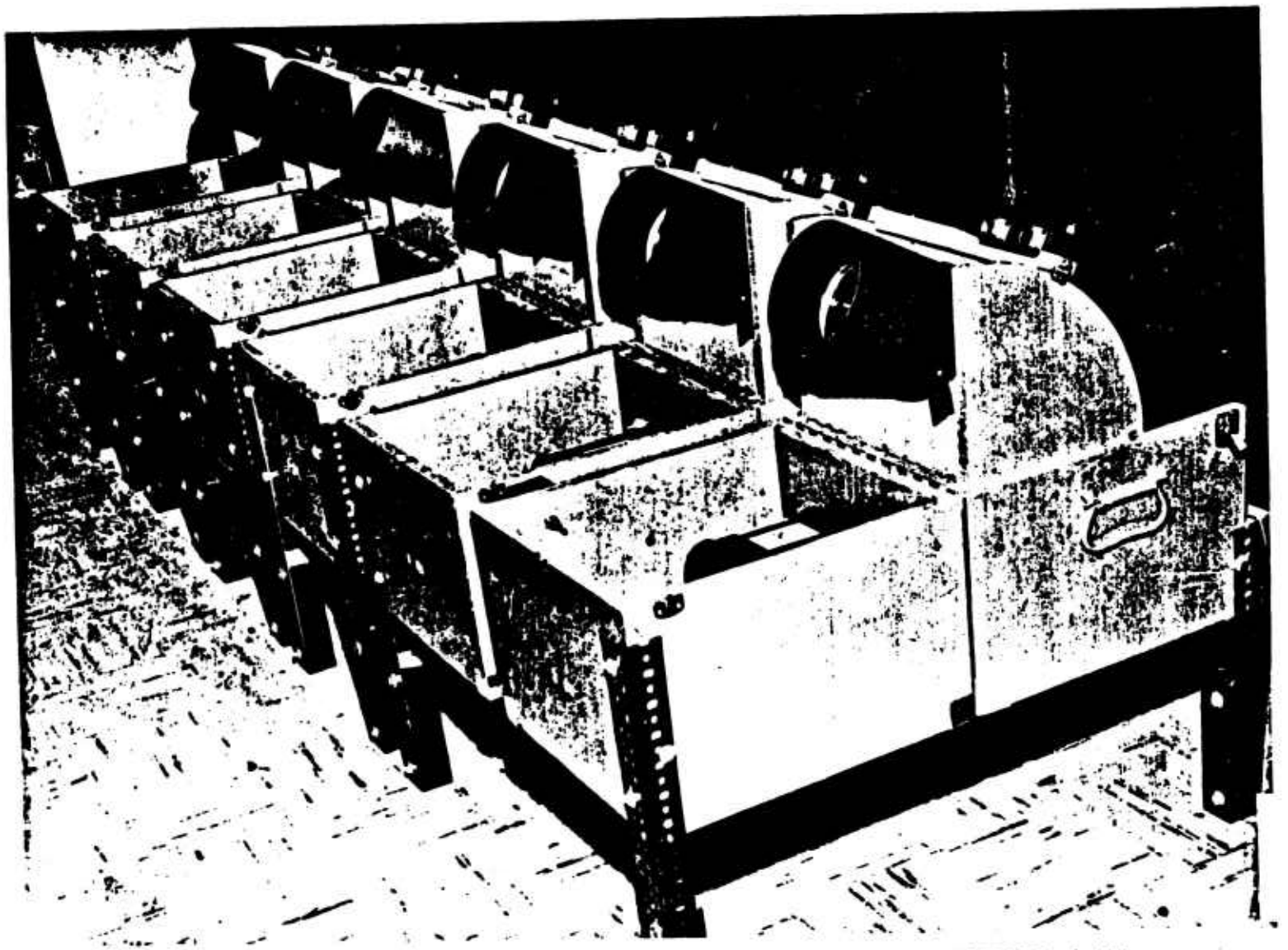

Figure 2.5 Six K-24 cameras mounted in operating position. (AFCRL photo)

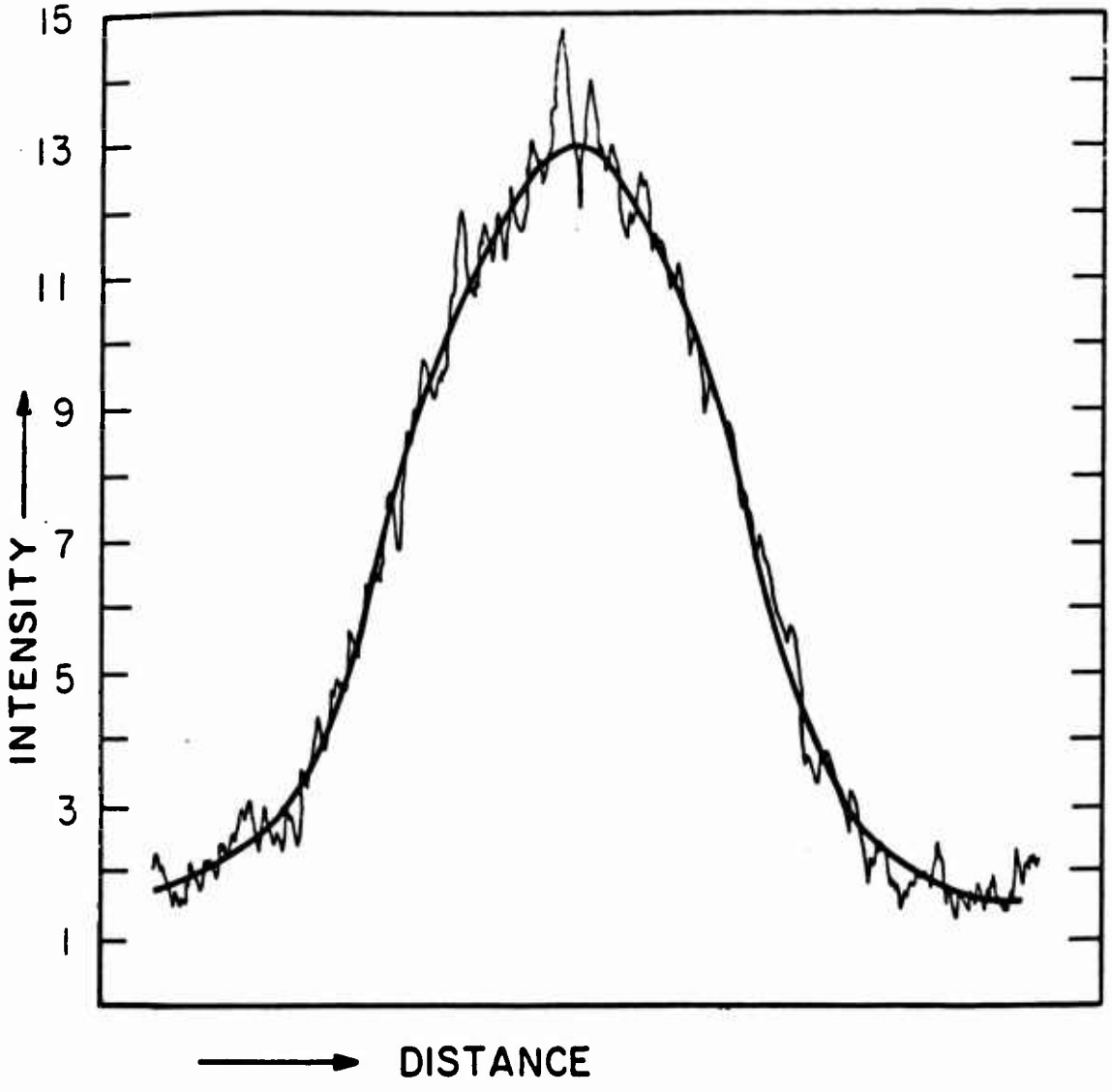

Figure 2.6 Densitometer trace, 2 November (AM), altitude 121 km, time after release 84 seconds.

CHAPTER 3

RESULTS

3.1 STAR FISH PRIME

Nike-Cajun rockets containing sodium trail packages were launched at dusk (2024 hours local time), 8 July, and dawn (0609:30 hours), 9 July, that is, at the twilight preceding and succeeding the successful nuclear detonation, Star Fish Prime. Continuous trails of sodium were released, starting at 36 km (40 seconds after launch), continuing through apogee, until exhaustion of the chemical supply at approximately 100 km (260 seconds after launch). Both rockets were skin-tracked by the Range Tracker. The peak altitude on the first rocket was 132 km and on the second rocket 131 km.

Figures 3.1, 3.2, 3.3, and 3.4 show a series of photographs of the trail the evening before Star Fish Prime.[a] The approximate times of the photographs, after launch of the rocket, are 1, 3, 5, and 9 minutes, respectively. In Figure 3.1 the rocket is emitting sodium and is at the upper tip of the visible trail. The rocket is in the same relative position in the next figure. The lowest part of the trail is at

[a] All photographs appearing at the end of this chapter were taken with the stereo cameras on Johnston Island with the exception of Figure 3.42 which came from a K-24 camera also located on Johnston Island.

the opposite end, coinciding with the end of the nearly complete circular portion. Starting with the lowest part of the trail, which clearly exhibits turbulence, and moving in a counterclockwise direction, followed by a sharp turn in the opposite direction and then continuing to the right, the trail can be followed to its end, a short distance past the rocket apogee. Figure 3.3 shows further development of the same pattern, with the addition of the relatively short downward portion of the trail. The trail is partially obscured by cloud in Figure 3.4. The results of this firing are depicted in Figure 3.5.

Figures 3.6, 3.7, 3.8, 3.9, 3.10, and 3.11 show a series of photographs of the trail at dawn following Star Fish Prime. The approximate times of the photographs, after launch of the rocket, are 2-1/2, 4-1/2, 6-1/2, 10-1/2, 14-1/2 and 20-1/2 minutes, respectively. Although the trail was partially obscured by cloud for much of the time, the photographs (particularly the negatives) are adequate for reduction of the data of the very important phenomena that were observed at this time. In Figure 3.6 the rocket is at the right and to its left is a U-shaped trail. In the next figure the rocket has traveled farther and created a longer trail. The U-shaped portion of the trail is covered by cloud but is still

faintly visible. The upper side of the U is developing into a bow which is enlarged and blown downward in the subsequent photographs.

In Figures 3.9 and 3.10, at the lower left top of the U, another section of the trail can be seen, joined to it by a shear region of approximately 180 degrees. It is obvious that the pattern in Figure 3.10 (say) is considerably different from the approximately 8-shaped pattern in Figure 3.4 which is more typical. Note the dramatic change in the descent portion of the trail between Figures 3.8 and 3.9. The descent section of the trail is deformed into a U similar in shape to that of the ascent portion. Compare Figure 3.10 with Figure 3.11.

Plotted in Figure 3.12 are the wind speeds and directions for this trail. The speeds (up to 180m/sec) are higher than usual, but it is the wind directions and shears which are completely unusual. The two approximately 180-degree shears which are usually separated by 20 to 30 kilometers in altitude are compressed into a single spiral (approximately 360 degrees) shear, at the top of which the wind is blowing toward the south instead of toward the west, which is always observed in this altitude region. No doubt this indicates

modification of the E- and F-region winds due to currents of electrons and ions induced in the north-south direction by charged particles trapped by the earth's magnetic field at higher altitudes.

3.2 BLUE GILL PRIME

A sodium trail was released at approximately 2020 hours (local time) on 25 July 1962. Although the subsequent nuclear test was unsuccessful, the data is of interest to see if any effects from Star Fish Prime persisted in this altitude region.

In Figures 3.13, 3.14, and 3.15 are shown successive phases of this trail at 3, 5 and 7 minutes after the launch of the rocket. In Figure 3.13 the position of the rocket (at the end of the diffuse, or broad section of the trail) is easy to identify. At the time of this photograph the rocket has just passed apogee. The trail can be followed downward, where it experiences a 180-degree bend, then upward where there is a bend of more than 90 degrees, right until a 180-degree bend is reached, and then left toward the center again, this being the lowest part of the trail. In Figure 3.15 the rocket has continued past apogee and made its descent. It can be seen in the photograph that the new part of the trail is higher than the other part which

crosses it. The marked turbulence in the lower portion of the trail is obvious in the photographs. In the vicinity of the upper altitude limit of turbulence, the photographs also illustrate the fact that, at a given pressure, turbulent diffusion is much more rapid than normal molecular diffusion.

The wind speeds and directions deduced from the above photographs are plotted in Figure 3.16. The wind pattern is almost normal in magnitude and direction, except for the superposition of an extremely strong (approximately 255 m/sec or 570 mph) wind toward the south at about 100 kilometers. This results in a strong north-south pseudo-shear due to the strong gradient in the wind speed in this direction.

3.3 BLUE GILL TRIPLE PRIME

The rocket scheduled for the evening twilight before Blue Gill Triple Prime had to be cancelled due to the heavy cloud cover at that time.

The rocket scheduled for the dawn twilight following this event was fired on 26 October 1962, at 0636 hours local time. The rocket and payload performance were completely normal. Since the solar depression at the time of launch was 9-1/2 degrees, the sodium was not visible until it reached an altitude above 90 kilometers. As time passed and the solar depression became less, the trail became sunlit

at lower altitudes. Sodium was emitted between about 50 kilometers and the rocket peak altitude of about 140 kilometers on the ascent of the flight and down again to about 90 kilometers on the descent.

Figures 3.17, 3.18, 3.19, and 3.20 show a series of photographs of this trail. The approximate times of the photographs, after launch of the rocket are 5-1/2, 7, 9-1/2, and 13 minutes, respectively. In Figures 3.17 the ascent portion starts near the center left side and can be followed to the center of the photograph. This portion exhibits the effects of atmospheric turbulence. It is also faint, as it was still within the earth's shadow. The peak is the widest portion and is just above the center of the photograph. The tip of the trail, near the bottom right corner of the figure, is the lower end of the descent portion. The pattern in Figure 3.18 is similar except that, due to a smaller solar depression angle, the lower parts of the ascent and descent are more clearly visible. In Figure 3.19 some of the trail is partially obscured by cloud. In Figure 3.20 atmospheric winds have spread the sodium over such a large region that a large part of the trail extends beyond the photograph.

It is of interest to watch the progress of the turbulent jets that have separated from the main cloud by the time the

exposure illustrated in Figure 3.17 was taken. The vertical motion is made apparent by a comparison of Figures 3.17, 3.18 and 3.19. As a negative temperature gradient is known to exist in this region, there can be little doubt that the gases in the globules are of a higher temperature than the ambient and that the motion is due to unstable convection. A comparison of Figure 3.19 with 3.20 shows that little vertical motion relative to the remainder of the cloud has taken place in the intervening 3-1/2 minutes, indicating that the convection has ceased and that the gases of the jets are approaching equilibrium with the ambient. The dimensions of the globular jets in Figure 3.20 have increased over those of Figure 3.19, suggesting that turbulent diffusion has, or is about to commence. There is also a very evident change in the density profiles of the globules between Figures 3.18 and 3.20.

Figure 3.21 shows the wind speeds and directions deduced from these photographs.

3.4 KING FISH

Three rockets were fired successfully after King Fish. One was fired on 1 November 1962, at 0638 hours local time

(H + 4-1/2 hours); the second was fired at 0638 hours, on 2 November (H + 28-1/2 hours); and the third at 1907 hours, on 2 November (H + 41 hours).

Figures 3.22, 3.23, 3.24, 3.25 show a series of photographs of the trail obtained at 0638 on 1 November 1962. The approximate times of the photographs after launch of the rocket are 4-1/2, 6-1/2, 8-1/2, and 11-1/2 minutes, respectively. Unfortunately, some sodium was obscured in each photograph due to scattered clouds moving across the field of view. In Figure 3.22 the lower portion of the photograph, including the lower ends of both the ascent and descent, is obscured by clouds. These parts of the trail are more clearly visible in Figure 3.23. The ascent starts as a faint turbulent region near the center of the photograph, moves to the right, then turns to the top of the photograph, turns left to the left corner, and then moves to the peak of the trail, which is located near the center of the photograph. The descent can be traced similarly. From the pattern and rate of spread of the trail, it is obvious that marked wind shears and high wind speeds existed at the time. This deduction is confirmed by Figure 3.26, which shows the wind speeds and directions computed from these photographs.

Figures 3.27, 3.28, 3.29, and 3.30 show photographs of the trail obtained at 0638 on 2 November 1962. The approximate times of the photographs after launch of the rocket are 4-1/2, 7-1/2, 10, and 12-1/2 minutes, respectively. Again, there was some, but not serious, obscuration of the trail by scattered moving clouds. In Figure 3.27 the ascent portion is near the bottom of the photograph, it curves toward the peak and the descent section, which ends near the center of the photograph. In Figure 3.28 the pattern formed by the descent is almost identical in shape and orientation, but smaller, than that formed by the ascent. Most of the ascent has spread beyond the limits of the photograph in Figure 3.29, and Figure 3.30 contains little more than the central portion of the trail. The corresponding wind speeds and directions are given in Figure 3.31.

Photographs of the trail obtained at 1907 hours on 2 November 1962 (3 November GMT) are shown in Figures 3.32, 3.33, 3.34, and 3.35. The photographs were taken at 4, 6, 8, and 10-1/2 minutes after the rocket was launched. In Figure 3.32 the rocket is still emitting sodium and is located at the tip of the trail. There is considerable turbulence exhibited by the ascent portion, which is near the bottom of the photograph. Note that the Cajun exhaust trail

is also visible. This is fainter in the next photograph. Figure 3.33 provides an excellent guide to the winds present, because both the ascending and descending sections are complete, and both exhibit the key characteristics of the winds. Starting at the peak of the cloud (the broadest portion) and moving upward on the photograph, the first wind shear is encountered. This bends ascending and descending portions into apparently opposite directions. The second sharp shear is next encountered in both portions of the trail. Continuing along the two portions, a third shear is seen, below which considerable turbulence is observed. The wind speeds and directions deduced from these photographs are given in Figure 3.36.

3.5 TIGHT ROPE

One rocket was fired before Tight Rope, at 1907 hours local time, 3 November 1962 (4 November GMT). The photographs in Figures 3.37, 3.38, 3.39, and 3.40 are of the accompanying sodium release. They were taken 3-1/2, 5, 7, and 9 minutes, respectively, after the rocket was launched. The rocket flight was normal, and from radar tracking, was found to reach a peak altitude of 133 km. Unfortunately, the sodium was above a cloud of cirrus, as can be seen in

the photographs. Nevertheless, the photographs are reasonable and quite adequate for data reduction.

At the time of the flight, winds were very strong from ground level (about 20 knots) up to the upper limit of rawinsonde observations. This trend continued in the region in which measurements were made with the sodium trail. It is for this reason that the trail was quickly dispersed.

In Figure 3.37 the Cajun exhaust trail, exhibiting the effects of strong wind shears, overlays the sodium and constitutes most of the image. At the time of the photograph, the rocket had just passed its apogee and is located at the tip of the trail. The sodium may be more clearly identified in Figure 3.38, starting at the tip of the trail (the lower end of the descent) near the center of the photograph and moving down the photograph to the first kink, which corresponds to the peak. The smooth trail can then be followed toward the lower right corner, where it makes a sharp change in direction to the left (and at the same time exhibits the effects of turbulence). This part of the trail curves until it ends almost touching the image of the peak. The rest of the turbulent trails in the photograph are due to the rocket exhaust. Due to dispersion and cloud cover,

only portions of the sodium are visible in Figures 3.39 and 3.40.

The corresponding wind speeds and directions are shown in Figure 3.41.

3.6 DIFFUSION COEFFICIENT DATA

The sodium trail at dusk on 25 July was densitometered at 107, 112, 118, and 120 km, as indicated in Figure 3.42. Some difficulty was encountered because of low contrast between the trail and sky background. The diffusion coefficients obtained are given in Table 3.1, and plotted in Figure 3.43. In Table 3.1 the "Time After Release" indicates the interval after release of the sodium for which photographs were studied. The K-24 photographs were taken at 20-second intervals and the stereo at 60-second intervals. Data up to 160 seconds after release was used to obtain the diffusion coefficient. At later times the plot of r^2 versus t deviated from a straight line, as predicted by Equation 1.12 . The values at 112, 118, and 120 km are consistent with theoretical values for molecular diffusion. The curves of r^2 versus t for 107 km are shown in Figure 3.44. The trail growth for about 100 seconds after release was due to molecular diffusion and yielded the values of the diffusion coefficient given in

Table 3.1. However, between 100 and 200 seconds the rate of growth rapidly increased due to the onset of turbulence. This gave an apparent diffusion coefficient which increased with time as indicated in Figure 3.43 (horizontal line at 107 km).

For isotropic (weak shear) turbulent diffusion the rate of growth is given by

$$r_o^2 = \frac{8}{3}\epsilon t^3\left[1 + \ell n\left(\frac{r_{o\ max}^2}{2r_e^2}\right) - \ell n\left(\frac{4/3\ \epsilon t^3}{r_e^2}\right)\right] \qquad (3.1)$$

where ϵ is the rate of viscous dissipation of turbulent kinetic energy, per unit mass (Reference 13). Equation 3.1 can be rearranged in the form

$$\frac{r_o^2}{t^3} = \frac{8}{3}\epsilon\left[1 + \ell n\ \frac{3r_{o\ max}^2}{8} - \ell n\, t^3\right]$$
$$= A - B\ \ell n\, t^3 \qquad (3.2)$$

where A and B are constants. r^2/t^3 versus t^3 is plotted in Figure 3.45 for several isophotes. These curves should have negative slopes according to Equation 3.2, and it can be seen that as turbulence took control this condition was attained.

The trail at dawn on 2 November was photometered at a series of altitudes between 109 and 128 km, as shown in

Figure 3.46. Between 111 and 128 km the diffusion was molecular and the values of the coefficient are given in Table 3.2. At early time, turbulence appeared to cease at 95 km. However, later exposures (say, six minutes after rocket launch) indicated visible turbulence as high as 109 km. A finite time for the onset of turbulence (particularly at higher altitudes) is usually observed. The diffusion coefficient for 109 km was obtained by using only photographs at early times before visible turbulence appeared. The values of the coefficients for 2 November are compared with theory and other experimental values in Figure 3.43 and agree well with both. Figure 3.47 illustrates r^2 versus t for 125 km. The curves for the different isophotes remain linear until about 150 seconds after release time. An increasing slope after 150 seconds would indicate a departure from an $r^2 \sim t$ dependence toward a $r \sim t$ relation symptomatic of shear turbulent diffusion (Reference 13), while a decreasing slope would indicate that molecular diffusion was still dominant and the third term in Equation 1.12 was becoming important. In the example cite, however, there is no clear cut trend for $t > 150$ seconds, and one cannot determine whether any change in the slope of the r^2 versus t curve is taking place.

TABLE 3.1 DIFFUSION COEFFICIENTS MEASURED WITH THE SODIUM TRAIL FROM ROCKET LAUNCHED AT 2020 LOCAL TIME 25 July 1962 (26 July GMT)

Altitude (km)	Time of Release[a] (sec)	Film Type	Time of Photographs	Diffusion Coefficient (cm^2/sec)	Time after Release (sec)
107	104	K-24	2024-2025	2.83×10^6	136-196
112	111	K-24	2024-2024:40	4.66×10^6	129-169
118	121	K-24	2024-2024:40	2.68×10^7	119-159
120	125	K-24	2024-2024:40	3.36×10^7	115-155

[a]Time after launch of rocket, from radar data.

TABLE 3.2 DIFFUSION COEFFICIENTS MEASURED WITH THE SODIUM TRAIL FROM ROCKET LAUNCHED AT 0638 LOCAL TIME 2 November 1962

Altitude (km)	Time of Release[a] (sec)	Film Type	Time of Photographs	Diffusion Coefficient (cm^2/sec)	Time after Release (sec)
109	106	K-24	1641-1643	4.97×10^6	74-194
111	109	K-24	1641-1643	4.15	71-191
112	111	stereo	1641-1643	6.42	69-189
114	114	stereo	1641:30-1644	1.15×10^7	96-246
121	126	stereo	1641-1643:30	3.98	94-204
125	134	stereo	1641-1644	5.93	46-226
128	138	stereo	1641-1643:30	8.05	42-192

[a]Time after launch of rocket, from radar data.

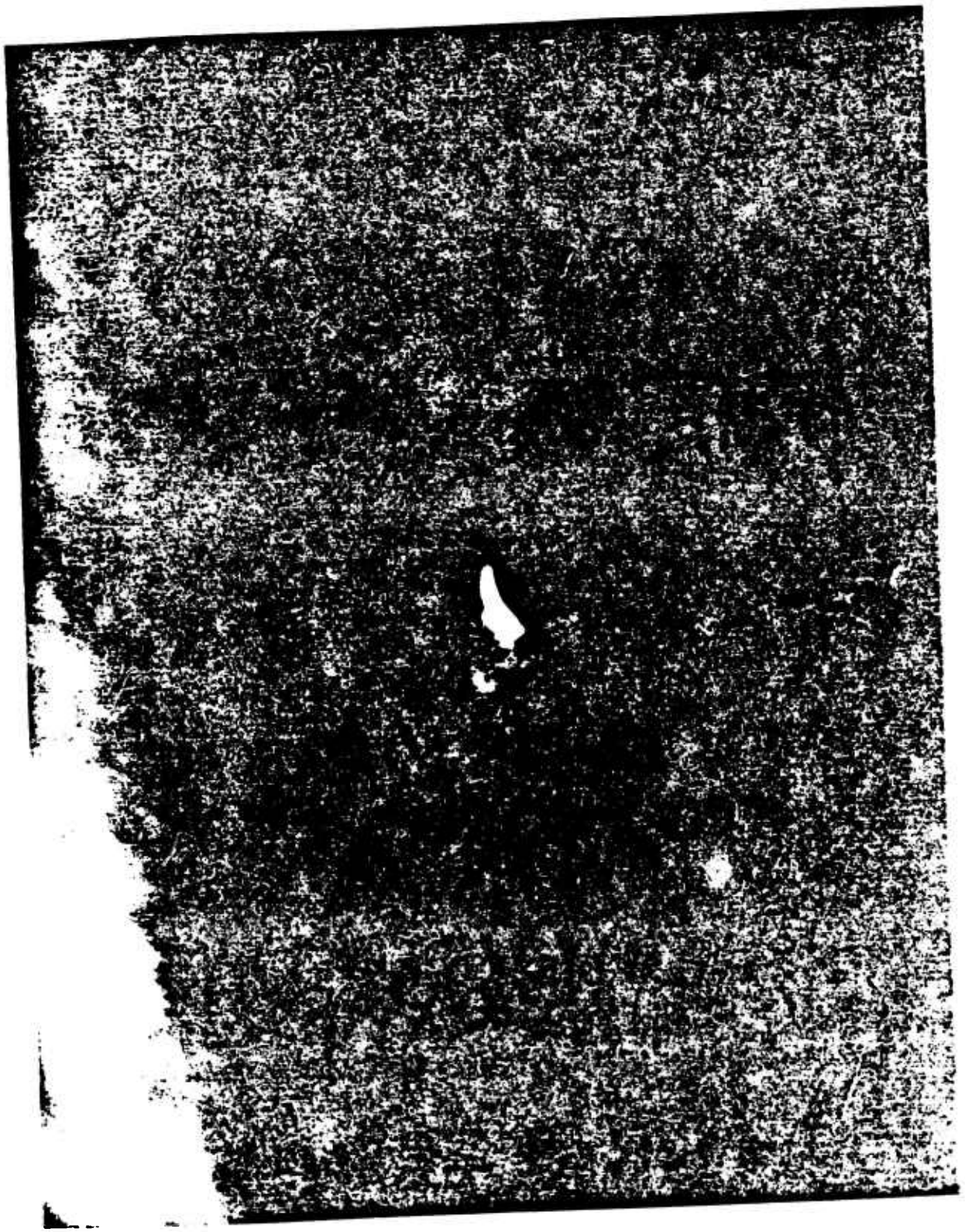

Figure 3.1 Sodium trail at dusk before Star Fish Prime. 1 minute after rocket launch.

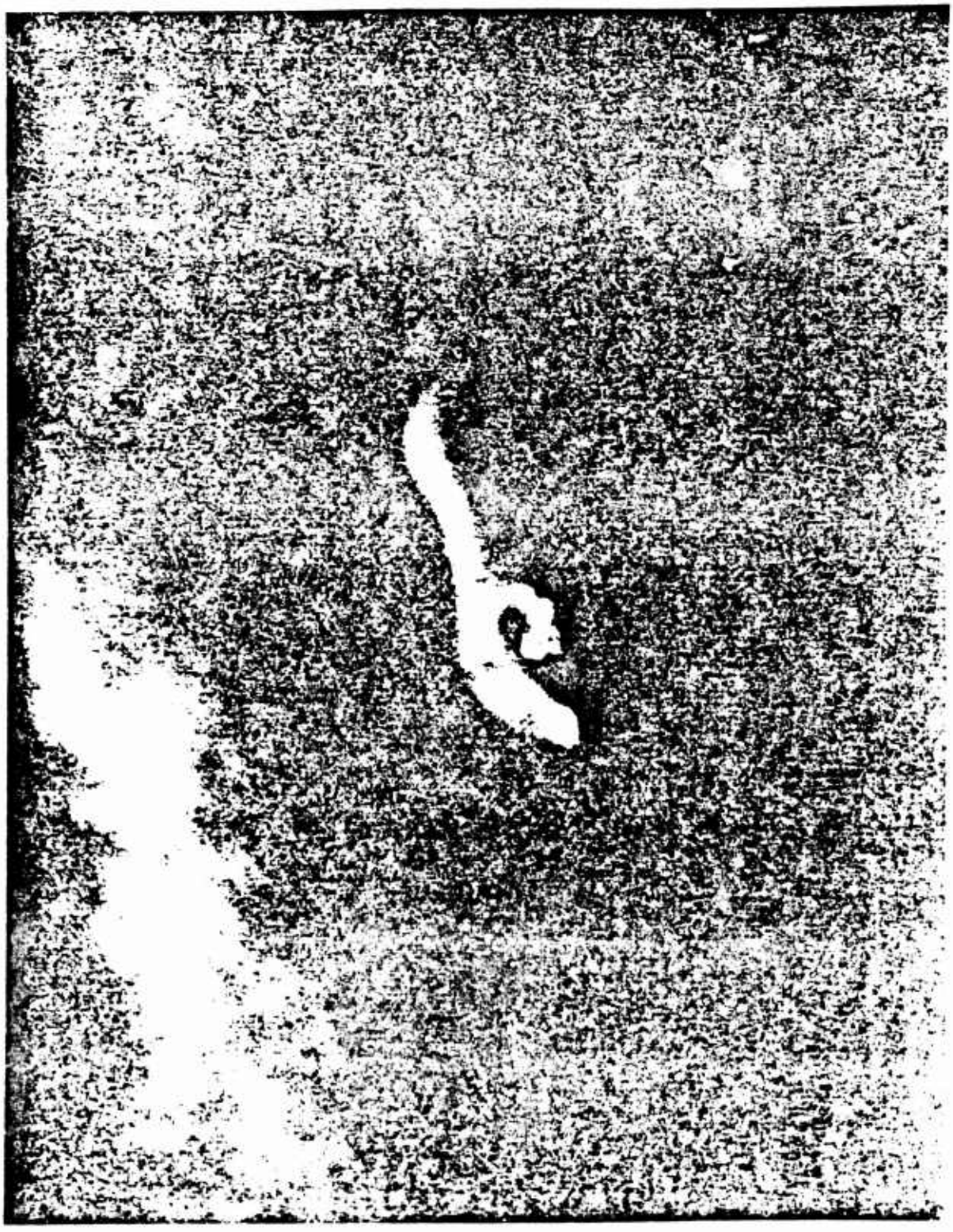

Figure 3.2 Sodium trail at dusk before Star Fish Prime, 3 minutes after rocket launch.

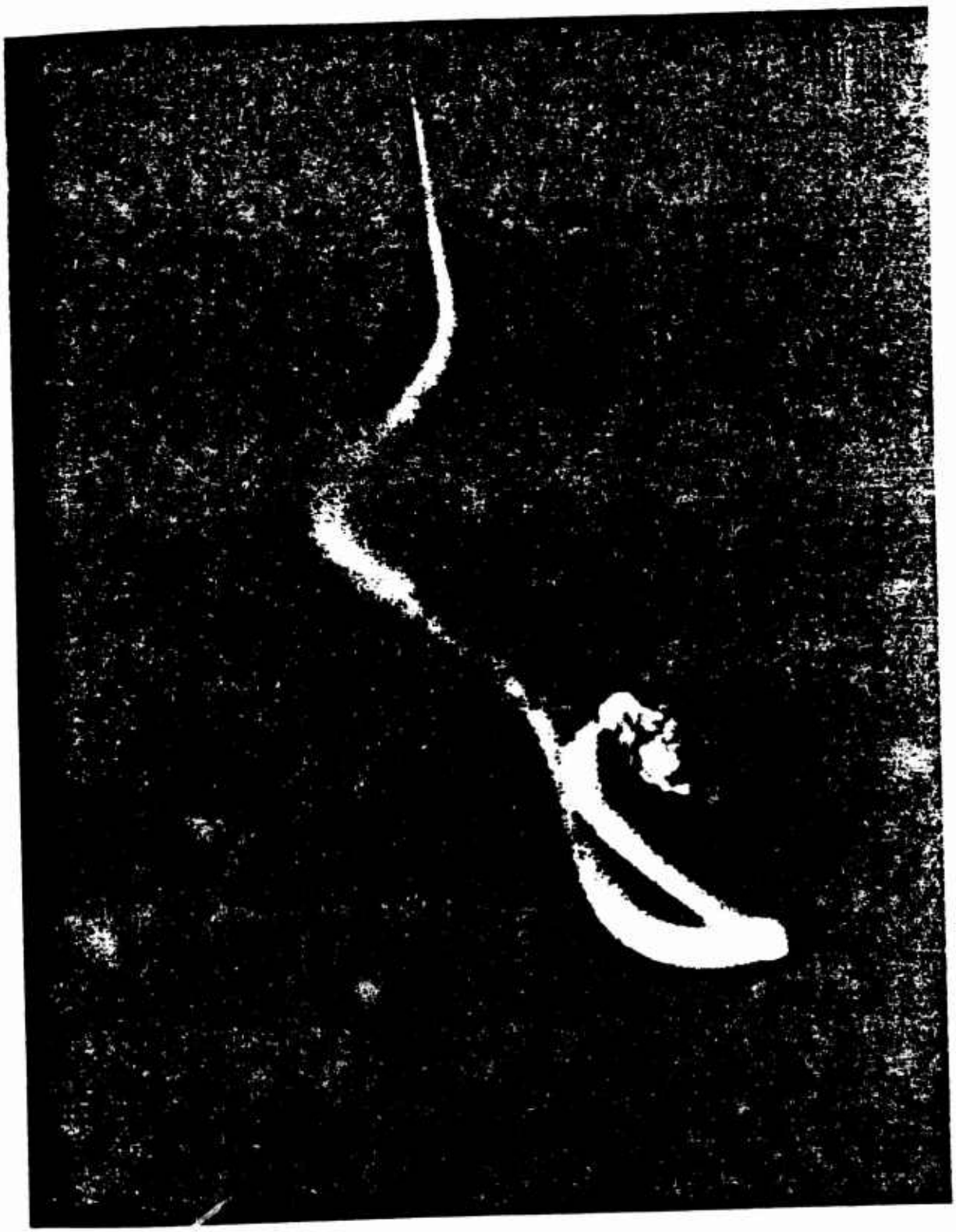

Figure 3.3 Sodium trail at dusk before Star Fish Prime, 5 minutes after rocket launch.

Figure 3.4 Sodium trail at dusk before Star Fish Prime, 9 minutes after rocket launch.

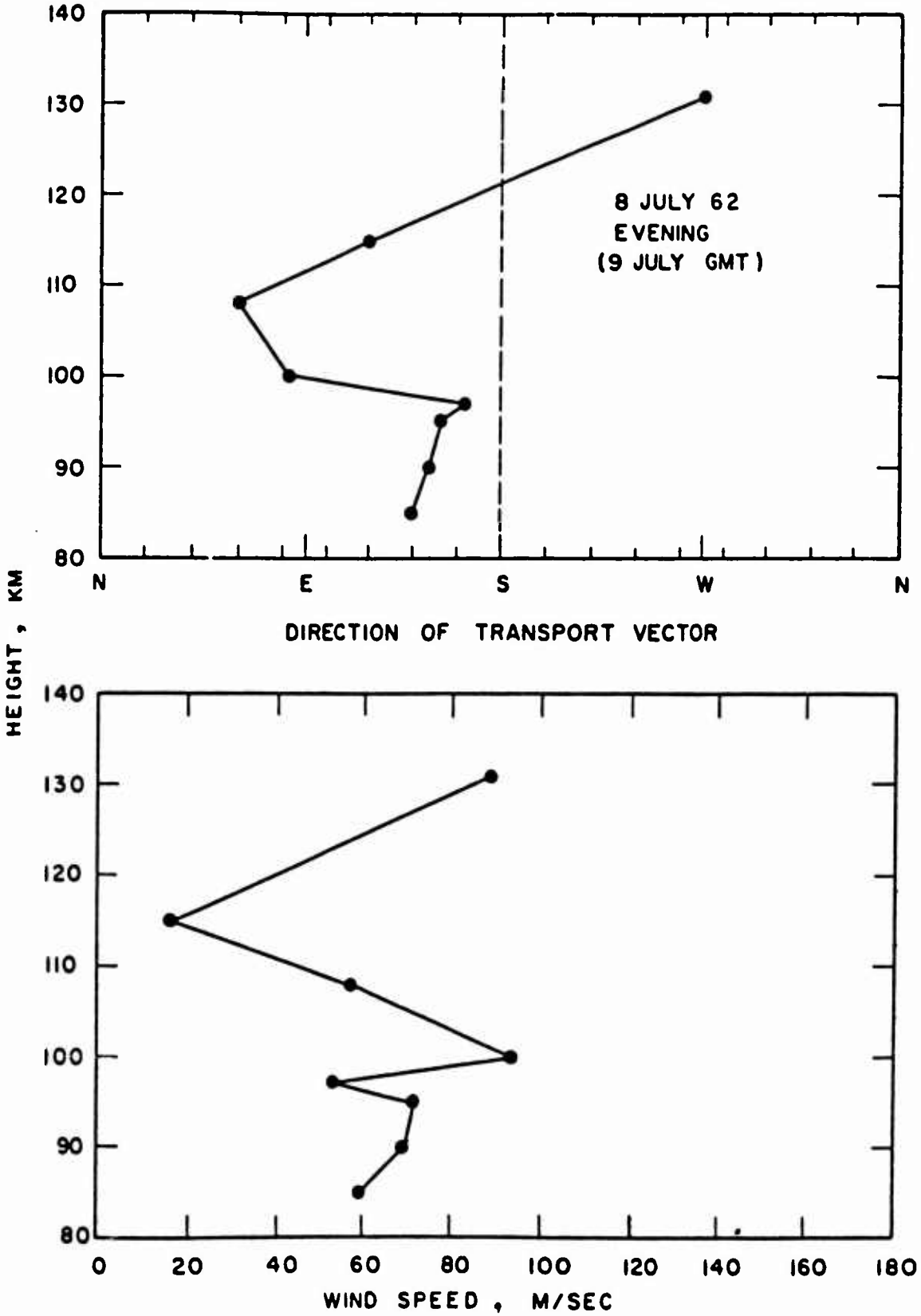

Figure 3.5. Upper atmosphere wind speeds and directions at dusk before Star Fish Prime.

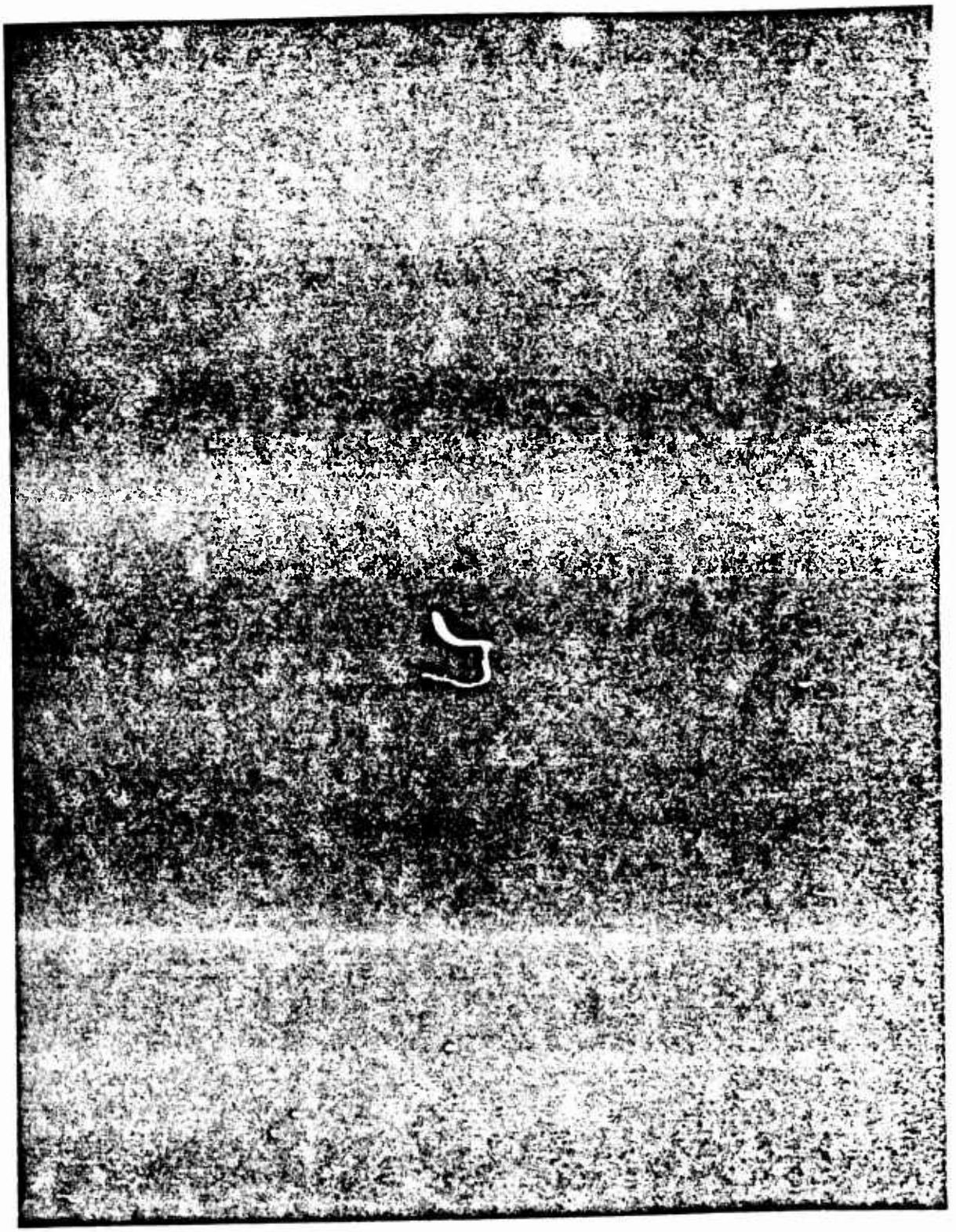

Figure 3.6 Sodium trail at dawn following Star Fish Prime, $2\frac{1}{2}$ minutes after rocket launch.

Figure 3.7 Sodium trail at dawn following Star Fish Prime, 4 ½ minutes after rocket launch.

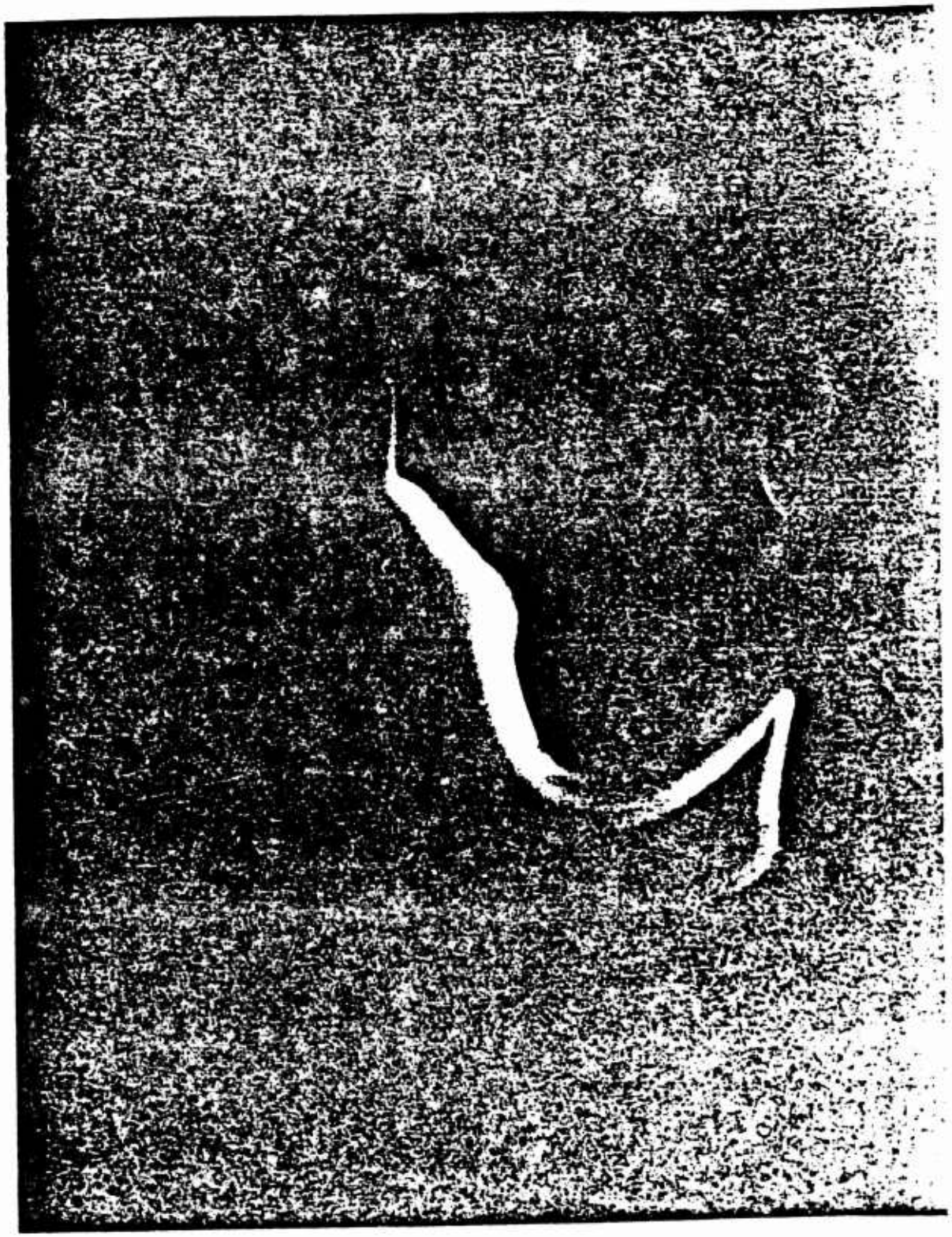

Figure 3.8 Sodium trail at dawn following Star Fish Prime $6\frac{1}{2}$ minutes after rocket launch.

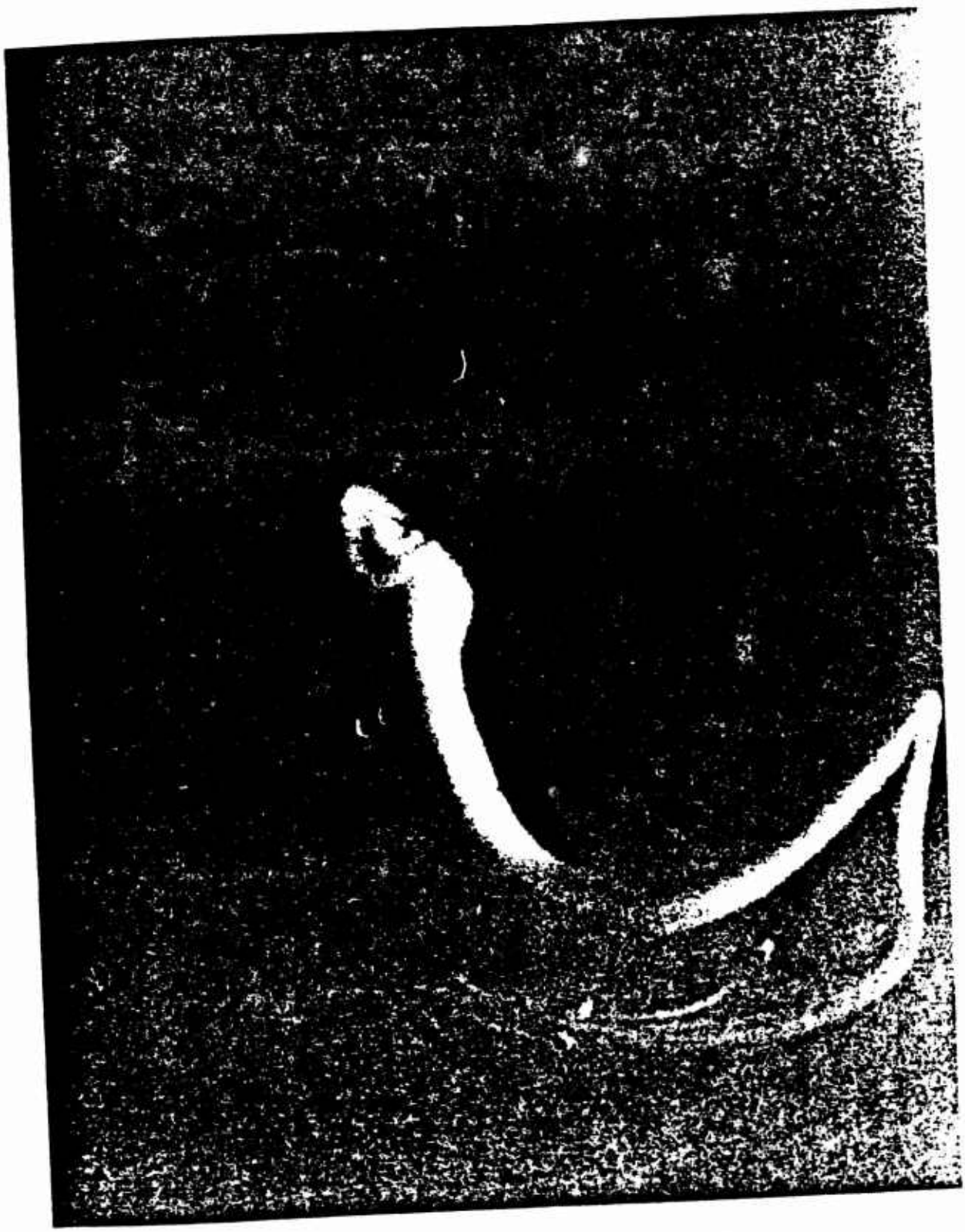

Figure 3.9 Sodium trail at dawn following Star Fish Prime, 10 ½ minutes after rocket launch.

Figure 3.10 Sodium trail at dawn following Star Fish Prime, 14½ minutes after launch.

Figure 3.11 Sodium trail at dawn following Star Fish Prime, 20 ½ minutes after launch.

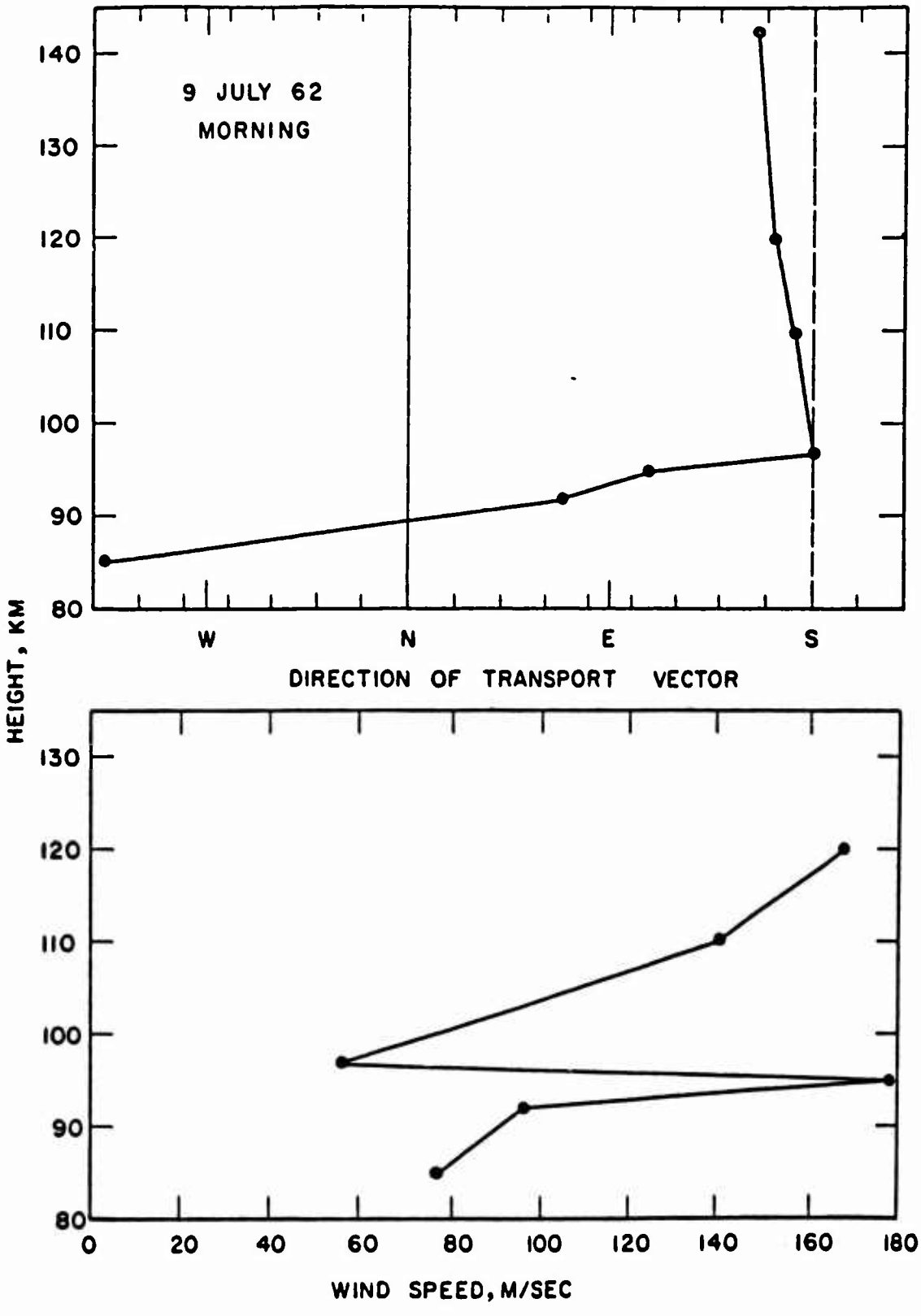

Figure 3.12. Upper atmosphere wind speeds and directions at dawn following Star Fish Prime.

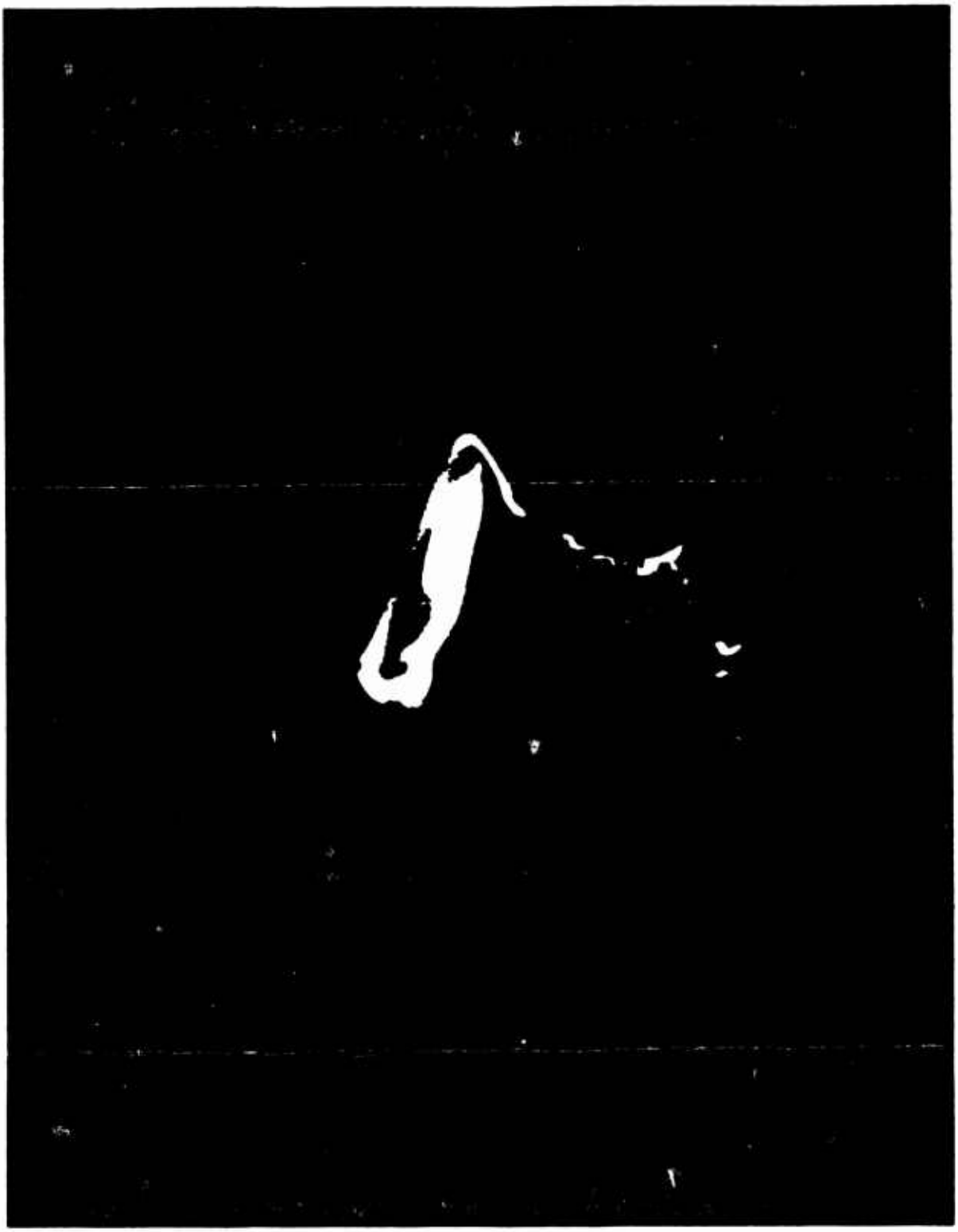

Figure 3.13 Sodium trail at dusk before Blue Gill Prime, 3 minutes after rocket launch.

Figure 3.14 Sodium trail at dusk before Blue Gill Prime, 5 minutes after rocket launch.

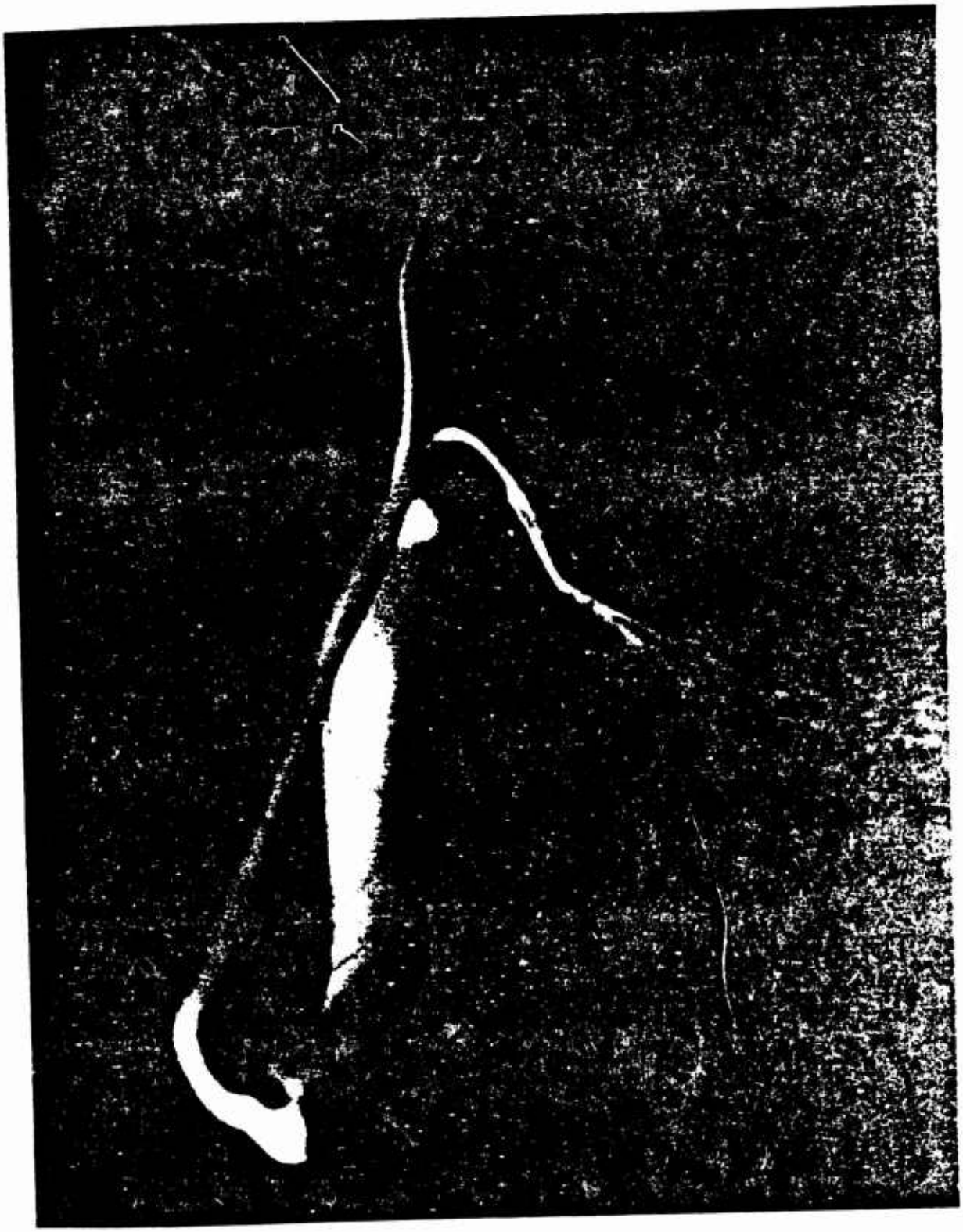

Figure 3.15 Sodium trail at dusk before Blue Gill Prime, 7 minutes after rocket launch.

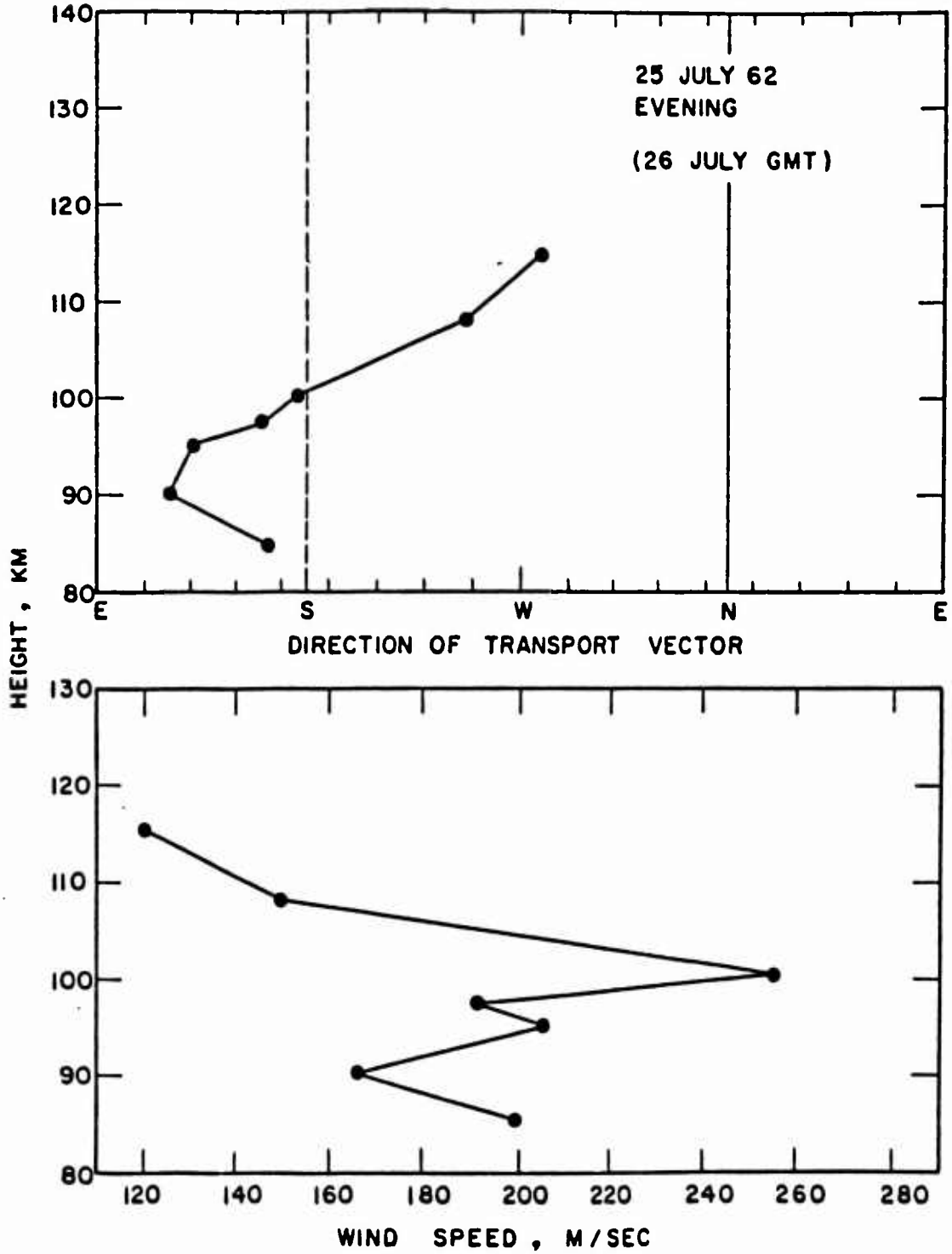

Figure 3.16. Upper atmosphere wind speeds and directions at dusk before Blue Gill Prime.

Figure 3.17 Sodium trail at dawn following Blue Gill Triple Prime, 5 ½ minutes after rocket launch.

Figure 3.18 Sodium trail at dawn following Blue Gill Triple Prime, 7 minutes after rocket launch.

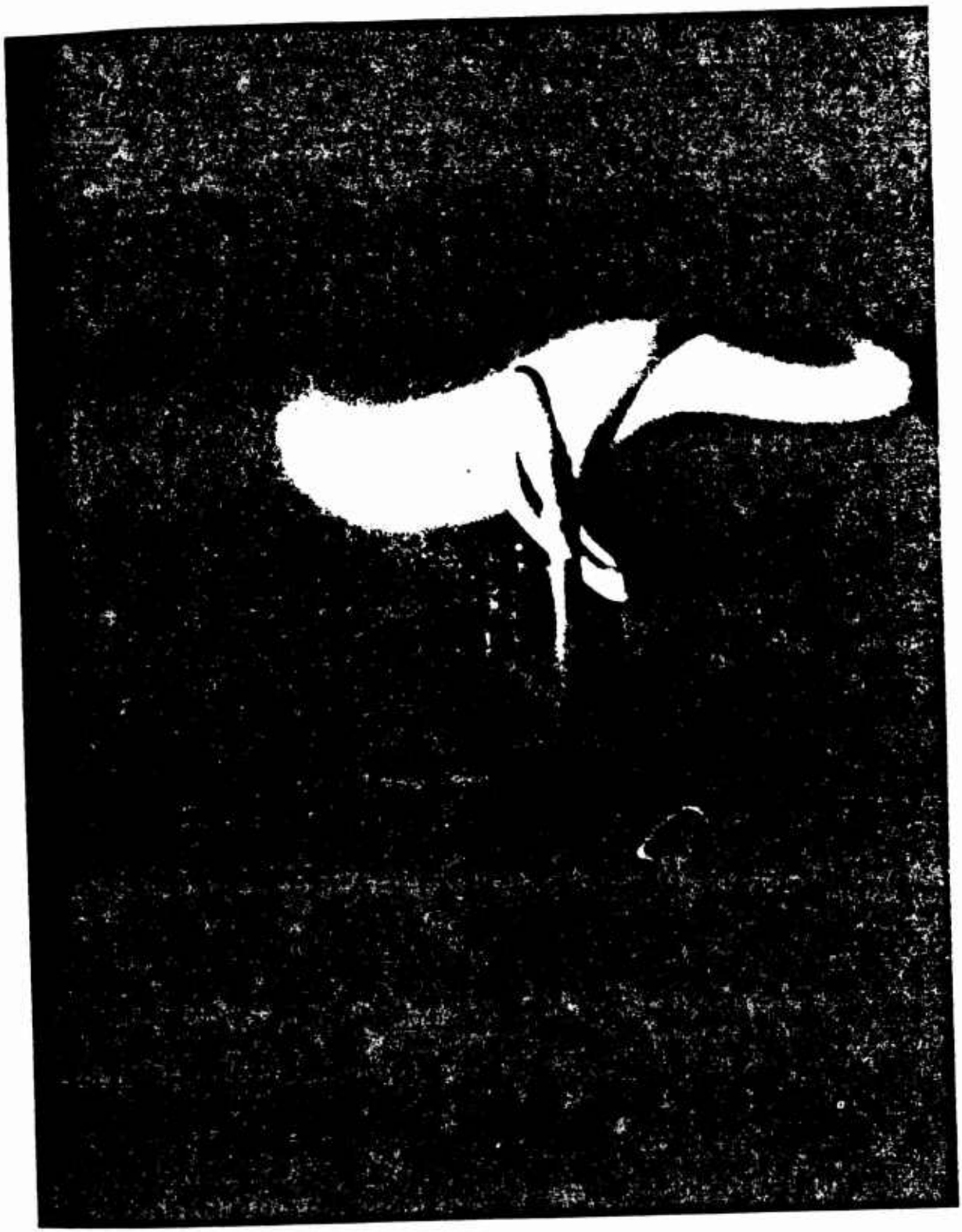

Figure 3.19 Sodium trail at dawn following Blue Gill Triple Prime, 9½ minutes after rocket launch.

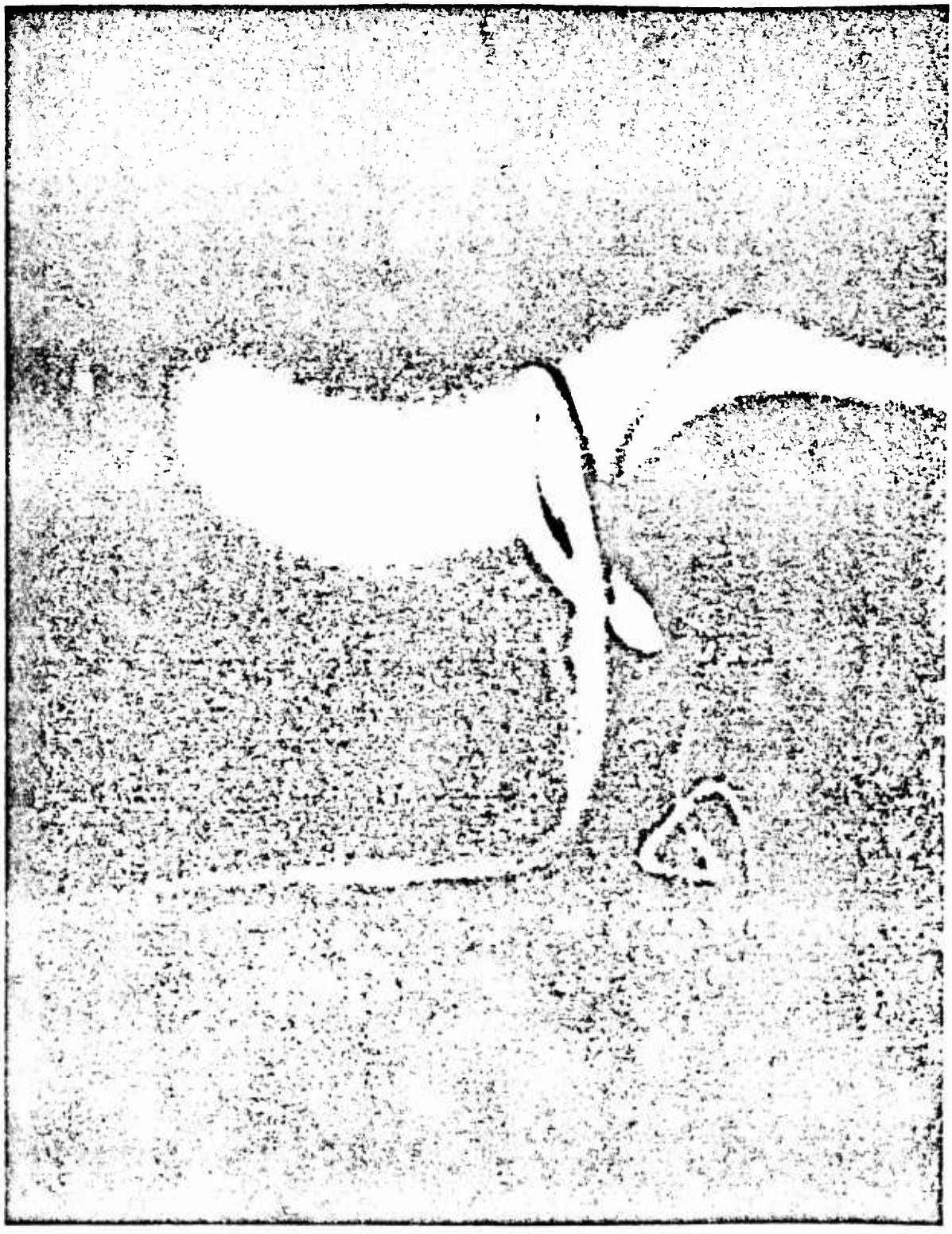

Figure 3.20 Sodium trail at dawn following Blue Gill Triple Prime, 13 minutes after rocket launch.

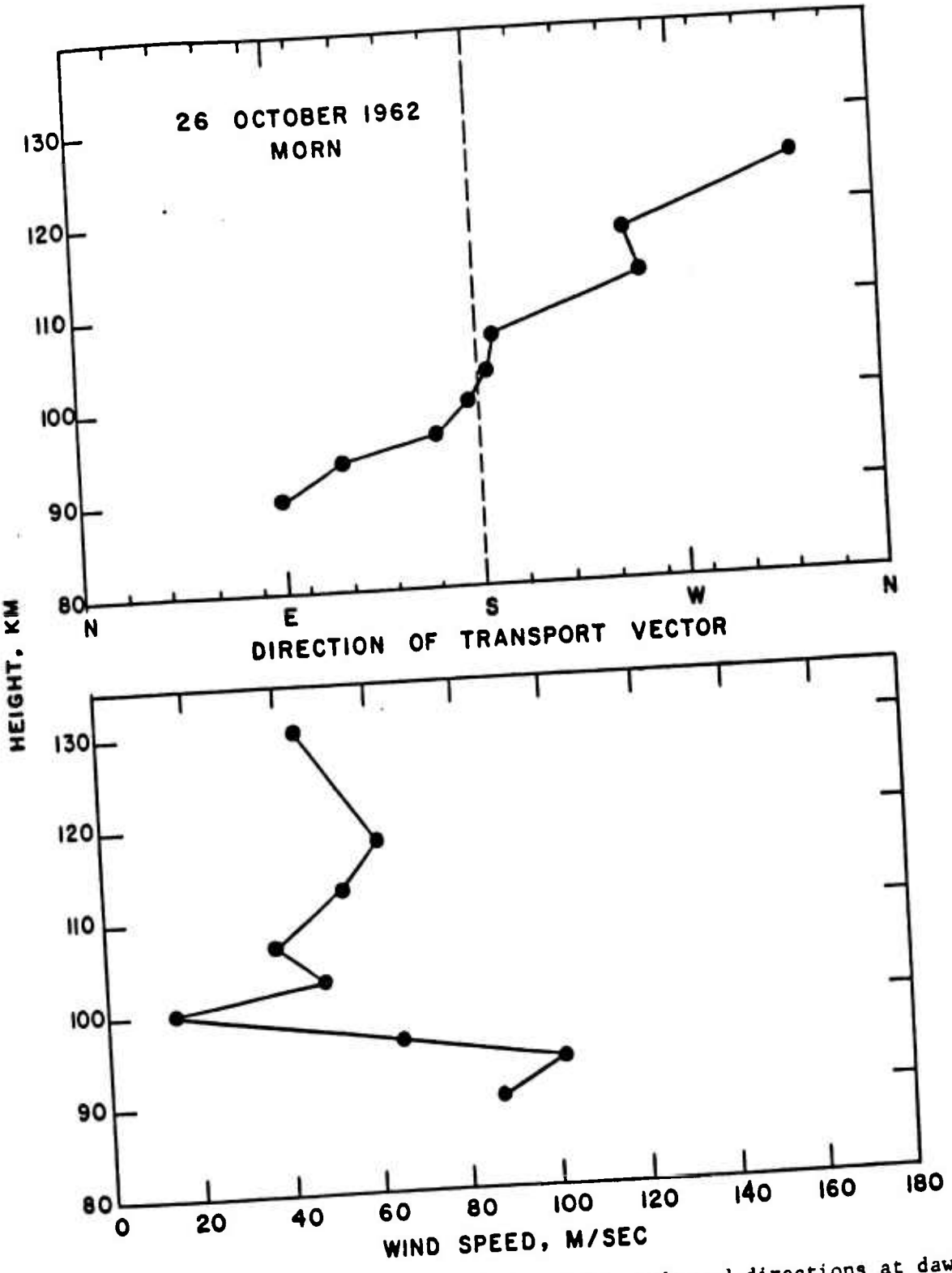

Figure 3.21. Upper atmosphere wind speeds and directions at dawn following Blue Gill Triple Prime.

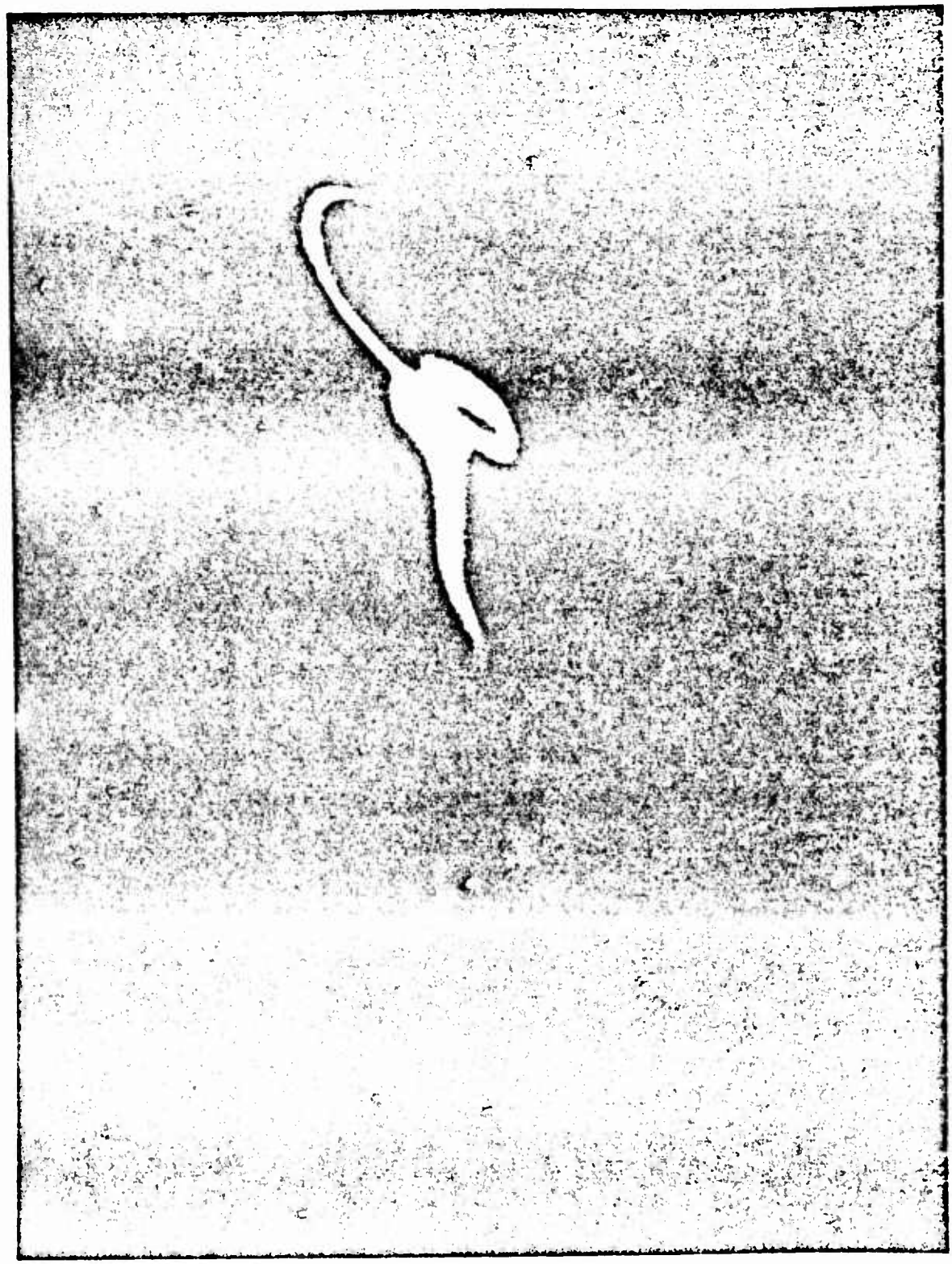

Figure 3.22 Sodium trail at dawn ($4\frac{1}{2}$ hours) after King Fish, $4\frac{1}{2}$ minutes after rocket launch.

Figure 3.23 Sodium trail at dawn (4½ hours) after King Fish, 6½ minutes after rocket launch.

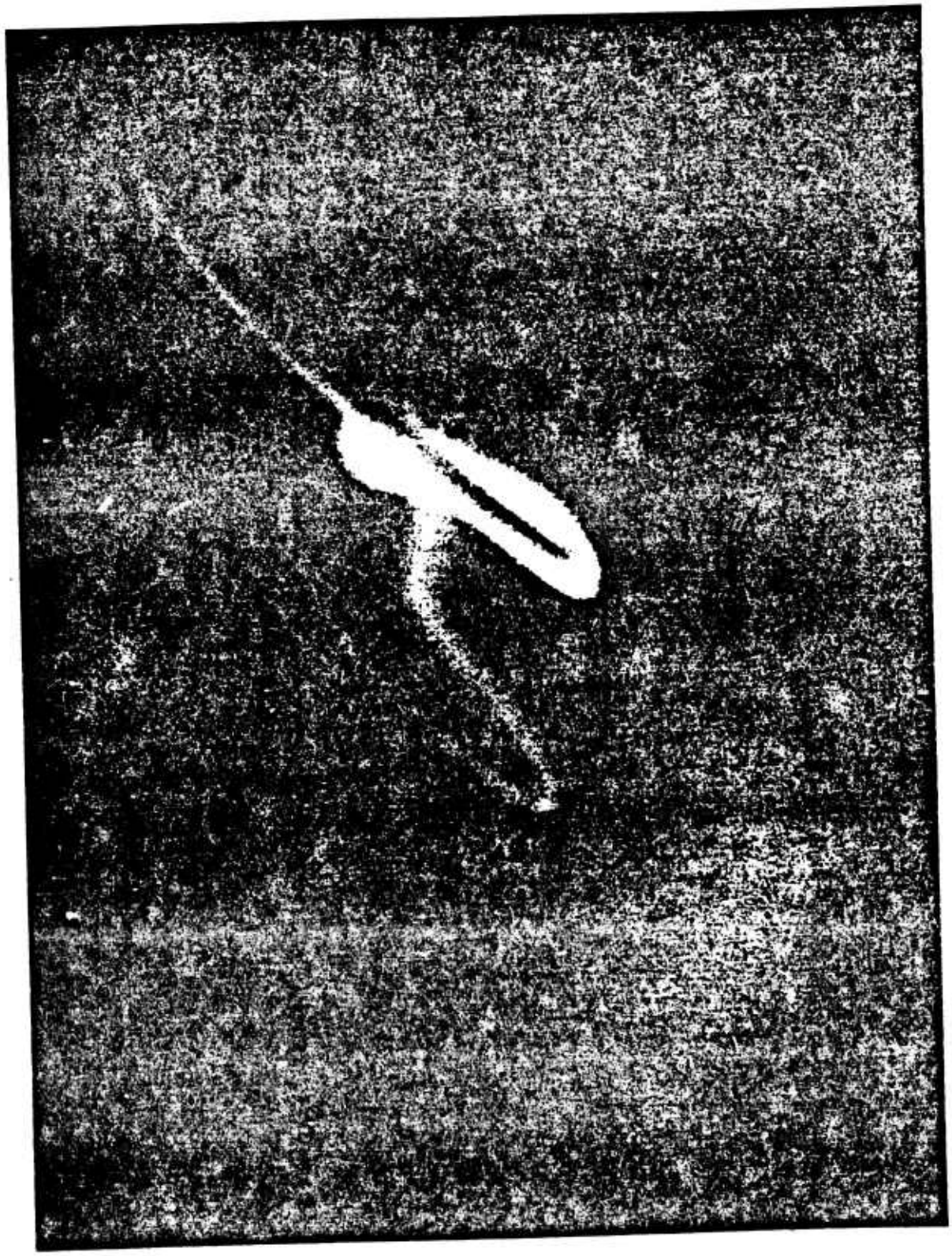

Figure 3.24 Sodium trail at dawn (4 ½ hours) after King Fish, 8 ½ minutes after rocket launch.

Figure 3.25 Sodium trail at dawn (4 ½ hours) after King Fish, 11 ½ minutes after rocket launch.

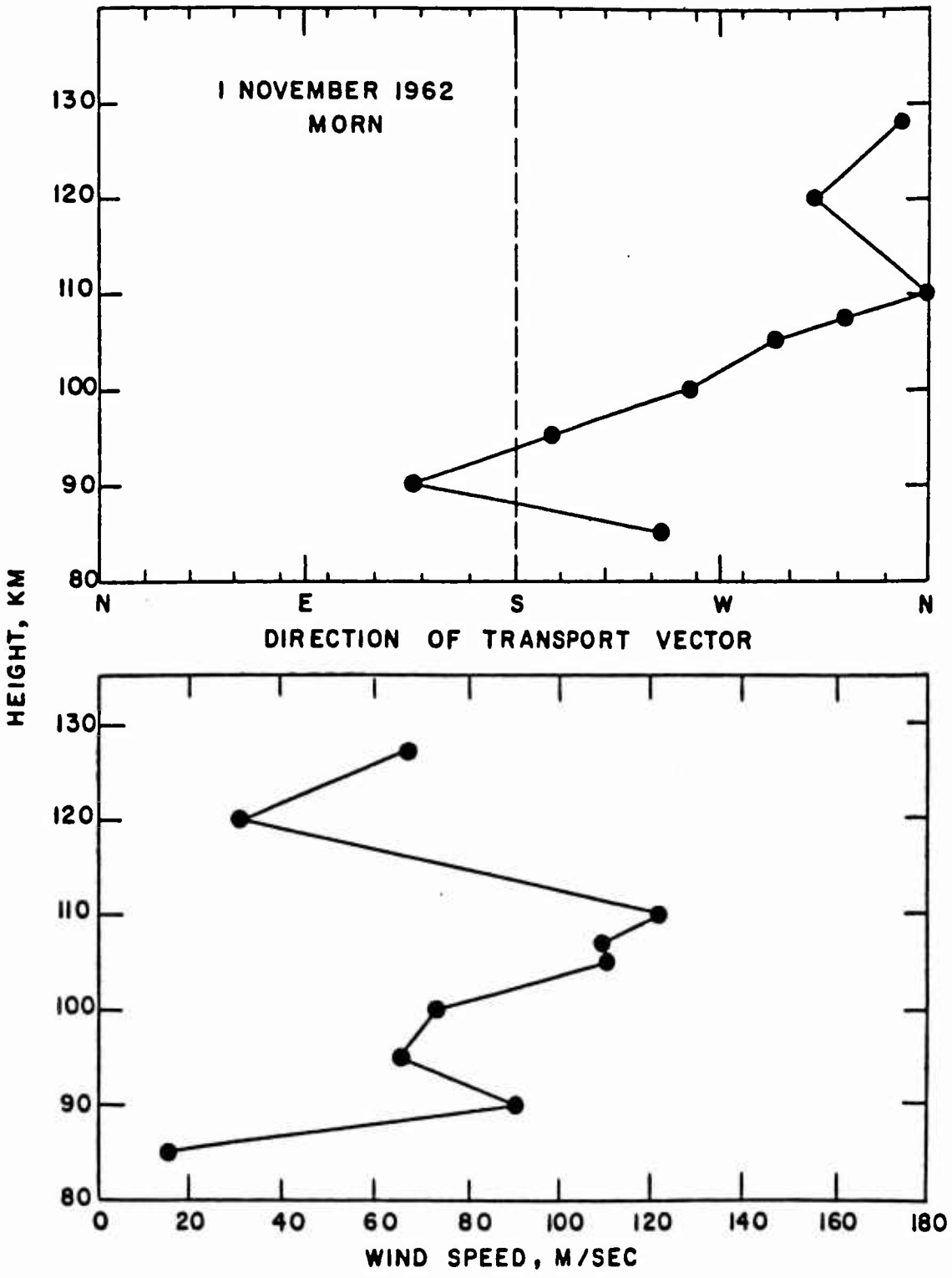

Figure 3.26. Upper atmosphere wind speeds and directions at dawn (4-1/2 hours) after King Fish.

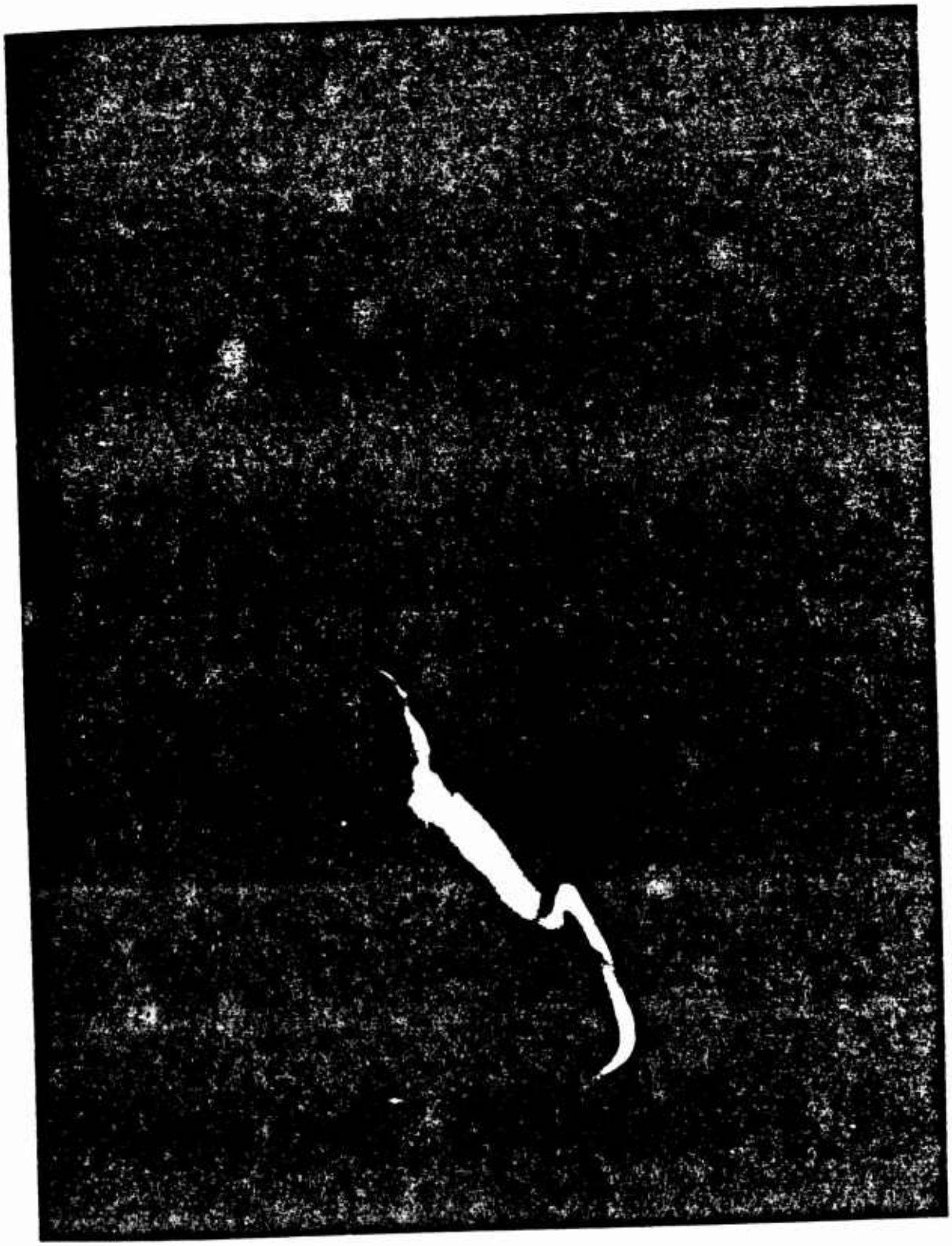

Figure 3.27 Sodium trail at dawn (28 ½ hours) after King Fish, 4 ½ minutes after rocket launch.

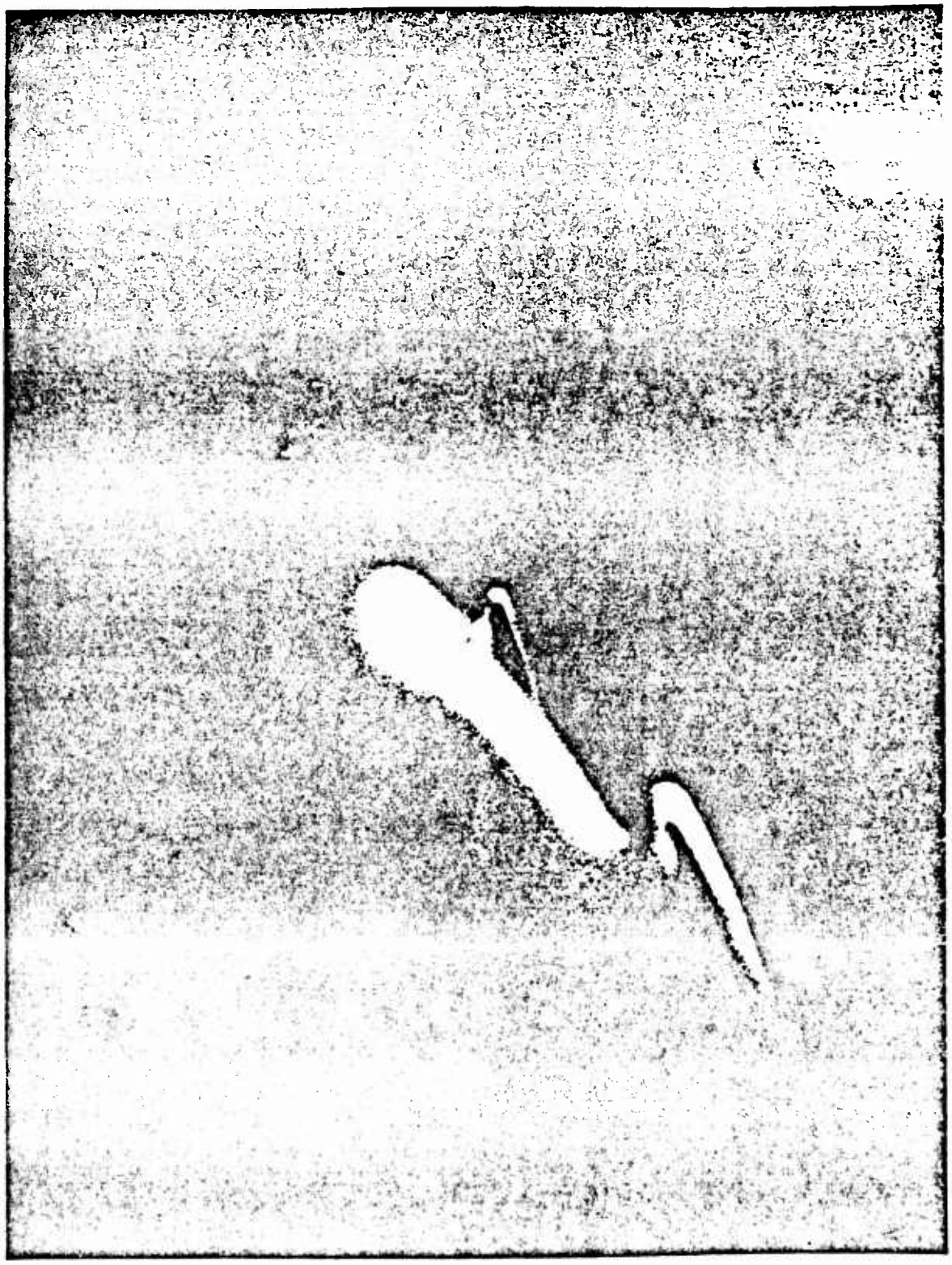

Figure 3.28 Sodium trail at dawn (2s$^{1}_{2}$ hours) after King Fish, 7$^{1}_{2}$ minutes after rocket launch.

Figure 3.29 Sodium trail at dawn (28½ hours) after King Fish, 10 minutes after rocket launch.

Figure 3.30 Sodium trail at dawn (28 ½ hours) after King Fish, 12 ½ minutes after rocket launch.

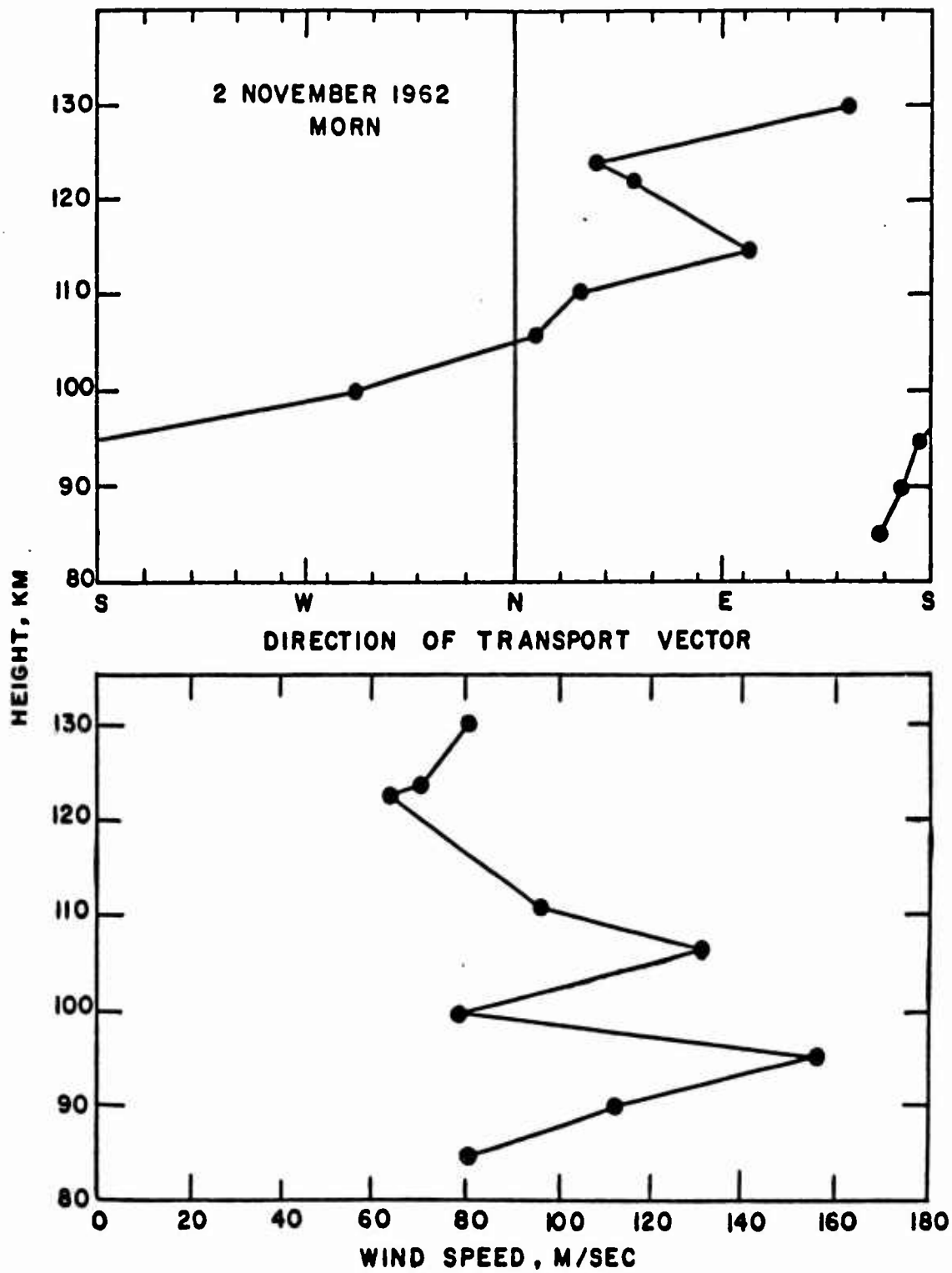

Figure 3.31. Upper atmosphere wind speeds and directions at dawn (28-1/2 hours) after King Fish.

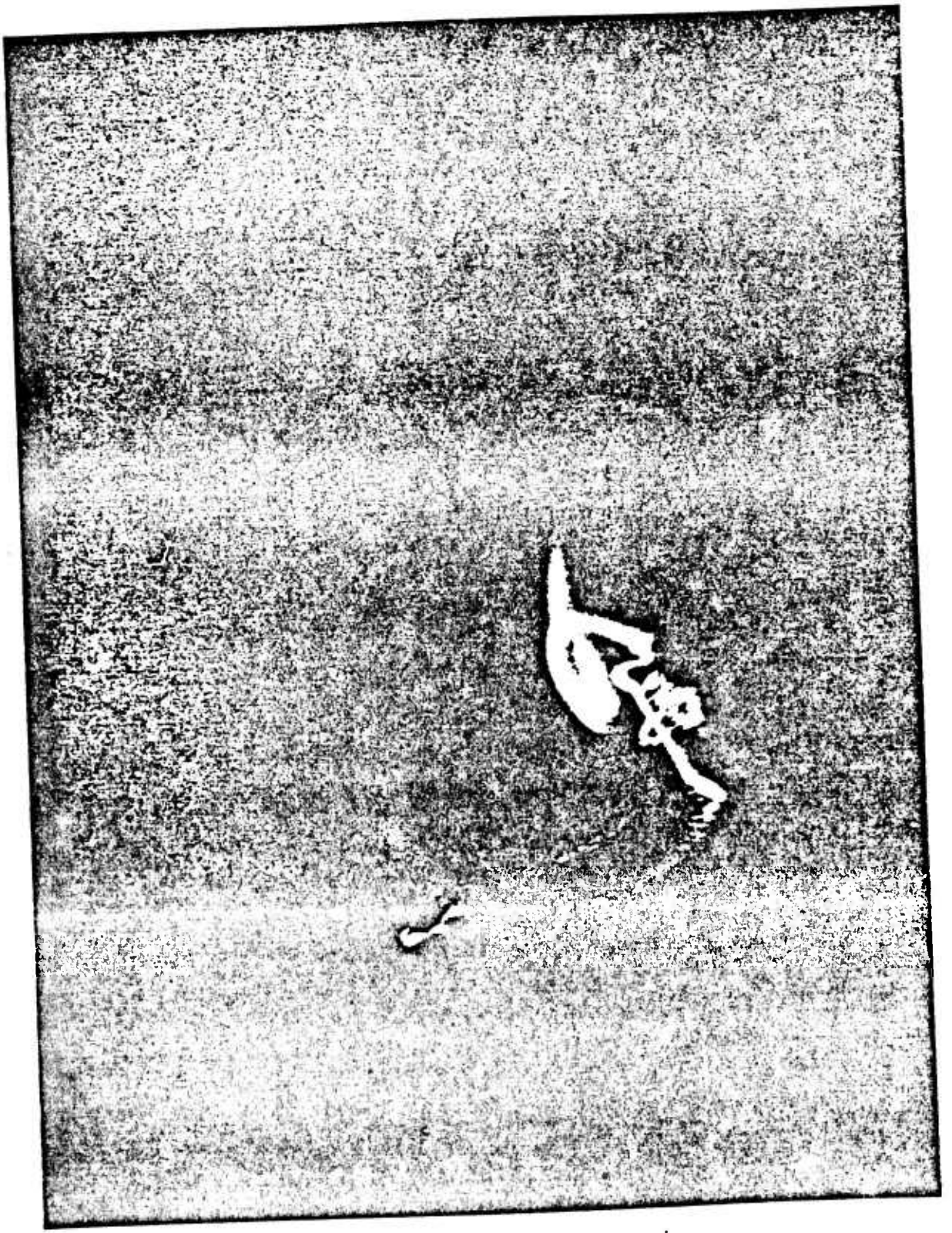

Figure 3.32 Sodium trail at dusk (41 hours) after King Fish, 4 minutes after rocket launch.

Figure 3.33 Sodium trail at dusk (41 hours) after King Fish, 6 minutes after rocket launch.

Figure 3.34 Sodium trail at dusk (41 hours) after King Fish, 8 minutes after rocket launch.

Figure 3.35 Sodium trail at dusk (41 hours) after King Fish, 10 ½ minutes after rocket launch.

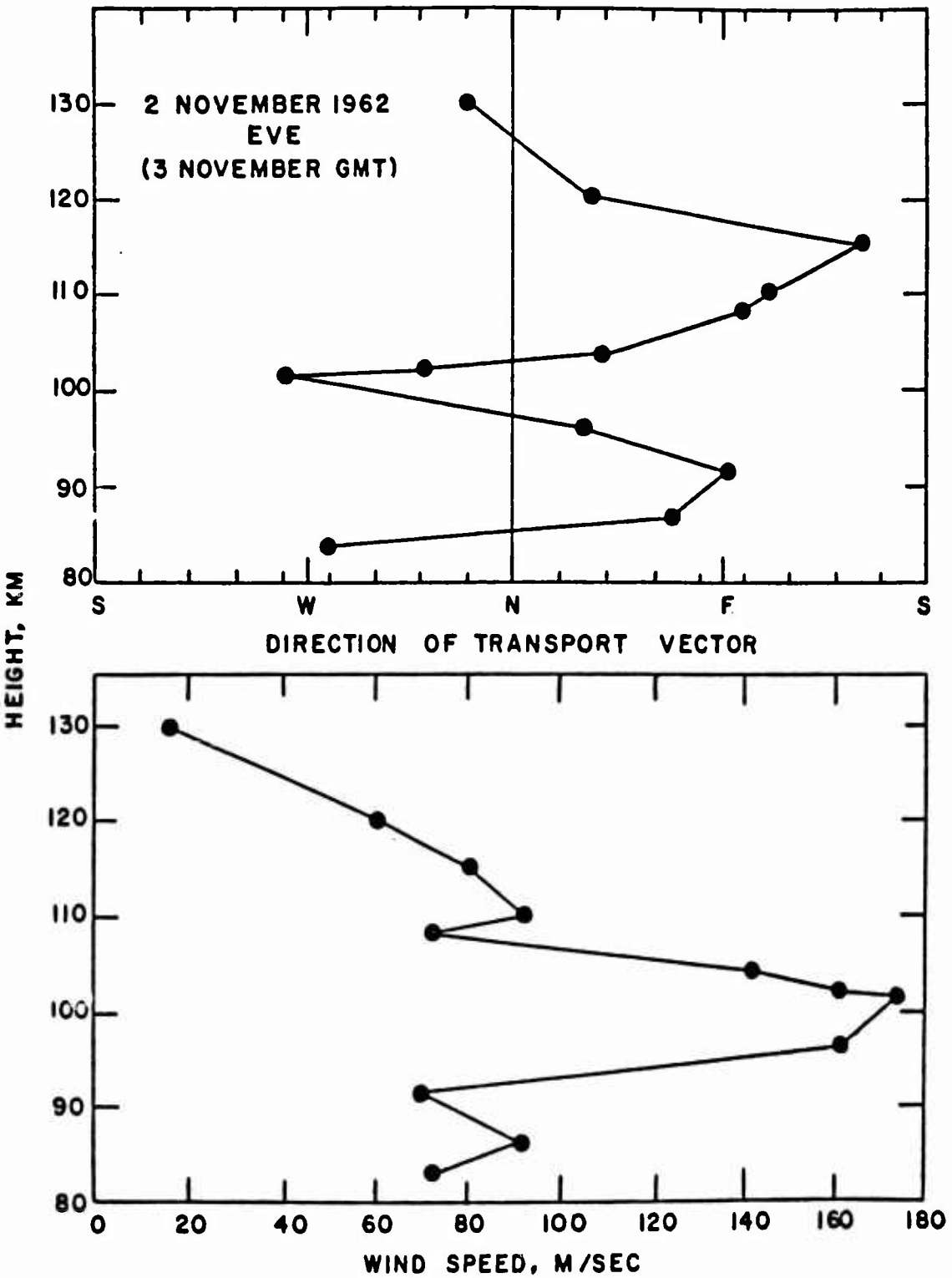

Figure 3.36. Upper atmosphere wind speeds and direction at dusk (41 hours) after King Fish.

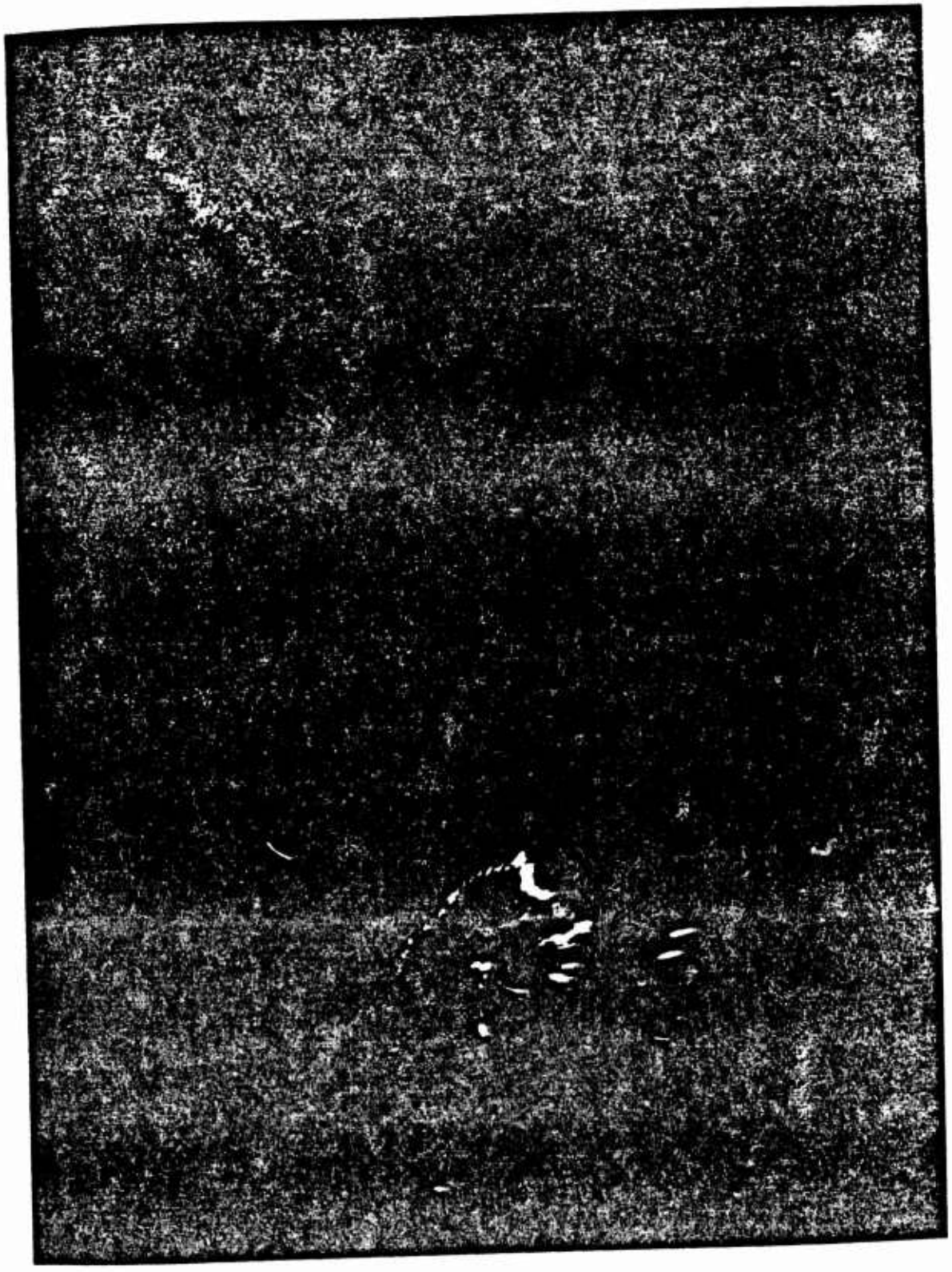

Figure 3.37 Sodium trail at dusk prior to Tight Rope, 3½ minutes after rocket launch.

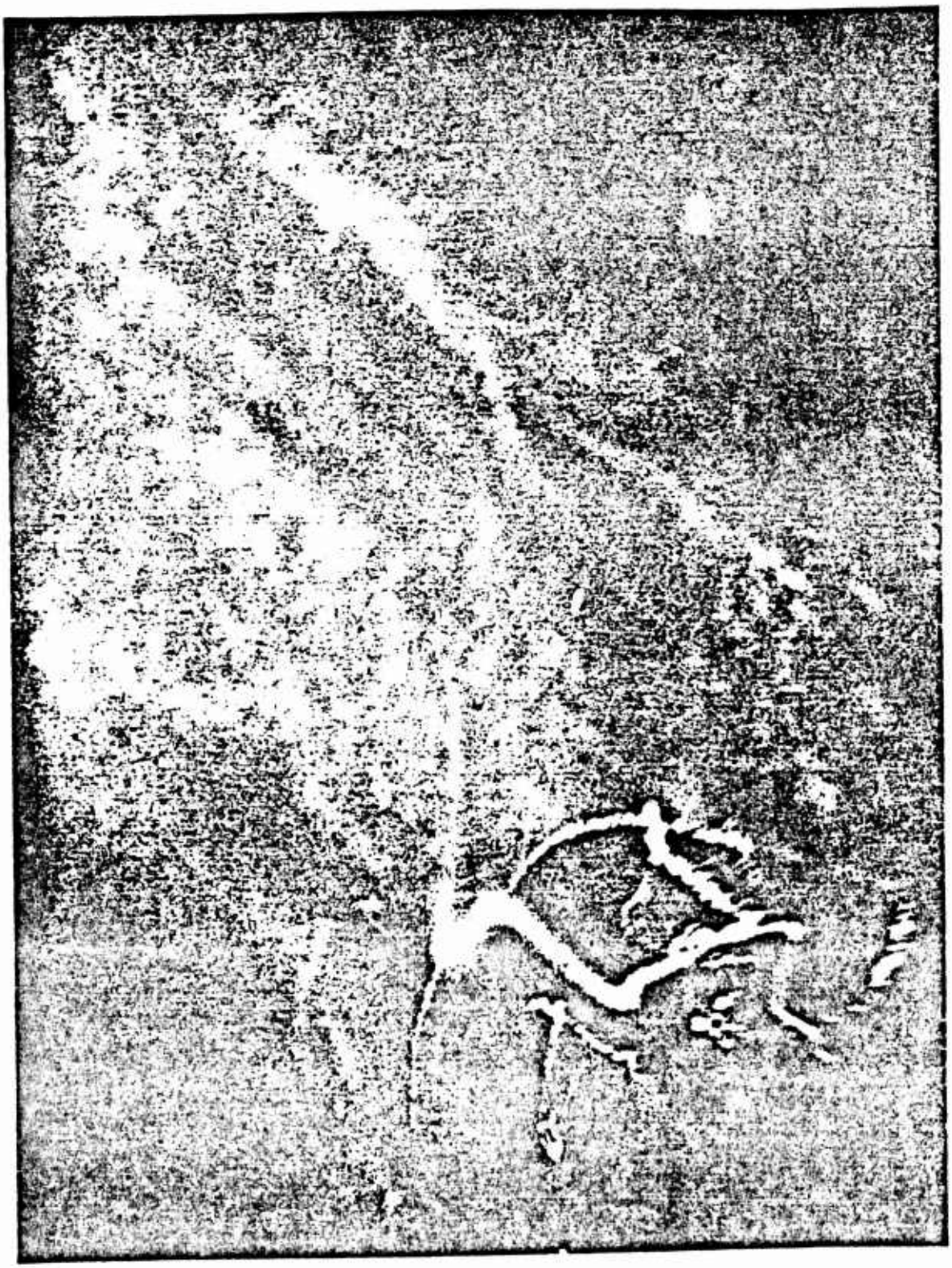

Figure 3.38 Sodium trail at dusk prior to Tight Rope, 5 minutes after rocket launch.

Figure 3.39 Sodium trail at dusk prior to Tight Rope, 7 minutes after rocket launch.

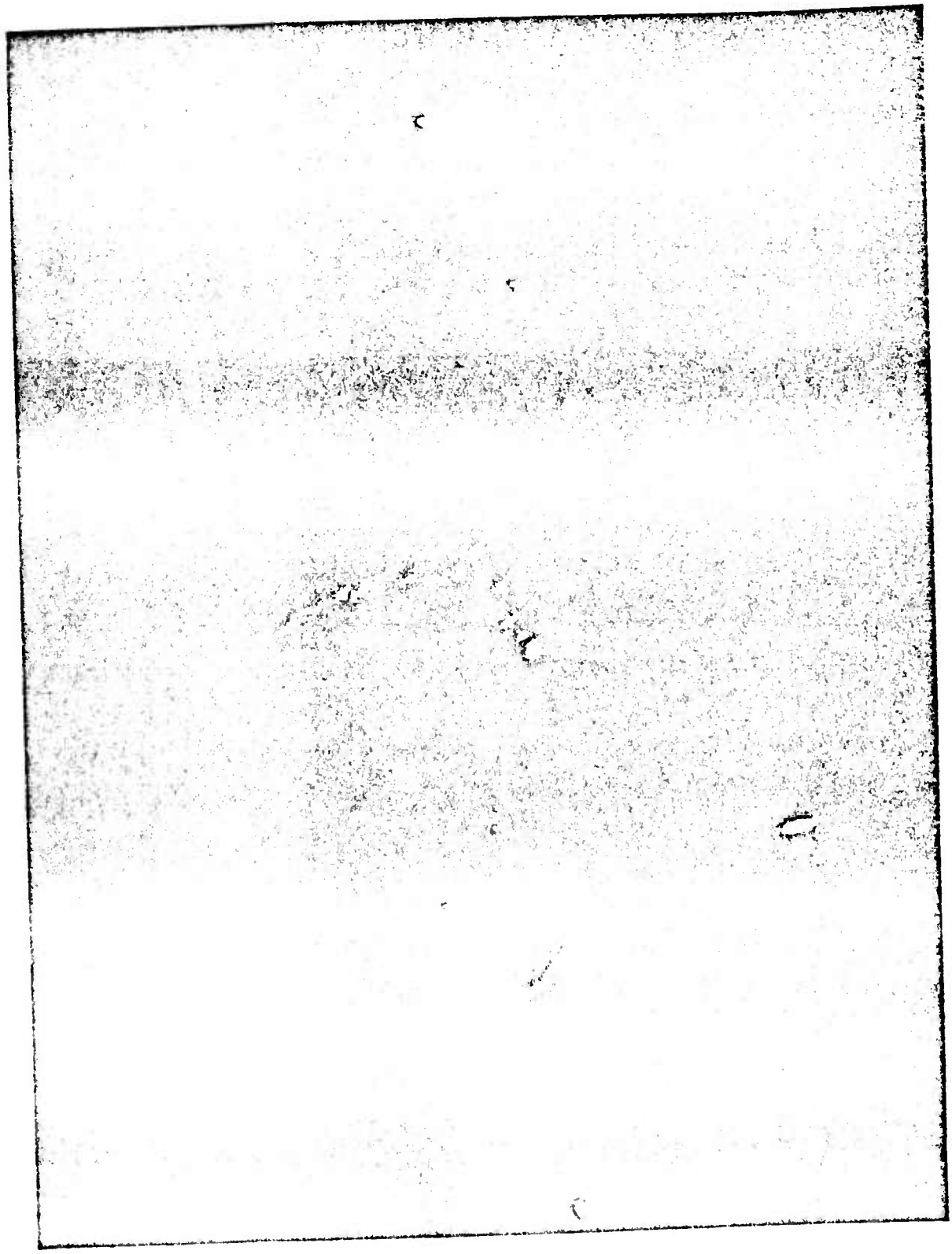

Figure 3.40 Sodium trail at dusk prior to Tight Rope, 9 minutes after rocket launch.

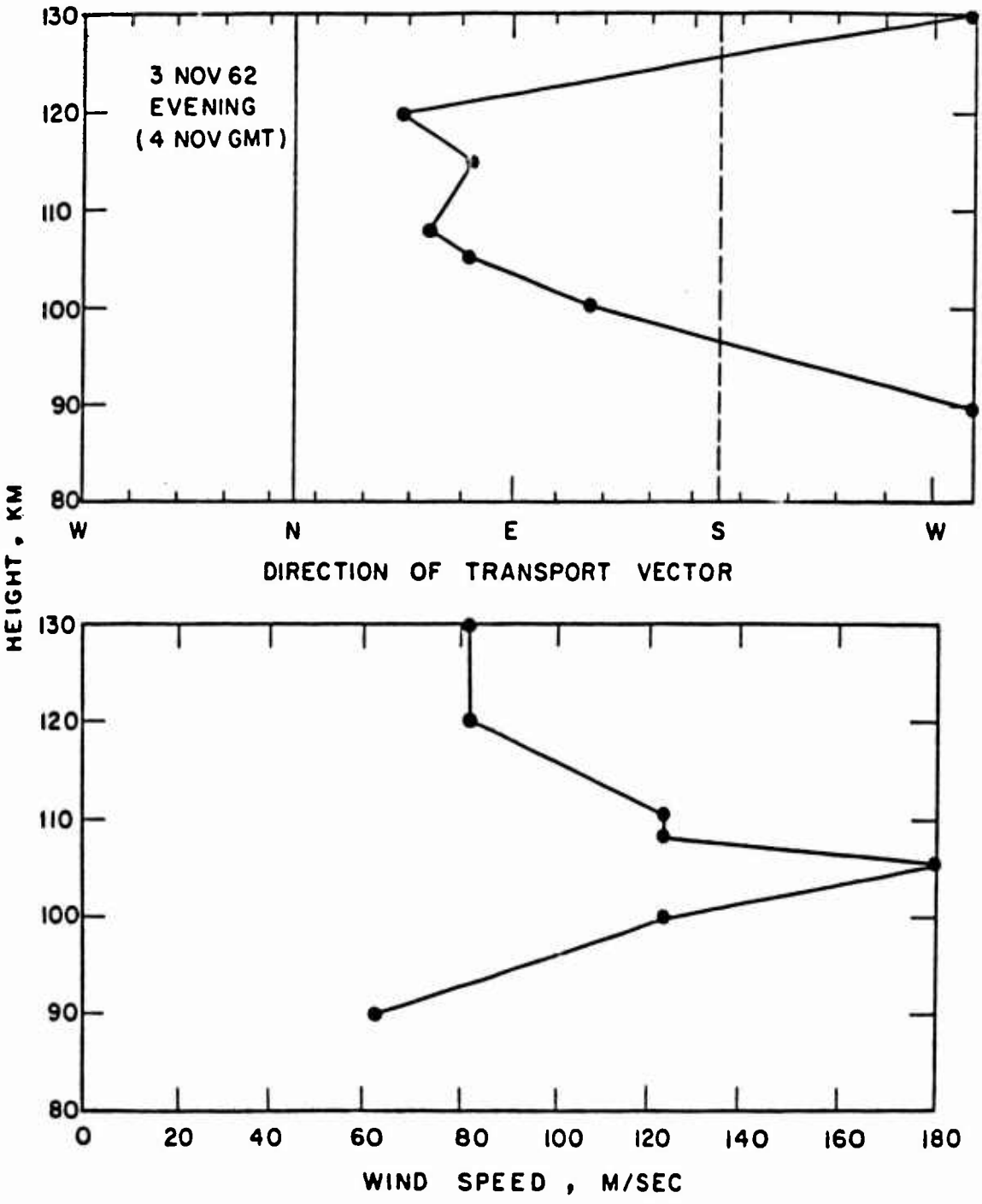

Figure 3.41. Upper atmosphere wind speeds and direction at dusk prior to Tight Rope.

Figure 3.42 Sodium trail 26 July 1962 (PM), including altitudes at which it was densitometered.

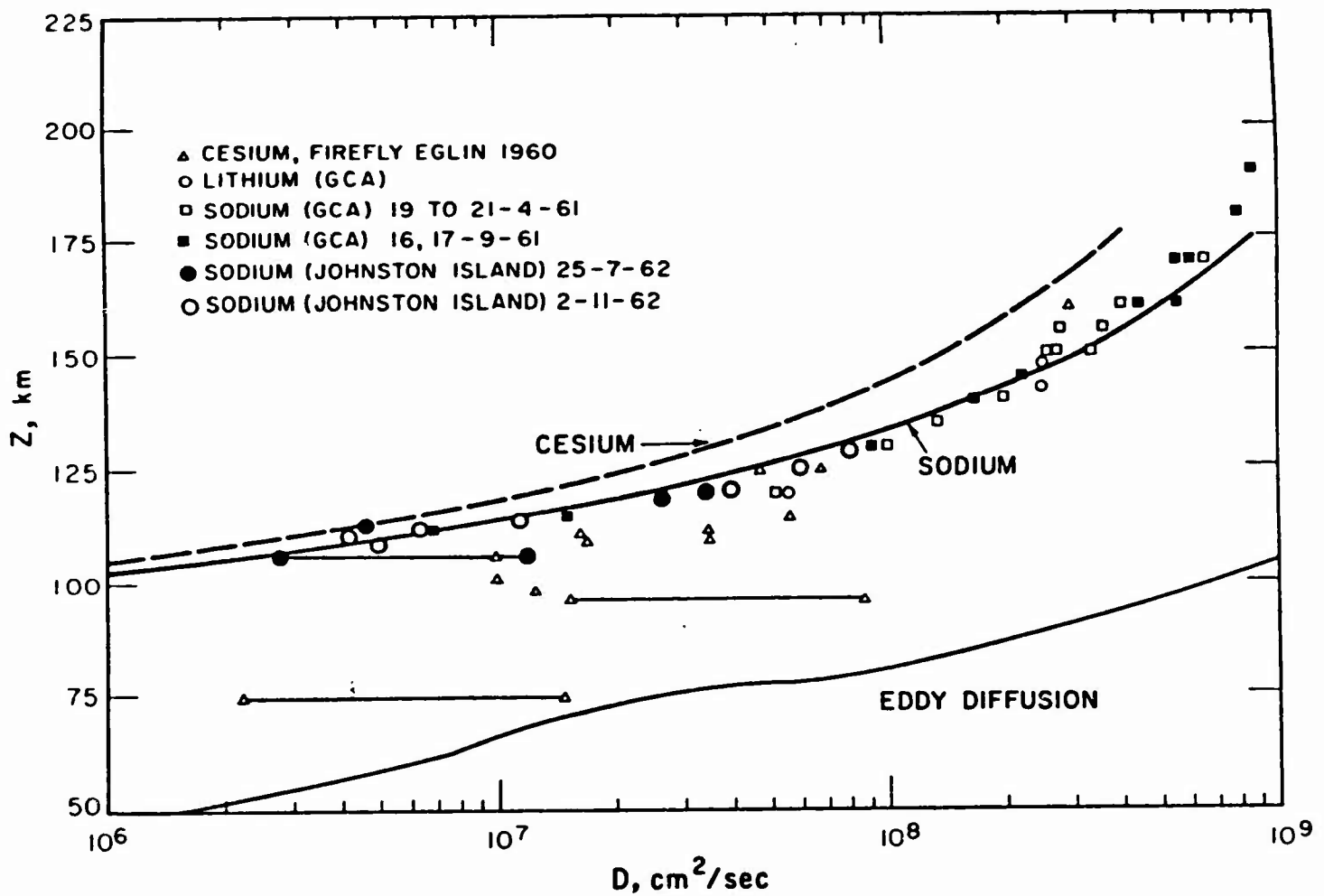

Figure 3.4? Comparison of theoretical curves of diffusion coefficients wit' some experimental results. The curves are for the diffusion of sodium and cesium in a nitrogen atmosphere. The measured turbulent diffusion coefficients are indicated by the horizontal lines. The curve labeled "eddy diffusion" is a theoretical estimate of the diffusion coefficient of large-scale eddies (Reference 13). See Figures 3.14 and 3.17 for examples of such eddies.

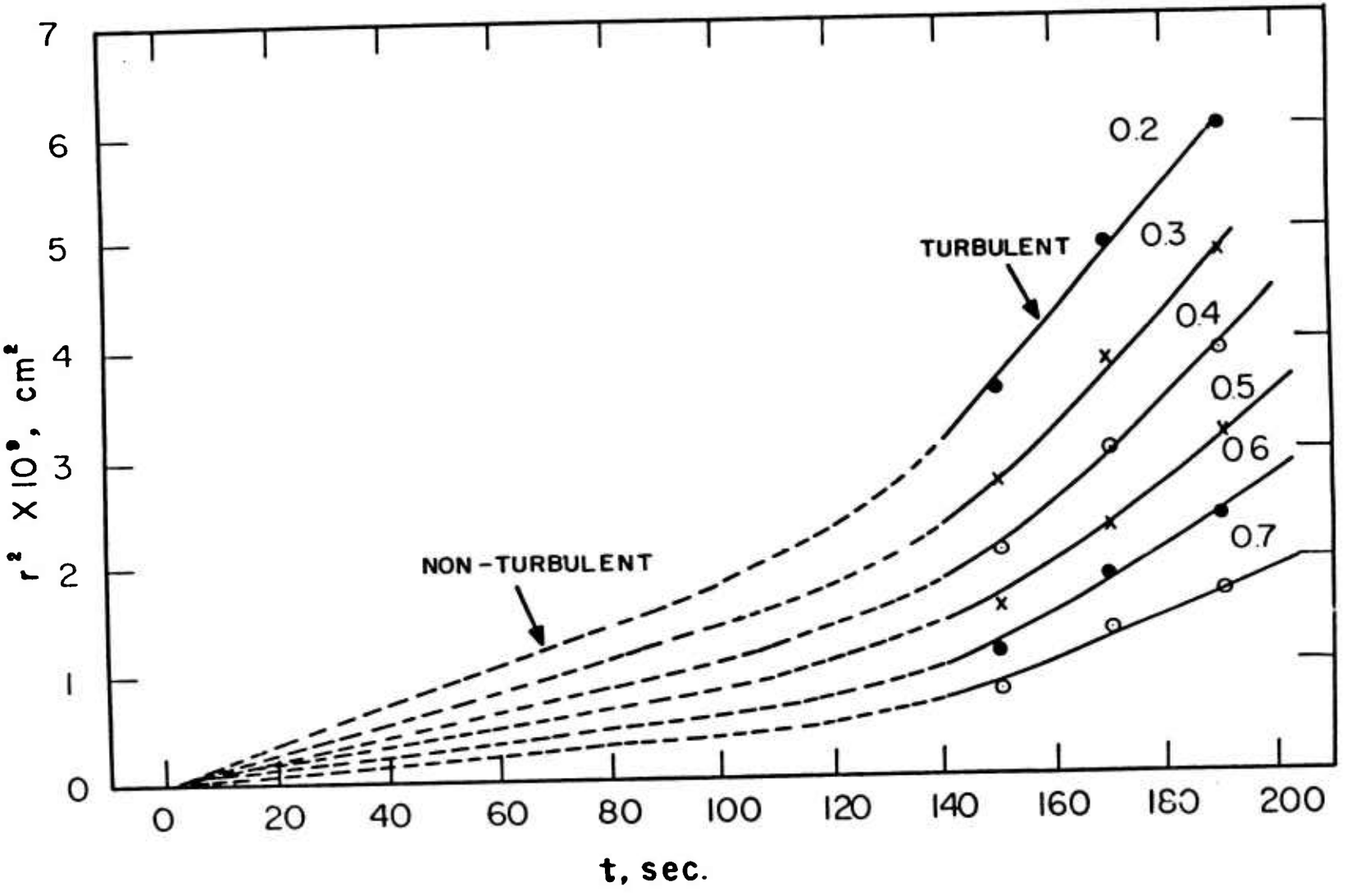

Figure 3.44 Plot of r^2 versus time for isophotes between 0.2 and 0.7 for trail of 26 July (PM), altitude 107 km. Note: release time was obtained from radar data.

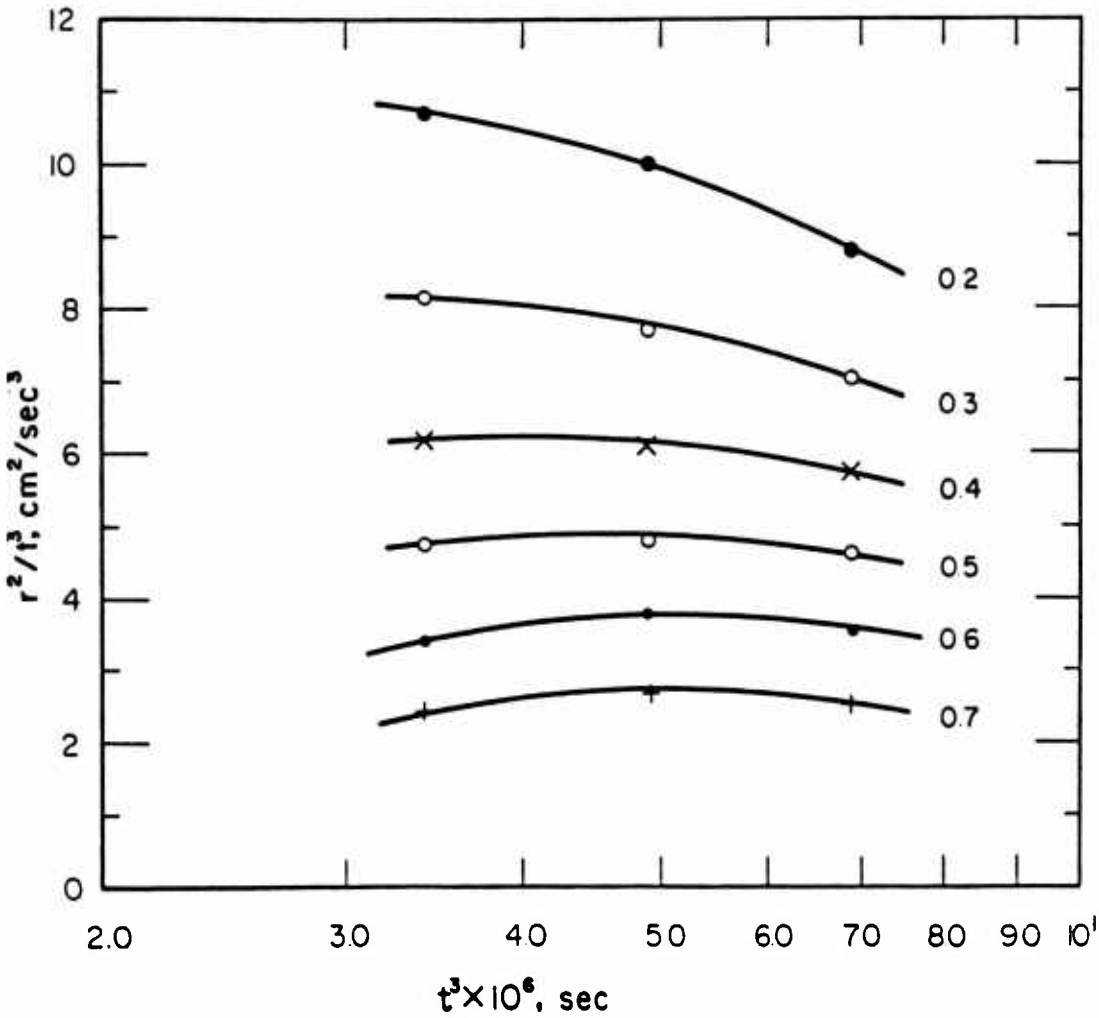

Figure 3.45 Plot of r^2/t^3 versus t^3 for isophotes between 0.2 and 0.8 for trail of 26 July (PM), altitude 107 km.

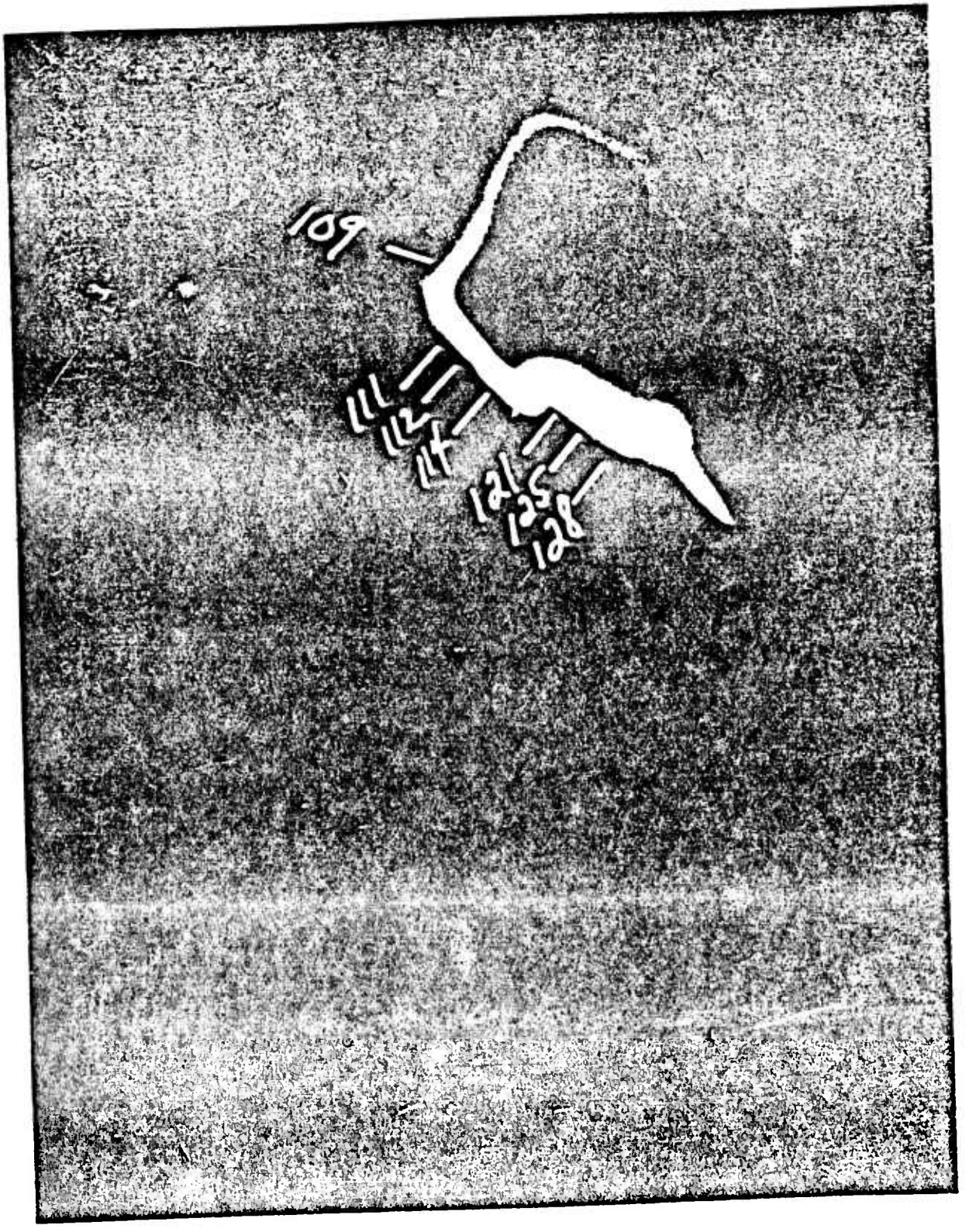

Figure 3.46 Sodium trail 2 November (AM), including altitudes at which it was densitometered.

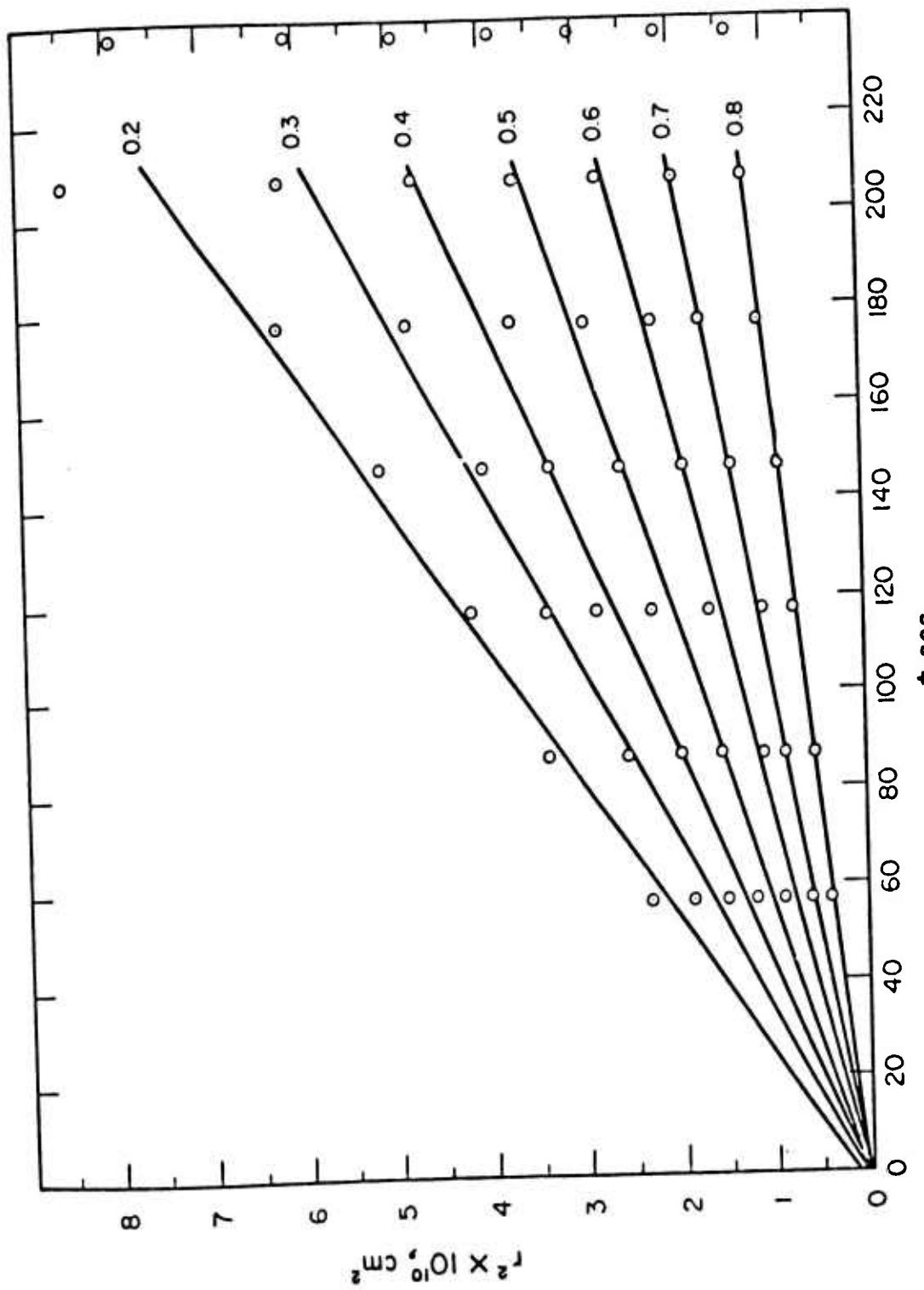

Figure 3.47. Plot of r^2 versus time for isophotes between 0.2 and 0.8 for trail 2 November (AM), altitude 125 km.

CHAPTER 4

DISCUSSION

Zonal wind components (Reference 2) are shown in Figure 4.1. These represent a typical wind pattern as a function of latitude for summer and winter, respectively. Note that the directions given are those from which the wind comes, which is the meteorological convention, and opposite to that used in this report. Vertical lines have been put in at 16.5 degrees latitude to indicate the location of Johnston Island. Very little wind data is available at high altitudes in the tropics. At the highest altitudes winds come from the east. There is a shear, which usually lies between 90 and 110 km, and whose exact altitude is determined by latitude and season, among other factors. Below this shear the wind is from a westerly direction.

In Figure 3.5 are shown the wind speeds and directions obtained for the evening before Star Fish Prime. Although the upper wind shear was higher than average, the wind speeds and directions observed are otherwise typical of summer conditions at this latitude. The winds shown in Figure 3.12 for July 9, morning, exhibit the highly disturbed conditions

following Star Fish Prime High wind speeds including very marked pseudoshears (or sharp changes in speed), were coupled with a unique pattern of wind directions. A double shear (or corkscrew change through 360 degrees) between 85 and 100 km was observed, instead of two approximately 180-degree shears, which are usually separated by about 30 km in altitude. Above this the wind was directed to the south instead of the west, as is invariably observed in this altitude region. This could be the return of material blasted to the north earlier. Ionized material travelled north and downward immediately following the detonation. The direction indicates the effect of magnetic field alignment on the motion of charged particles.

The wind speeds and directions obtained for 25 July, evening, are shown in Figure 3.16. The wind pattern was reasonably typical except for the presence of a north-south pseudoshear indicated in the previous chapter.

The high-speed north-south wind suggests the effect of a magnetic disturbance, inducing currents in the E-region which, by means of collisions with the neutral atmospheric gases, cause the observed wind. The observed wind was in some ways analogous to that measured the morning after Star Fish Prime, and it is tempting to postulate that it was due

to some residual effects from Star Fish Prime, for example, related to high-altitude trapped radiation. However, there are important differences in the winds. Following Star Fish Prime the wind was to the south at all altitudes (for which measurements were made) above 95 km. In this case, there was a strong wind to the south only between about 95 and 105 km.

Inspection of values of K_p (geomagnetic index) for the month of July shows that, by coincidence, the wind measurements were made at the time of highest magnetic activity for the month of July (6^+ at 0600Z on 26 July). This unusual activity was probably related to an observed sudden ionospheric disturbance

The wind patterns following the later nuclear detonations were not simple. This is probably due to three main reasons. One is that later detonations were of smaller yield, resulting in smaller, and hence less clearcut, perturbations. Secondly, the detonations were at lower altitudes, resulting in complicated hydrodynamical effects rather than the relatively simpler magnetohydrodynamical effects which dominated the Star Fish Prime event. Finally, the later detonations were so close together in time, including some large air-drop detonations, that changes in wind patterns were not simply related to a single detonation.

The wind measurements after Blue Gill Triple Prime were made at the following dawn, approximately six hours forty minutes after the detonation. (The data plotted in Figure 3.21 constitutes a revision of that in the interim report.) A comparison between the revised data and the rather limited data collected prior to the tests indicates that there was no significant perturbation in the wind patterns as a result of Blue Gill Triple Prime. However, the turbulent jets illustrated in Figures 3.18, 3.19, and 3.20 are unusual and possibly indicate enhanced turbulence persisting after the detonation.

The three occasions (Table 2.2) at which winds were measured following King Fish were 4-1/2, 28-1/2, and 41 hours after the detonation. Revised results are shown in Figures 3.26, 3.31, and 3.36. The results are puzzling since the perturbation appears to increase for some time before starting to return to normal again. The wind vector gradually rotated clockwise. On 1 November morning (H + 4-1/2 hours) it was displaced about 90 degrees clockwise compared with what would be expected. The following morning (H + 28-1/2 hours) the directions were little different up to 110 km, but above that altitude there was a further displacement of about 90 degrees. The evening (3 November PM) above 115 km the directions started to return to normal. Between 115 and

100 km they are approximately the same as in the morning, followed by a curious transition to an almost normal set of directions between 80 and 90 km.

The next measurement was made 24 hours later (4 November PM) just before Tight Rope. The maximum wind speed, 180 m/sec, was still high. The altitude separation of the wind shears (30 km) was normal, but their actual altitudes (97 and 127 km) were about 20 km above even their average summer altitudes. In early November the shears would normally be about 15 km below their summer altitudes, as the atmosphere cools toward its winter conditions. This suggests that residual energy deposition in the atmosphere following the nuclear detonations caused the change.

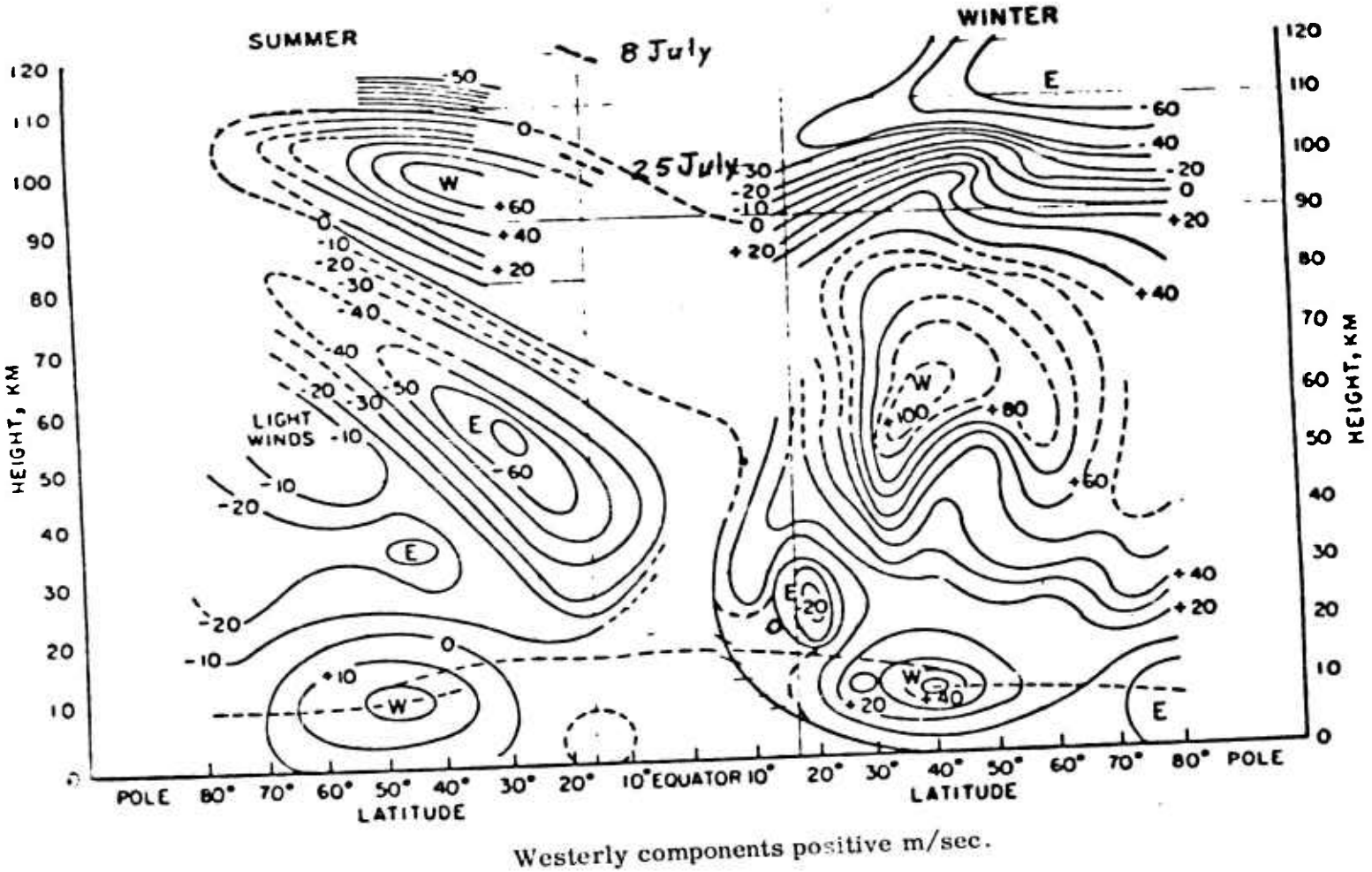

Figure 4.1 Variation of zonal wind components with latitude and altitude, summer and winter.

CHAPTER 5

CONCLUSIONS AND RECOMMENDATIONS

Wind speeds and directions, in the altitude range 80 to 130 km, have been determined from all eight sodium trails discussed in this report. Diffusion coefficients and turbulence distribution have been obtained for two of the trails. Both the wind velocities and diffusion coefficients can be used to determine the rate and direction of dispersal of the nuclear debris. The diffusion coefficients obtained depend strongly on the amount and type of turbulence present. Turbulence can change the magnitude of diffusion coefficient by as much as one or two orders of magnitude at a particular altitude. Because of the variation of these properties with altitude, long-term debris tracking (several days) is complicated unless the precise altitude of the material is known.

In addition, it has been possible to study intermediate and long-term effects of nuclear detonations, of various yields at several different altitudes, on winds in the ionosphere. The most pronounced and clear-cut effects were caused by Star Fish Prime. Blue Gill Triple Prime did not produce significant long-term effects on the wind circulation pattern between 80 and 130 km. All three measurements following King Fish showed winds that were unusual. However, their interpretation and variation with

time are not simple. This probably should not be surprising, since the measurements followed a period when a number of nuclear devices were detonated at various altitudes, separated only by short intervals of time. The perturbations of the wind circulation patterns caused by a nuclear detonation may be greater during October and early November, which are part of a period of transition between summer and winter wind flow patterns.

It is recommended for future high-altitude nuclear tests that wind measurements be made, not only at dawn and dusk using sodium trails, but also during the very night of the detonation, minutes before, and after, the event. Chemicals, such as nitric oxide and trimethyl aluminum, which form a persistent glow as a result of chemiluminescence, could be used.

REFERENCES

1. L.B. Smith; "The Measurements of Winds Between 100,000 and 300,000 Feet by Use of Chaff Rockets"; J. Meteor., 1960, Vol. 17, pages 296-310; Unclassified.

2. R.J. Murgatroyd; "Winds and Temperatures Between 20 km and 100 km —a review"; Quart. J.R. Meteor. Soc., 1957, Vol. 83, pages 417-458; Unclassified.

3. E.S. Batten; "Wind Systems in the Mesosphere and Lower Ionosphere"; J. Meteor., 1961, Vol. 18, pages 283-291; Unclassified.

4. K.S.W. Champion and S.P. Zimmerman, "Winds and Turbulence at 200,000 to 400,000 Feet from Chemical Releases"; Proc. of National Symposium on Winds for Aerospace Design, AFCRL-62-273 (II), 1962; Air Force Cambridge Research Laboratories, Bedford, Massachusetts; Unclassified.

5. J.F. Bedinger, E.R. Manring, and S.N. Ghosh; "Study of Sodium Vapor Ejected into the Upper Atmosphere"; J. Geophys. Research, 1958, Vol. 63, pages 19-29; Unclassified.

6. E. Manring and others; "Some Wind Determinations in the Upper Atmosphere Using Artificially Generated Sodium Clouds"; J. Geophys. Research, 1959, Vol. 64, pages 587-591; Unclassified.

7. E. Manring and others; "Upper Atmospheric Wind Profiles Determined from Three Rocket Experiments"; GCA Technical Report, No. 61-1-N, February 1961; Geophysics Corporation of America, Bedford, Massachusetts; Unclassified.

8. S.P. Zimmerman, "Upper Atmosphere Turbulences Near the 100 km Level"; Annales de Geophysique, Jan-March 1962, Vol. 18, No. 1; Unclassified.

9. S.P. Zimmerman, S.K. Majumdar and K.S.W. Champion; "Turbulence in the Upper Atmosphere"; Fluid Dynamics Div. of American Physical Society, Baltimore, March 1961; Unclassified.

10. S.P. Zimmerman and K.S.W. Champion; "Shear Turbulence in the Upper Atmosphere"; First Western National Meeting of American Geophysical Union, Los Angeles, December 1961; Unclassified.

11. S.K. Majumdar, S.P. Zimmerman and K.S.W. Champion; "Turbulence in the Upper Atmosphere"; Project Firefly, Semiannual Report, AFCRL Part I, July 1961; Air Force Cambridge Research Laboratories, Bedford, Massachusetts; Unclassified.

12. S.P. Zimmerman and K.S.W. Champion; "Molecular and Turbulent Diffusion in the Upper Atmosphere"; Project Firefly, AFCRL 256, Part I, 1961; Air Force Cambridge Research Laboratories, Bedford, Massachusetts; Unclassified.

13. S.P. Zimmerman and K.S.W. Champion; "Transport Processes in the Upper Atmosphere"; J. Geophysical Research, 1963, Vol. 68, page 3049; Unclassified.

14. E. Manring and H. Knaflich; "Some Measurements of the Coefficient of Diffusion in the Upper Atmosphere"; GCA Technical Report, No. 61-3-N, March 1961; Geophysics Corporation of America, Bedford, Massachusetts; Unclassified.

15. A.G. Weisner; "Diffusion of an Artificial Cloud of Neutral Atomic Sodium"; Unpublished memo. Evans Signal Lab, Belmar, New Jersey, 9 August 1951; Unclassified.

16. C.D. Shane; Lick Obs. Bull., 1941, Vol. 19, pages 119; Unclassified.

17. M. Minnaert; "The Sun"; U. Chic. Press, page 92; Unclassified.

18. T.M. Donahue and A. Foderaro; J. Geophys. Research, 1955, Vol. 60, page 75; Unclassified.

19. "Development and Testing of Ignition System for Rocket-Borne Sodium Vaporizer"; GCA Technical Report, No. 60-1-N, Nov. 1960; Geophysics Corporation of America, Bedford, Massachusetts; Unclassified.

Pages 167 and 168 deleted.